**INSTITUTO DE GEOGRAFÍA**
**FACULTAD DE HISTORIA, GEOGRAFÍA Y CIENCIA POLÍTICA**
**PONTIFICIA UNIVERSIDAD CATÓLICA DE CHILE**

# GEOMORFOLOGÍA Y GEOCRONOLOGÍA ($^{10}$BE) DE LAS FLUCTUACIONES DEL GLACIAR UNIVERSIDAD EN LOS ANDES CHILENOS SUBTROPICALES (34° S) DESDE EL ÚLTIMO MÁXIMO GLACIAL AL PRESENTE: IMPLICACIONES PALEOCLIMÁTICAS

Por

HANS ANDRÉS FERNÁNDEZ NAVARRO

Tesis presentada al Instituto de Geografía, Facultad de Historia, Geografía y Ciencia Política de la Pontificia Universidad Católica de Chile para optar al grado académico de Doctor en Geografía.

**Profesor guía:**
DR. JUAN-LUIS GARCÍA BARRIGA
**Comisión revisora:**
DR. SAMUEL U. NUSSBAUMER
DR. ESTEBAN SAGREDO TAPIA
DR. JOSÉ ARAOS ESPINOZA

Enero, 2023
Santiago de Chile

**DERECHOS DE AUTOR**

© 2023, Hans Andrés Fernández Navarro

Se autoriza la reproducción total o parcial, con fines académicos, por cualquier medio o procedimiento, incluyendo la cita bibliográfica que acredita al trabajo y a su autor.

**AGRADECIMIENTOS**

A Mariela y Luis, mi madre y mi padre, quienes siempre han sido un apoyo incondicional. Al Dr. Rodrigo Hidalgo, por invitarme a postular al Doctorado en Geografía UC. Al Dr. Juan Luis García, por aceptar y conducir mi propuesta de investigación hacia niveles de excelencia. Al Dr. Samuel U. Nussbaumer, quien también orientó mi proceso de formación y me abrió las puertas de la Universidad de Zúrich. A la Dra. Alessa J. Geiger, por su ayuda tanto en terreno como en la elaboración de los manuscritos. Al Dr. Esteban Sagredo, por las preguntas y comentarios que enriquecieron la ciencia de mi tesis.

Al Dr. Dmitry Tikhomirov y Dr. Markus Egli, ambos pertenecientes al Laboratorio de Exposición Superficial de la Universidad de Zúrich (Surface Exposure Laboratory - UZH), por facilitar el proceso de fechado de muestras. A Francia Pérez, del Laboratorio de Isótopos Cosmogénicos y Paleoclima del Cuaternario del Instituto de Geografía de la Pontificia Universidad Católica, por su incansable y valiosa colaboración. Al equipo de Glaciología y Geomorfodinámicas de la Universidad de Zúrich y a los profesores y colegas del World Glacier Monitoring Service (WGMS) por su recibimiento y ayuda en el fortalecimiento de mi trabajo. A mis compañeras y compañeros del doctorado, particularmente a Einer Sepúlveda, Rodrigo Soteres y Sebastián Ruiz.

A todas mis profesoras y profesores por guiarme en el camino de la Geografía, el cual me ha llenado de felicidad a lo largo de estos años.

A los Andes, por ser uno de los paisajes más conmovedores e inspiradores que he recorrido.

**CONTENIDO**

RESUMEN ..... 7
ABSTRACT ..... 10
1. INTRODUCCIÓN ..... 13
1.1. Evolución glaciar y climática del último siglo ..... 15
1.2. Glaciaciones cuaternarias de los Andes centrales de Chile y Argentina ..... 18
1.3. Preguntas de investigación ..... 21
1.4. Hipótesis ..... 22
1.4.1. Hipótesis #1 ..... 22
1.4.2. Hipótesis #2 ..... 22
1.5. Objetivos de investigación ..... 23
1.5.1. Objetivo General ..... 23
1.5.2. Objetivos específicos ..... 23
2. DE-ICING LANDSYSTEM MODEL FOR THE UNIVERSIDAD GLACIER (34° S) IN THE CENTRAL ANDES OF CHILE DURING THE PAST ~660 YEARS ..... 24
2.1. Introduction ..... 25
2.1.1. Conceptual models of de-icing ..... 26
2.2. Regional setting ..... 28
2.3. Materials and methods ..... 31
2.3.1. Geomorphological mapping ..... 31
2.3.2. Geochronology ..... 32
2.4. Results ..... 34
2.4.1. Geomorphology of the glacier forefield ..... 34
2.4.1.1. Moraine ridges ..... 35
2.4.1.2. Hummocky terrain ..... 40
2.4.1.3. Flutes ..... 43
2.4.2. The debris-covered glacier snout ..... 45
2.4.3. Geochronology ..... 48
2.5. Discussion ..... 49
2.5.1. Timing of morphogenesis ..... 49
2.5.2. Active ice derived landforms ..... 51
2.5.3. Stagnant ice-derived landforms ..... 54
2.5.4. Current deglaciation ..... 57
2.5.5. De-icing conceptual model ..... 59
2.6. Conclusions ..... 62

3. FLUCTUATIONS OF THE UNIVERSIDAD GLACIER IN THE ANDES OF CENTRAL CHILE (34° S) DURING THE LATEST HOLOCENE DERIVED FROM A 10BE MORAINE CHRONOLOGY ..... 64
3.1. Introduction ..... 65
3.2. Study area ..... 70
3.3. Material and methods ..... 73
3.3.1. Geomorphological mapping ..... 73
3.3.2. Geochronology ..... 73
3.4. Results ..... 75
3.4.1. Geochronology of the UNI IV moraine complex ..... 75
3.5. Discussion ..... 78
3.5.1. Geochronology ..... 78
3.5.2. Glacier records for the central Andes of Chile and Argentina ..... 84
3.5.3. Paleoclimate context ..... 85
3.5.4. Paleoclimate forcing ..... 86
3.5.5. Wider implications at regional and hemispheric scale ..... 89
3.6. Conclusions ..... 90
4. EVIDENCE OF LAST GLACIAL MAXIMUM AND A LATE GLACIAL ADVANCE IN UNIVERSIDAD GLACIER VALLEY (34° S), ANDES OF CENTRAL CHILE: PALEOCLIMATE IMPLICATIONS ..... 91
4.1. Introduction ..... 92
4.2. Study area ..... 95
4.3. Material and methods ..... 98
4.3.1. Geomorphological mapping ..... 98
4.3.2. Geochronology ..... 99
4.4. Results ..... 101
4.4.1. Glacial geomorphology ..... 101
4.4.2. Geochronology ..... 107
4.5. Discussion ..... 113
4.5.1. Glacial geomorphology ..... 113
4.5.2. Geochronology ..... 116
4.5.3. Paleoclimate forcings of the LGM and LGT ..... 121
4.5.4. Conclusions ..... 129
5. CONCLUSIONES GENERALES ..... 131
6. REFERENCIAS ..... 135
ANEXOS ..... 162
Characteristics of the sampled boulders in the moraine UNI IV ..... 162

## LISTA DE FIGURAS

Figure 1. location of the study area in the central Chile (30–35°s)..... 30
Figure 2. Glacial geomorphology and geochronology of the Universidad Glacier forefield.. ..... 34
Figure 3. Frontal ridges of moraines A and B. ..... 36
Figure 4. Overview of the forefield and moraines $D_1$ and $D_2$..... 37
Figure 5. Universidad Glacier front. ..... 39
Figure 6. Geomorphological attributes of hummocky terrain..... 41
Figure 7. Different types of glacial flutes on the hummocky terrain. ..... 44
Figure 8. The debris-covered glacier snout. ..... 47
Figure 9. De-icing model for the Universidad Glacier..... 61
Figure 10. Location of the study area in the Andes of central Chile..... 69
Figure 11. $^{10}$Be geochronology of the UNI IV moraine complex at the Universidad Glacier..... 72
Figure 12. Sampled boulders within the UNI IV moraine complex. ..... 77
Figure 13. Probability density of exposure ages for the UNI IV moraine complex (=20)..... 78
Figure 14. Frequency of $^{10}$Be exposure ages available for the UNI IV moraine complex represented in calendar years (n=20)..... 81
Figure 15. Universidad Glacier $^{10}$Be chronology (in gray) compared to climate indexes for the latest Holocene. ..... 88
Figure 16. Study area in the hemispherical and regional context. ..... 96
Figure 17. Moraines UNI I, UNI II and UNI III on the right side of the valley. ..... 102
Figure 18. Surface of the left lateral moraine UNI I. ..... 103
Figure 19. The left latero-frontal moraine UNI I. ..... 105
Figure 20. Boulders on the lower section of the moraine UNI II (LGM). ..... 106
Figure 21. Last glacial period $^{10}$Be chronology of the Universidad Glacier. ..... 107
Figure 22. $^{10}$Be exposure ages of the moraines UNI I and UNI II in the Universidad Glacier valley. .. 109
Figure 23. $^{10}$Be exposure ages of the moraines UNI II and UNI III in the Universidad Glacier valley. 110
Figure 24. Probability density plot of $^{10}$Be exposure ages. ..... 111
Figure 25. Paleoclimate context in which late-Quaternary fluctuations of the Universidad Glacier occurred..... 123

## LISTA DE TABLAS

Table 1. Geographical data, analytical data, and exposure ages of 10Be samples of the UNI IV moraine of Universidad glacier..... 50
Table 2. Analytical data used for age calculation of the samples of the UNI IV moraine complex of the Universidad Glacier ..... 82
Table 3. Geomorphic context and $^{10}$Be exposure ages of the samples of the UNI IV moraine complex of the Universidad Glacier. The samples are arranged according to their morphostratigraphical position.. 83
Table 4. Geographical and analytical data of $^{10}$Be samples of the UNI I, UNI II and UNI III moraines. ..... 112
Table 5. $^{10}$Be exposure ages of the samples from moraines UNI I, UNI II and UNI III in the Universidad Glacier valley..... 125

**RESUMEN**

Los glaciares ubicados en los Andes de Chile central (29°—35° S) son altamente sensibles a los cambios del clima. Por lo cual, reconstruir la evolución de los glaciares través de registros geológicos tales como morrenas, brindan una oportunidad para reconstruir las variaciones climáticas en distintas escalas de tiempo. Además, los glaciares de los Andes de Chile central representan una valiosa fuente de recursos hídricos para cerca de 10 millones de personas en periodos secos como el actual. En este trabajo se reconstruyó la evolución del Glaciar Universidad (34° 42' S, 70° 20' O) desde el Último Máximo Glacial al presente. Para aquello se confeccionó un mapeo geomorfológico a lo largo de los ~20 km del valle del Glaciar Universidad. El mapeo permitió identificar cuatro morrenas, denominadas desde la más distal a la más proximal como UNI I–IV. Las morrenas se distribuyen entre los ~1100 y 2500 m.s.n.m. Complementariamente, se aplicó datación por exposición superficial ($^{10}$Be) en cuarenta y nueve bloques granodioríticos emplazados principalmente en la superficie de las morrenas. El fechado por exposición superficial de cada una de las morrenas ha permitido obtener una de las geocronologías glaciales más completas de la región. Los resultados de la tesis se dividen en tres capítulos, los que a su vez presentan como investigaciones independientes en formato de artículo científico. Cabe destacar que la numeración de figuras y tablas es correlativa a la tesis doctoral, por lo cual no guardan exclusiva relación con cada uno de los capítulos.

El capítulo "*De-icing landsystem model for the Universidad Glacier (34° S) in the central Andes of Chile during the past ~660 years*", que se encuentra publicado en Geomorphology (doi.org/10.1016/j.geomorph.2021.108096; doi.org/10.1016/j.geomorph.2022.108426 [Corrigendum]) brinda un marco conceptual y geocronológico de la evolución geomorfológica del deshielo del Glaciar Universidad en el último milenio. Se ha definido que desde, al menos, los últimos ~660 años, el Glaciar Universidad ha evolucionado desde un glaciar limpio, a un glaciar con su frente cubierto de escombros, a una morrena con núcleo de hielo y, finalmente, a una topografía masiva y acolinada de hielo muerto. Esta transición geomorfológica ha sido interrumpida y retrabajada por múltiples reavances del hielo, lo que ha permitido la configuración de un complejo morrénico (morena UNI IV) en la actual área proglacial.

El capítulo "*Fluctuations of the Universidad Glacier in the Andes of central Chile (34° S) during the latest Holocene derived from a* $^{10}$*Be moraine chronology*", que está disponible en Quaternary Science Reviews (doi.org/10.1016/j.quascirev.2022.107884), establece la geocronología de las principales fluctuaciones glaciares del último milenio y discute acerca de los forzantes climáticos de dichos cambios. Los Andes de Chile central se encuentran entre el margen sur del Anticiclón del Pacífico Subtropical (APS) y el margen norte de los Vientos del Oeste (VO). El dominio de la APS en la región se asocia a condiciones cálidas y secas, mientras que la migración de los VO a Chile central se vincula con condiciones más frías y húmedas. Por medio del muestreo y fechado de veinte bloques granodioríticos se identificó que en el último milenio el Glaciar Universidad ha tenido, al menos, dos avances máximos. El primer avance máximo ocurrió entre el siglo 13 y 16, mientras que el segundo reavance máximo fue durante la primera mitad del siglo 19. Los avances del Glaciar Universidad desde el siglo 13 hasta la primera mitad del siglo 19 retrabajaron el área proglacial (morrena UNI IV). Los datos sugieren que los avances glaciares

fueron una respuesta a la migración de los VO a latitudes medias durante una fase negativa del Modo Anular del Sur (SAM) que se extendió desde el año ~1400 al 1850. El último avance del Glaciar Universidad ocurrió a mediados del siglo 20, también en un periodo negativo del SAM. Después de ese reavance el Glaciar Universidad solo ha tendido a decaer.

El capítulo "*Evidence of the Last Glacial Maximum and a late-glacial advances in the Universidad Glacier valley (34° S), Andes of central Chile: paleoclimate implications*", próximamente a ser enviado a una revista científica internacional por definir, aborda la geocronología de las fluctuaciones glaciares desde el Último Máximo Glacial (UMG) al periodo de la Última Terminación Glacial (UTG). Además, se debate en torno a los forzantes orbitales y a las condiciones atmosféricas que posibilitaron los avances glaciares del Cuaternario tardío. Tres bloques granodioríticos obtenidos desde la morrena UNI I brindaron edades de exposición pre-Último Máximo Glacial (51.4±2.7 a 135.9±7.1 ka; 1 ka= hace 1000 años), por lo cual no fue posible establecer relación alguna entre su periodo de construcción y un evento climático especifico. Catorce edades de exposición obtenidas desde la Morrena UNI II fluctuaron entre los 17.0±0.8 y 19.9±1.0 ka (promedio= 18.2±0.7 ka), lo que coincide con el UMG. Desde la morrena UNI III se obtuvieron seis edades de exposición que variaron entre 9.7±0.5 y 14.4±1.1 ka (promedio=11.8±1.8 ka), lo que implica un reavance tardiglacial ocurrido durante la UTG y comienzos del Holoceno. El principal factor climático que explica los avances glaciares que construyeron las morrenas UNI II y UNI III, radica en la migración de los VO hacia Chile central, lo cual implicó el transporte de condiciones atmosféricas más húmedas y frías desde regiones subantárticas hacia latitudes subtropicales.

El último capítulo, de conclusiones generales de la tesis, se ha construido como un abordaje integrador a las preguntas e hipótesis de esta investigación.

**ABSTRACT**

Glaciers located in the Andes of central Chile (29° —35° S) are highly sensitive to climate changes. Therefore, reconstructing the evolution of glaciers through geological records such as moraines provides an opportunity to reconstruct climate variations on different time scales. In addition, glaciers in the Andes of central Chile represent a valuable source of fresh water for about 10 million people in dry periods such as the present. A broad vision of glacial changes in the context of climate warming and drying could provide technical support for the generation of public policies associated with water resource management and the conservation of high mountain environments. Here, I reconstructed the evolution of the Universidad Glacier (34° 42' S, 70° 20' W) from the Last Glacial Maximum to the present. For this purpose, I made a geomorphological mapping along the ~20 km of the Universidad Glacier valley. The mapping allowed the identification of four moraines labeled from distal to the most proximal position as UNI I-IV. The moraines are distributed between ~1100 and 2500 m asl. Additionally, surface exposure dating ($^{10}$Be) was applied on forty-nine granodioritic boulders resting mainly on the top of the moraines. The dating by surface exposure allowed us to obtain one of the most complete glacial geochronologies of the region. The results of this thesis are divided into three chapters, which in turn are presented as independent research in paper format. It should be noted that the numbering of figures and tables is correlative to the doctoral thesis, so they are not exclusively related to each of the chapters.

The chapter "*De-icing landsystem model for the Universidad Glacier (34° S) in the central Andes of Chile during the past ~660 years*", which is published in Geomorphology (doi.org/10.1016/j.geomorph.2021.108096; doi.org/10.1016/j.geomorph.2022.108426 [Corrigendum]), provides a conceptual and geochronological framework of the geomorphological de-icing of the Universidad Glacier during the last millennium. I defined that since, at least the last ~660 years, the Universidad Glacier has evolved from a clean glacier to a glacier with its debris-covered front, to an ice-cored moraine, and finally into a massive dead ice moraine topography. This geomorphological transition has been interrupted and reworked by multiple readvances of the glacier, which has allowed the configuration of a moraine complex (UNI IV moraine) in the current proglacial area.

The chapter "*Fluctuations of the Universidad Glacier in the Andes of central Chile (34° S) during the latest Holocene derived from a $^{10}$Be moraine chronology*", which is available in Quaternary Science Reviews (doi.org/10.1016/j.quascirev.2022.107884) establishes the geochronology of the major glacial fluctuations of the last millennium and discusses the atmospheric forcing of these changes. The Andes of central Chile lies between the southern margin of the Subtropical Pacific Anticyclone (SPA) and the northern margin of the Southern Westerly Winds (SWW). The dominance of the SPA in the region is associated with warm and dry conditions, while the migration of the SWW to central Chile is related to cooler and wetter conditions. By sampling and dating twenty granodioritic boulders, I identified that in the last millennium the Universidad Glacier had two maximum advances. The first maximum glacier advance occurred between the 13$^{th}$ and 16$^{th}$ centuries, while the second glacier readvance was during the early to mid-19$^{th}$ century. These glacier advances covered and reworked the entire proglacial area (moraine UNI IV). The data suggest that the glacial advances were a response to the migration of SWW to mid-

latitudes during a negative phase of the Southern Annular Mode (SAM) that extended from ~1400 to 1850 CE. The latest readvance of the Universidad Glacier occurred in the mid-20$^{th}$ century, also during a negative SAM phase. After that pulse, the Universidad Glacier has only tended to decay.

The chapter "*Evidence of the Last Glacial Maximum and a late-glacial advances in the Universidad Glacier valley (34° S), Andes of central Chile: paleoclimate implications"*, soon to be submitted to an international journal, addresses the geochronology of glacial fluctuations from the Last Glacial Maximum (LGM) to the Last Glacial Termination (LGT). Moreover, I discussed the orbital forcing and atmospheric conditions that made possible the glacial advances of the Late Quaternary. Three granodioritic blocks obtained from the UNI I moraine provided pre-Last Glacial Maximum exposure ages (51.4±2.7 to 135.9±7.1 ka; 1 ka= 1000 years ago), so it was not possible to establish any relationship between their period of construction and a specific climatic event. Fourteen exposure ages obtained from the UNI II moraine ranged from 17.0±0.8 to 19.9±1.0 ka (mean=18.2±0.7 ka), which coincides with the Last Glacial Maximum. Six exposure ages were obtained from UNI III Moraine ranging from 9.7±0.5 to 14.4±1.1 ka (mean=11.8±1.8 ka), implying a late-glacial advance that occurred during the Last Glacial Termination and early Holocene. The main climatic factor explaining the glacial advances that built the UNI II and UNI III moraines is the migration of the SWW towards central Chile, which implied the transport of cooler and wetter atmospheric conditions from sub-Antarctic regions to subtropical latitudes.

The last chapter, the general conclusions of this thesis, has been constructed as an integrative approach to the questions and hypotheses of this research.

# 1. INTRODUCCIÓN

La sensibilidad de los glaciares a los cambios climáticos hace que los registros geológicos producidos por las fluctuaciones del hielo sean una valiosa fuente de información para la reconstrucción de las condiciones atmosféricas del pasado (Mackintosh et al., 2017). Además, el mapeo de las geoformas generadas por los cambios del hielo permite tener nociones de las respuestas de los glaciares a los periodos cálidos o fríos (Evans and Twigg, 2002; Evans, 2011; 2013). Al generar una compresión integrada de la historia glacial a través del estudio de las geoformas de origen glacial presentes en el paisaje se obtienen nociones de la evolución de la criósfera y de la alta montaña en el contexto del calentamiento climático actual y futuro (Knight and Harrison, 2014).

Los Andes de Chile central (29°—35° S) se encuentran la zona de transición de dos importantes sistemas atmosféricos del hemisferio sur (Garreaud, 2009). Por una lado se encuentra el Anticiclón del Pacífico Subtropical (APS), que se centra entre los 25° a 30° S y que durante el invierno austral se extiende hasta los 45° S (Pizarro et al., 1994; Flores-Aqueveque et al., 2020). El fortalecimiento del APS ha sido vinculado a periodos cálidos y secos en Chile central (Boisier et al., 2018; Garreaud et al., 2020). Por otro lado, se encuentran los Vientos del Oeste, un cinturón circumpolar que transporta humedad desde el océano al continente y que tiene su núcleo entre los 50° y 55° S (Moreno et al., 2018). Durante el invierno austral y debido al debilitamiento del APS, los Vientos del Oeste migran hacia el norte, hasta los 27.5° S, transportando bajas temperaturas y precipitaciones hacia el continente (Lamy et al., 2000). Así, los glaciares de Chile central responden principalmente al aporte de nieve generados por la llegada de los Vientos del Oeste a la región (Sagredo et al., 2014; Masiokas et al., 2016).

Por lo anterior, la reconstrucción de los cambios glaciares de Chile central durante el Cuaternario tardío puede permitir establecer correlaciones entre periodos cálidos y secos o fríos y húmedos con los cambios latitudinales del APS y los Vientos del Oeste.

## 1.1. Evolución glaciar durante último siglo

La temperatura promedio del aire en la vertiente oeste de la cordillera de Andes (33° S) ha ascendido entre 0.2 a 0.4°C entre 1979 y 2006 (Falvey y Garreaud, 2009). Debido a esta tendencia se ha proyectado que para el periodo 2070-2100 la Altitud de Línea de Equilibrio glaciar ascenderá desde los 3800 a ~4300 m.s.n.m. a los 34° S (Carrasco, Casassa y Quintana, 2005). Además, desde el año 2010 un déficit de precipitaciones que fluctúa entre el 20 y 40% ha afectado al territorio comprendido entre los 29° y 39° S (Garreaud et al., 2020), lo que ha generado la reducción acelerada de la cobertura glaciar de Chile central (Dirección General de Aguas, 2022a). Se espera que el aumento de la temperatura promedio del aire y la falta de precipitación nival se traduzca durante las próximas décadas en la disminución del área englaciada, el adelgazamiento del hielo y cambios morfológicos en los frentes glaciales (Rivera et al., 2002; Bown et al., 2008;), lo que tiene implicancias con la disponibilidad de recursos hídricos regionales (Janke et al., 2015).

Si bien se han hecho trabajos de mapeo del cambio del cambio del frente glaciar y pérdida de área englaciada en los Andes de Chile central (Bown et al., 2008; Le Quesne et al., 2009; Malmros et al., 2016), también hay investigaciones que han sugerido que la degradación de los glaciares en periodos cálidos y secos va acompañada por el desarrollo de una capa detrítica supraglacial que promueve la formación y subsecuente degradación de un hielo subsuperficial (García et al., 2014; Janke et al., 2015). Así, la acumulación de una cobertura de escombros en los glaciares ha sido interpretado como parte de la transición morfogenética desde un glaciar limpio, a glaciar cubierto a, posiblemente, un glaciar de roca (Janke et al., 2015; Monnier and Kinnard, 2015; 2017). La degradación del hielo y producción de escombros en los frentes glaciares puede entenderse en el marco de los procesos paraglaciales, los cuales son entendidos

como hacen referencia a la inestabilidad del paisaje y al reajuste sedimentario que ocurre en la transición de un ambiente glacial a periglacial (Ballantyne, 1995; 2002). Los procesos paraglaciales se manifiestan a través de la liberación de una alta cantidad de sedimentos desde laderas de las montañas recientemente deglaciarizadas (Church & Ryder, 1972; Eichel et al., 2018; Oliva et al., 2020). Depósitos de derrumbes, conos de escombros, conos aluviales o deslizamientos de laderas son resultado del desencadenamiento de la actividad paraglacial (Knight & Harrison, 2014, 2018). Se ha catastrado en distintas áreas montañosas que, desde mediados del siglo 20, el reajuste paraglacial en laderas de montaña ocurre en las mismas zonas donde los frentes glaciares se están degradando (Eichel et al., 2018; van Woerkom et al., 2019). La producción de sedimentos desde las laderas de montaña recientemente deglaciarizadas es un factor que incide en el desarrollo de la cobertura detrítica supraglacial en los frentes glaciares (van Woerkom et al., 2019).

La transición geomorfológica desde glaciares limpios a glaciares cubiertos de escombros se ha modelado para distintas zonas montañosas del mundo. En Islandia se estableció que dicho cambio está dominada por el desarrollo de morrenas con núcleo de hielo en los márgenes glaciares cubiertos de escombros (Krüger and Kjær, 2000; Kjær and Krüger, 2001; Schomacker, 2007; Krüger et al., 2010). En los Himalyas, Benn y Owen (2002) han destacado que los frentes glaciares pueden estar forzados a fases estacionarias debido a la deposición de escombros que caen desde la secciones altas de la cordillera del Karakórum. En el Glaciar Sachen del Nanga Parbat, Shroder et al. (2000) observaron el desarrollo de una cobertura de escombros en el área de ablación desde finales del siglo 19, lo que ha provocado que la posición del frente glaciar se haya mantenido relativamente estable desde, al menos, comienzos de 1934. La degradación de los glaciares cubiertos de escombros ha sido abordada desde el monitoreo de las morrenas con núcleo de hielo tanto en los Alpes (Reid & Brock, 2014) como en los Himalayas (Shroder et al.,

2000). Se ha sugerido que la degradación completa de las morrenas con núcleo de hielo genera un paisaje de geomorfología masiva, acolinada y con características superficiales tales como subsidencias rellenas por escombros y alineamientos de sedimento grueso embebidos en el terreno (Krüger and Aber, 1998; Krüger and Kjær, 2000; Kjær and Krüger, 2001; Krüger et al., 2010).

Una topografía masiva con una superficie acolinada han sido descrita para áreas proglaciales de los Andes centrales de Chile y Argentina (Wayne and Corte, 1983; García et al., 2014; Iturrizaga and Charrier, 2021; Janke et al., 2015). Este relieve también se han descrito como complejos morrénicos cercanos a los frente glaciares actuales (Espizua, 2005; Sagredo et al., 2017). Tanto la topografía masiva y los complejos morrénicos no han sido estudiados en tanto su evolución geomorfológica ni geocronológica. Por lo que develar la evolución de los cambios glaciares en la última parte del Holoceno en los Andes de Chile central proporciona un mejor entendimiento de la evolución actual y subactual de criósfera respecto a los cambios del clima.

## 1.2. Glaciaciones cuaternarias de los Andes centrales de Chile y Argentina

La evolución glaciar de los Andes centrales durante el Cuaternario cuenta con un restringido número de estudios, lo cual ha impedido reconstruir las respuestas de la criósfera a los cambios del clima en el corto, mediano y plazo. Lo estudios holocénicos se han concentrado principalmente en los últimos 1.0 ka (1 ka=1000 años). Röthlisberger (1986), en un trabajo pionero, utilizó fechado radiocarbónico (14-C) en paleosuelos bajo material morrénico y estableció que el glaciar Cipreses (34° S) tuvo un avance hace 0.5±0.2 cal ka. El desarrollo de nuevas técnicas de datación por exposición superficial de minerales ha permitido fechar directamente morrenas en los Andes de Chile central, permitiendo establecer nuevas cronologías de fluctuaciones glaciales. Así, Sagredo et al. (2017), utilizando Nucleidos Cosmogénicos Terrestres (NCT; 10-Be), estableció que el glaciar Cipreses tuvo un avance entre los últimos 0.9 y 0.5 ka. Al norte de los Andes de Chile central, en el glaciar el Tapado (30° S), el uso de NCT (36-Cl) ha dado cuenta de avances glaciares ocurridos hace 1.0 y 0.5 ka (Sagredo et al., 2017). En los Andes de Argentina central también se han llevado a cabo estudios para determinar la historia reciente de los glaciares. En el valle del glaciar Las Damas (34° S) se obtuvieron edades mínimas desde paleosuelos bajo superficies morrénicas de avances glaciares ocurridos hace ~0.4±0.1 y <0.3 cal ka (Espizua & Pitte, 2009). En los valles de El Azufre (35° S) y El Peñón (35° S) se obtuvieron edades de avances glaciares en torno a 0.4±0.1 cal ka (Espizua, 2005) y <0.3 cal ka (Espizua & Pitte, 2009). Los datos disponibles sugieren que las últimas fluctuaciones glaciares en los Andes de Chile y Argentina central en el último milenio ocurrieron principalmente entre los siglos 14 y 19.

Uno de los trabajos pioneros en reconstruir las fluctuaciones glaciares del Pleistoceno fue el realizado por Santana (1967) en la cuenca del río Cachapoal (34° S). Su trabajo describe una posición de margen glaciar a los ~1200 m.s.n.m., lo que coincide con la actual confluencia de los ríos Cachapoal y Cipreses. Según Santana, la zona denominada como "El Manzanar" exhibe morrenas laterales en forma de terrazas a >15 m de altura respecto al lecho fluvial. Caviedes y Paskoff (1975) realizaron observaciones geomorfológicas y estratigráficas en la cordillera de la región de Valparaíso (33° S), sugiriendo la existencia de, al menos, cuatro avances glaciares durante el Cuaternario. Los autores proponen que el afloramiento rocoso con rasgos de abrasión glacial que se observa en el sector del Salto del Soldado (1300 m.s.n.m.) serían formaciones heredadas de la Pre-Penúltima Glaciación; las morrenas encontradas en Guardia Vieja (1600 m.s.n.m.) estarían vinculadas con la Penúltima Glaciación; mientras que las dos morrenas mapeadas en El Portillo (2900 y 2650 m.s.n.m.) corresponderían respectivamente a un avance ocurrido en la Última Glaciación y a un pulso post glacial.

En el lado argentino (33° S) se describieron cinco posiciones de morrenas cuaternarias (Espizua, 1993, 2004). El depósito morrénico más distal, denominado como Glaciación *Uspallata*, está a los 1850 m.s.n.m. y a 80 km de distancia del Monte Aconcagua. La Glaciación *Uspallata* fue fechada en 170±50 ka BP; un segundo deposito llamado *Punta de Vacas* lo marcaría una morrena lateral parcialmente cubierta por conos aluviales que se encontraría a los 2350 m.s.n.m. y a más de 39 km de distancia de la posición del hielo actual. La glaciación *Punta de Vacas* fue estimada en una edad mínima de 134±32 ka BP; una morrena terminal (3100 m.s.n.m.) con aspecto monticulado a 18 km del frente del glaciar Horcones Superior marcaría el tercer avance llamado como *Penitentes*. Hermanns et al. (2015) han reanalizado y fechado a través de $^{36}$Cl exposición superficial el depósito de *Penitentes*, y han concluido material de origen glacial se mezcló con derrumbes holocénicos de hace 11.2±2 ka. El cuarto depósito corresponde a *Horcones*, una

morrena terminal de aspecto monticulado ubicada a 15 km del hielo actual y a los 2750 m.s.n.m. Mientras que el quinto depósito morrénico denominado *Almacenes*, localizado a 8 km del hielo actual y los 3200 m.s.n.m, ha sido vinculado a un avance glaciar ocurrido entre 10 y 14 cal ka BP. Tanto el depósito de *Horcones* y *Almacenes* han sido posteriormente asociados derrumbes holocénicos ocurridos hace 10.4±1.1 ka (Hermanns et al., 2015).

El uso de NCT ha brindado nuevos datos asociados a las glaciaciones pleistocénicas de la región. En los Andes Chile central, Zech et al. (2017) recalculó las edades de exposición superficial ($^{10}$Be) obtenidas por Zech et al. (2007, 2006) en morrenas laterales y terminales del valle del Encierro (29° S) y en el Cordón de Doña Rosa (30° S) entre 3600 y 3800 m.s.n.m., respectivamente. Las edades recalculadas para el valle del Encierro fluctuaron entre 17.2±0.8 a 20.5±1.0 ka, mientras que las edades de exposición obtenidas en el Cordón de Doña Rosa variaron entre 18.1±0.7 a 21.8±0.8 ka. Recientemente, Aguilar et al. (2022) obtuvo nuevas edades de exposición desde el valle del Encierro y que variaron entre 17.4±0.7 y 18.8±0.7 ka. Charrier et al. (2019) obtuvo edades de exposición de 18.9 y 20.4 ka desde una morrena lateral a los ~1600 m.s.n.m. en la cuenca del Cachapoal (34° S). En el valle del Glaciar Cipreses (34° S), Sagredo et al., (2017) mapearon cuatro morrenas entre los 1730 a 1770 m.s.n.m. y desde ellas obtuvieron trece edades que fluctuaron entre 15.0±0.2 ka a 0.6 ka. En la vertiente oriental de los Andes centrales (33° S), Moreiras et al. (2017) mapeó y dató las morrenas Angostura (2900 m s.n.m) y Los Morteritos I (2500 m s.n.m) en 15.3±1.3 ka y 25.2±2.2 y, respectivamente. Avances glaciares más jóvenes fueron reportados a los ~3300 m s.n.m. en el cordón morrénico de la Plata en los Andes orientales (33° S), siendo fechados entre 11.9±1.0 y 15.3±1.3 ka (Moreiras et al., 2017).

A pesar de estos estudios, la magnitud, la cronología y las causas de las glaciaciones cuaternarias siguen siendo poco entendidas. Por esos motivos en este trabajó se buscó reconstruir la historia

de las fluctuaciones del Glaciar Universidad (34° S, 70° O) durante Holoceno y Pleistoceno tardío utilizando un mapeo geomorfológico en detalle y el fechado de geoformas de origen glacial a través de datación por exposición superficial ($^{10}$Be). Los datos presentados en esta tesis buscan establecer una geocronología robusta de las fluctuaciones glaciares cuaternarias de la región, que contribuya, a su vez, a entender los cambios en el sistema atmosférico subtropical y las respuestas de la criósfera andina en el corto, mediano y largo plazo.

## 1.3. **Preguntas de investigación**

**Capítulo 1**

¿Cuáles son los procesos geomorfológicos que ocurren durante periodos cálidos y secos en las cuencas englaciadas de Chile central? ¿Los glaciares retroceden abruptamente o se derriten gradualmente *in situ* bajo una cobertura de escombros?

**Capítulo 2**

- ¿Cuándo ocurrieron las principales fluctuaciones glaciares durante la última parte del Holoceno? ¿Qué condiciones paleoclimáticas generaron aquellos cambios?

**Capítulo 3**

- ¿Cuándo ocurrieron los principales avances glaciares del Pleistoceno tardío en Chile central? ¿Estos avances glaciares respondieron a forzamientos climáticos hemisféricos o globales?

## 1.4. **Hipótesis**

### 1.4.1. Hipótesis #1

Si las condiciones climáticas más secas y cálidas en los Andes de Chile central provocan un reajuste paraglacial, entendido como el periodo de transición desde un ambiente glacial a no glacial en el cual sedimentos condicionados glacialmente comienzan a ser retrabajados (Ballantyne, 1995, 2002), la alta transferencia de escombros desde el entorno de alta montaña hacia los márgenes del hielo debería provocar que la degradación de los frentes glaciales sea bajo una cobertura de escombros y, por lo tanto, la geomorfología resultante de aquel proceso correspondería a la fusión de hielo subsuperficial (Krüger and Aber, 1998; Krüger and Kjær, 2000; Schomacker, 2007; Krüger et al., 2010). Si la hipótesis es correcta, el área recientemente deglaciada del Glaciar Universidad debería tener registros geomorfológicos asociados a la degradación de morrenas con núcleo de hielo.

### 1.4.2. Hipótesis #2

Hay evidencia en los Andes de Chile central que sugiere la expansión de glaciares durante el Holoceno tardío (Röthlisberger, 1986;Sagredo et al., 2017) y Pleistoceno tardío (Zech et al., 2017; Charrier et al., 2019). Dichas expansiones estarían asociadas a la migración de los Vientos del Oeste hacia latitudes medias (Heusser, 1989; Denton et al., 1999; Jenny et al., 2002; Toggweiler et al., 2006; Sagredo et al., 2017). Si las condiciones climáticas del Cuaternario tardío fueron más húmedas y frías que el presente debido a la migración de a los Vientos del Oeste, los avances de glaciares en Chile central deben ser sincrónicos con la expansión de glaciares de latitudes más australes.

## 1.5. **Objetivos de investigación**

### 1.5.1. Objetivo General

Establecer un modelo geomorfológico y geocronológico de las fluctuaciones del Glaciar Universidad para el Holoceno y Pleistoceno tardío utilizando registros geológicos.

### 1.5.2. Objetivos específicos

a) Definir y caracterizar los procesos geomorfológicos que ha tenido el Glaciar Universidad a lo largo del Holoceno y Pleistoceno tardío.
b) Definir el estilo geomorfológico de deshielo que ha sido mediado por una cobertura de escombros supraglacial en el Glaciar Universidad
c) Determinar la geocronología de las variaciones del Glaciar Universidad durante el Holoceno y Pleistoceno tardío
d) Explorar mecanismos climáticos forzantes de la glaciación en Chile central desde una perspectiva regional, hemisférica e interhemisférica.

## 2. DE-ICING LANDSYSTEM MODEL FOR THE UNIVERSIDAD GLACIER (34° S) IN THE CENTRAL ANDES OF CHILE DURING THE PAST ~660 YEARS

Este segundo capítulo se presenta como artículo científico y por ese motivo está escrito en inglés. El artículo y su *corrigendum* están publicados en la revista Geomorphology: Fernández, H. García, J.-L., Nussbaumer, S.U., Geiger, A.J., Gärtner-Roer, I., Pérez, F., Tikhomirov, D., Christl, M., Egli, M., 2022a. De-icing landsystem model for the Universidad Glacier (34° S) in the Central Andes of Chile during the past ~660 years. Geomorphology 400. El acceso al artículo puede realizarse a través del siguiente enlace: doi.org/10.1016/j.geomorph.2021.108096; doi.org/10.1016/j.geomorph.2022.108426 [Corrigendum]. La numeración de figuras y tablas es correlativa a toda la tesis doctoral, por lo cual las figuras y tablas expuesta aquí no guardan exclusiva relación con este capítulo.

## 2.1. **Introduction**

Glacial landforms in high mountains are unique indicators of morphogenetic processes linked to distinct glacial dynamics and climatic fluctuations (Benn and Evans, 2014; Mackintosh et al., 2017). Despite the existence of well-preserved Holocene glacial landforms in the Andes of central Chile (29—35°S), only a few studies have aimed at understanding the geomorphological transition from glacial to non-glacial landscapes in response to climate warming (Bodin et al., 2010; García et al., 2014; Janke et al., 2015; Monnier and Kinnard, 2017; Iturrizaga and Charrier, 2021). Notable unresolved questions include:

- What are the geomorphic processes that occur during warm and dry periods in a glaciated basin of the Andes of central Chile?
- Do glacier fronts retreat abruptly or by progressive de-icing with standstills and/or re-advances phases during the overall deglaciation?
- Is it possible to define the latest Holocene deglaciation landsystem model for a prominent glacier system in the Andes of central Chile based on geomorphic records?

In this paper, we aim to build a conceptual model of deglaciation that better characterizes the response of glaciers to warm and dry periods in the Andes of central Chile. Our model is based on detailed geomorphic mapping of the latest Holocene glacier record constrained by $^{10}$Be exposure dating in the forefield of the Universidad Glacier (34° 42' S, 70° 20' W). This approach provides temporal context for the deglaciation of the 20$^{th}$ and 21$^{st}$ centuries and insights into the long-term deglacial process for this mountain area. Our study area in the hinterland of the most populated area in Chile represents one of the main sources of freshwater for human and agricultural uses (Bellisario et al., 2013; Ayala et al., 2016). Understanding the response of local glaciers to climate change is essential for sustainable water planning.

### 2.1.1. Conceptual models of de-icing

Geomorphological processes related to ice melting are enhanced in high mountains. In these areas, the deglacial process that follows a glacial expansion includes a long-term period of sediment and geomorphic adjustment (Ballantyne, 1995, 2002, 2008; Benn and Owen, 2002; Evans and Twigg, 2002; Curry et al., 2006) characterized by a high rate of debris mobilization and deposition at the lower margin of glaciers due to negative mass balance and ice stagnation (Eyles, 1979; Kjær and Krüger, 2001; Lukas et al., 2005, 2007; Schomacker, 2007; Evans, 2014). The debris generally comes from mass movement of ice-free adjacent valley slopes (Eyles and Rogerson, 1978; Eyles, 1979; Curry et al., 2006; Evans, 2009; Eichel et al., 2018) or avalanches (Owen, 1991; Shroder et al., 2000; Hambrey et al., 2008). Englacial debris accumulates on the glacier surface when the ice is thinning (Janke et al., 2015). In the transition between the active glacier and the stagnant snout, subglacial sediments can be thrust up to the supraglacial environment (Glasser and Hambrey, 2002; Swift et al., 2018).

Geomorphological models of deglaciation have been constructed for the Andes, Himalayas, and Europe to understand the current de-icing process. According to Janke et al. (2015), the present-day evolution of glacial landscapes in the Andes of central Chile could be better understood as a continuous transition from clean to debris-covered glaciers and, possibly, glaciogenic rock glaciers. Complementarily, García et al. (2014) suggested that a transitional state from clean glaciers to debris-covered glaciers may be ice-cored moraines: buried bodies of ice detached from the active or stagnant glacier up-valley (Kjær and Krüger, 2001; Lukas et al., 2007; Evans, 2014). In both cases, ice melt produces an upper layer of rock material that mostly insulates underlying ice (García et al., 2014; Janke et al., 2015). In the Himalayas, Shroder et al. (2000) suggested that the transition from debris-covered glaciers to rock glaciers depends on the

sediment transfer rate from ablation zones to glaciofluvial systems. An inefficient transfer would thicken the supraglacial layer, increasing the insulation of internal ice (Shroder et al., 2000; Jones et al., 2019). Other investigations in Central Asia found that the main causes of mass loss in debris-covered snouts are supraglacial melt-out ponds and ice cliffs (Sakai et al., 2000; King et al., 2020; Buri et al., 2021). In this manner, surface lowering is associated with the development and subsequent degradation of dead-ice zones (Benn and Owen, 2002).

In Europe, the degradation of ice-cored moraines has been well-established. Backwasting of the ice front and glacier downwasting become a significant cryogeomorphic process during warm periods (Kjær and Krüger, 2001; Krüger et al., 2010; Reid and Brock, 2014). The variable thickness of the glacier's debris cover results in differential downwasting rates in the ablation area, producing a hummocky topography (Patterson, 1998; Schomacker, 2008; Evans, 2009; Oliva and Ruiz-Fernández, 2015). Features associated with a karstic evolution on stagnant ice may be identifiable, such as funnel-shaped sinkholes (*sensu* Clayton, 1964; Kjær and Krüger, 2001; Schomacker and Kjær, 2008) and debris-filled stripes, which are produced from tension cracks (Eyles, 1979; Kjær and Krüger, 2001). Complete de-icing of the ice-cored moraines results in a dead-ice moraine with massive ice-free hummocky topography (Kjær and Krüger, 2001; Schomacker and Kjaer, 2007; Krüger et al., 2010).

Debris-covered glacier de-icing models contrast inactive ice at the terminus with active flowing ice up-valley in the same glacier tongue (Kjær and Krüger, 2001; García et al., 2014; Phillips et al., 2017).This results in a stationary ice front, unlike the retreating ice front typical of clean mountain glaciers during negative mass balance periods (Bennett et al., 2000; Krüger et al., 2010).

## 2.2. **Regional setting**

The highest peaks in the Andes of central Chile reach ~6000 m a.s.l (Figure 1a). The Andes' rugged topography is characteristic of active tectonic uplift, volcanism, and incised glacial basins (García et al., 2014; Charrier et al., 2019). Its altitude and physical setting promote different sizes and types of glaciers (Lliboutry, 1998), such as clean glaciers; clean glaciers with debris-covered snouts; debris-covered glaciers. Periglacial landforms such as rock glaciers also occur in the Andes of central Chile. Clean glaciers and debris-covered glaciers are more common to the south of 33° S, but rock glaciers dominate the North (Azócar and Brenning, 2010).

The entire glacier-covered area in the Andes of central Chile has been shrinking dramatically since at least the middle of the 20$^{th}$ century (Barcaza et al., 2017). Between 2000 and 2019, an accelerated loss of glacier mass has been observed (Hugonnet et al., 2021). Moreover, the present mega-drought is the longest dry period in the last millennium (Garreaud et al., 2020). Malmros et al. (2016) confirmed a total reduction of the exposed ice area in the Andes of central Chile and Argentina (32°- 33° S) from 134 to 94 km$^2$ between 1955 and 2014. The loss of glaciated area and projections for a warmer climate have turned attention to debris-covered glaciers and rock glaciers as important regional water resources (Azócar and Brenning, 2010; Bellisario et al., 2013; Janke et al., 2015; Fernández and Ferrando, 2018).

The Andes of central Chile are south of the Pacific side of the Arid Diagonal (Abraham et al., 2020). In this region, winter precipitation produced by the southern westerlies dominates (Garreaud, 2009). 80% of the annual precipitation occurs between May and August, mostly in the form of snow. According to regional climate data from the Embalse El Yeso station (33° 40' S, 70° 5' W, ~2400 m a.s.l.), the mean annual air temperature is 8.3 °C, and the mean annual precipitation adds up to 515 mm (Barcaza et al., 2017). The local climate defines the equilibrium

line altitude (ELA) of the glaciers at 4300- 4400 m a.s.l. in the North, declining gradually to 3700 - 3800 m a.s.l. at 34° S (Brenning, 2005; Azócar and Brenning, 2010).

The Universidad Glacier is surrounded by high elevated summits. The highest peaks on the west side of the catchment area include Cerro Alto Los Arrieros (4990 m a.s.l.), El Portillo (4957 m a.s.l.), and Cerro El Brujo (4458 m a.s.l.). To the east, the highest peaks include the volcano El Palomo (4860 m a.s.l.) and other peaks at ~3500 m a.s.l. El Palomo has no volcanic activity at present. The main mountain lithologies surrounding the Universidad Glacier are granodiorites, rhyolites and, andesites (Charrier and Lillo, 1973) (Figure 1b).

The mountain range that surrounds the Universidad Glacier also hosts three other glaciers, that, together, cover an area of ~50 $km^2$ (Dirección General de Aguas, 2014): Cipreses Glacier to the northwest, Cortaderal Glacier to the east, and the Palomo Glacier to the north (Figure 1b).The Universidad Glacier has the largest surface area in the Andes of central Chile with 28.1 $km^2$ (Wilson et al., 2016), and a notable length of ~10 km. The Universidad Glacier originates from the El Palomo volcano and merges down-valley with “Manke” glacier (Figure 1c). At present, the Universidad Glacier flows down-valley from 4540 to ~2500 m a.s.l (Le Quesne et al., 2009). Aerial photographs available since 1944 allow tracing the evolution of the ice front since then. In the 1944 Trimetrogon photographs, the ice front was 1.5 km further down-valley than at present (Figure 1d). Between 1944 and 1955, the ice margin retreated 1 km (HYCON flight, 1955). Since 1955, the ice front has retreated about 300 m.

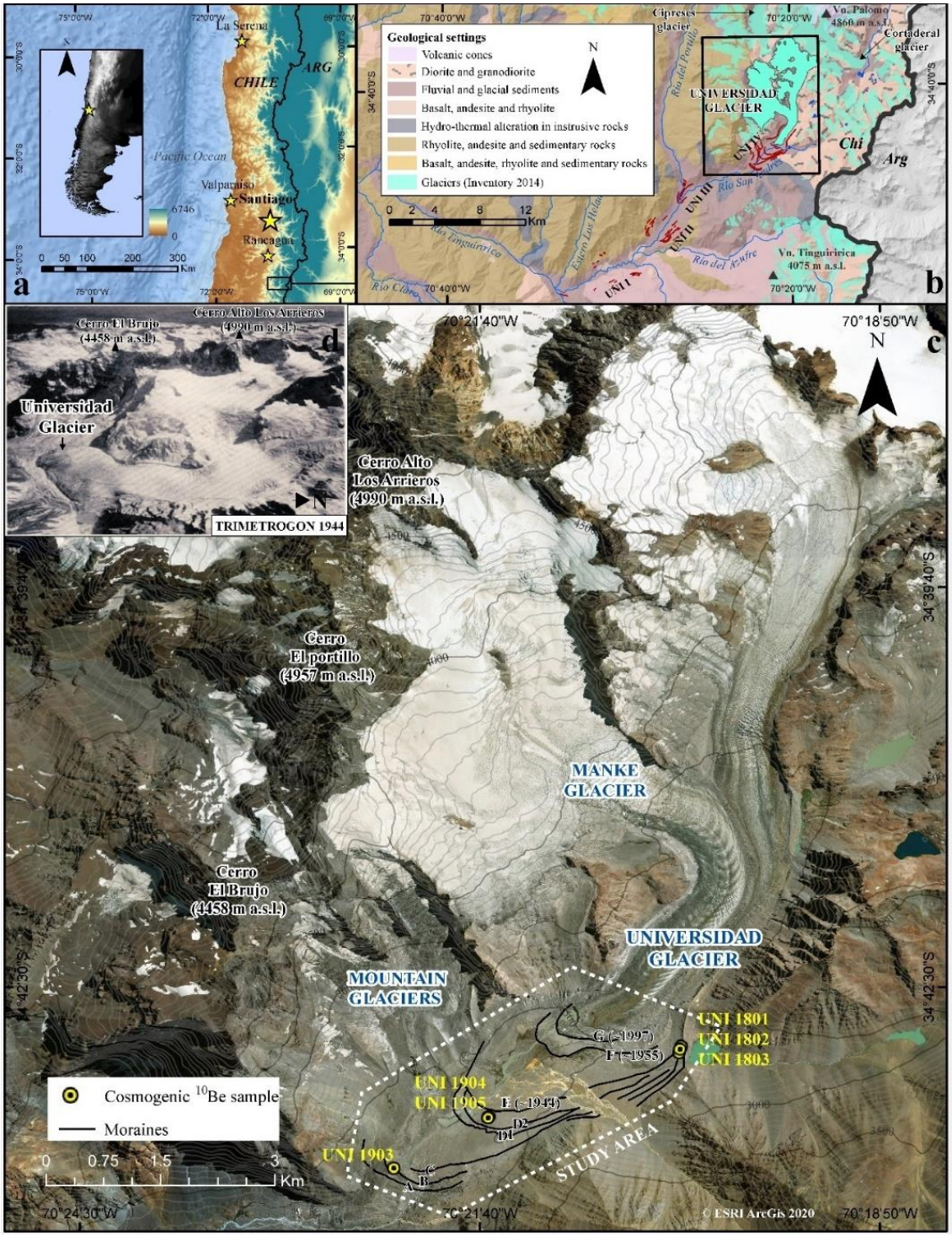


**Figure 1. location of the study area in the central Chile (30–35° S). (a)** Location of the study area in South America and the central Chile. Main cities near of the Universidad Glacier are marked with yellow stars; **(b)** The glacier inventory (Dirección General de Aguas, 2014) and the geological setting of the study area, with reconstructed Quaternary and holocenic moraines (red lines) mapped along the Universidad Glacier valley; **(c)** Universidad Glacier and the latest Holocene UNI IV moraine complex (white dotted line) and moraine ridges (black lines); **(d)** The oldest historical imagery of the Universidad Glacier from 1944 with view to the west.

## 2.3. **Materials and methods**

### 2.3.1. Geomorphological mapping

Our geomorphological mapping is based on interpretation of satellite images, field visits, and stereoscopic interpretation of aerial photographs. We analyzed aerial photos from 1997 (1:50,000, produced by GEOTEC flight, Servicio Aerofotogramétrico (SAF), Chile) and 1955 (1:70,000, produced by HYCON flight, SAF Chile). We acquired recent terrain imageries from GeoEye (2015), DigitalGlobe (2018), and ESRI ArcGIS (2020). We composited a Digital Elevation Model (DEM) with 12.5 m resolution from the ALOS-PALSAR data (https://vertex.daac.asf.alaska.edu/). In addition, were retrieved geological data from the national and regional geological databases to compile a map (1:500,000) (Charrier and Lillo, 1973; SERNAGEOMIN, 2004) (Figure 1b).

Once we identified main glacial features through geomorphological mapping on remotely sensed data, we carried out three fieldwork campaigns (in January and April of 2019 and in January of 2020, for a total of 30 days) to check and improve the remotely mapped glacial geomorphology. The terminal glacier zone, the upper ablation zone, and the glacier forefield were explored extensively. We used a handheld GPS device with ± 3 m horizontal accuracy to document sample and landform's locations. We used ESRI ArcGIS 10.3 to produce our geomorphic maps, applying the glacial geomorphology symbology of Barsch and Liedtke (1980) and Kneisel (1988).

### 2.3.2. Geochronology

To establish a general geochronological time frame, we collected rock samples (>1.5 kg) from the top (upper < 2 cm) of six granodiorite boulders (Table 1) resting on moraine ridges and flute fields for *in situ* terrestrial cosmogenic nuclide dating (TCND, $^{10}$Be), following standard procedures (Gosse and Phillips, 2001). The sampling focused on boulder ranging in size between 90 and 240 cm above the surrounding surface with minimal surface weathering, fractures, or evidence of gravitational movement or post-deposition exhumation. Each boulder had glacial erosional features such as striations. We collected rock samples with hammer and chisel, blasts, and handheld circular saw. Clean quartz was extracted at the Pontificia Universidad Católica de Chile - Cosmogenic Isotope Laboratory, while Beryllium was isolated at the Surface Exposure Lab at the University of Zurich, following a procedure adapted from Kohl and Nishiizumi (1992). All $^{10}$Be/$^{9}$Be ratios were measured at the ETH Zurich Tandy AMS system (Christl et al., 2013) and normalized to the ETH in-house AMS standards S2007N and S2010N ($^{10}$Be/$^{9}$Be = $28.1\cdot10^{-12}$ and $3.3\cdot10^{-12}$, respectively), which were calibrated to the ICN 01-5-1 standard (Nishiizumi et al., 2007). All AMS standards are associated with a $^{10}$Be half-life of 1.387±0.012 Myr (Chmeleff et al., 2010; Korschinek et al., 2010). $^{10}$Be/$^{9}$Be sample ratios were corrected with the weighted average of the two chemistry blanks (Table 1). We calculated $^{10}$Be exposure ages with the CRONUS-Earth online calculator (http://hess.ess.washington.edu/math/) version 3 (Balco et al., 2008). We used the local calibration dataset developed by Kaplan et al. (2011) to obtain the $^{10}$Be production rate for southern South America. The calibration data was obtained from the online ICE-D platform (http://calibration.ice-d.org/). We excluded both erosion and shielding by snow and/or sediment from the exposure age calculations due to the boulders' visible striations, indicating low surface weathering rates from the time of deposition. The height of the sampled boulders above the surrounding topography makes snow/sediment shielding less likely. It is also

very difficult to determine snow cover density and duration; therefore, our exposure ages should be regarded as minimum ages. All exposure ages reported here are in the $^{10}$Be time-dependent scaling scheme (Lm) after Lal (1991) and Stone (2000) (Table 1). Outputs from other scaling schemes do not change our final interpretations of exposure ages presented here.

## 2.4. **Results**

### 2.4.1. Geomorphology of the glacier forefield

The Universidad Glacier valley has four distinct moraines within a distance of 20 km, located between ~1100–2500 m a.s.l. We labeled them from outer to inner as UNI I to UNI IV (Figure 1b). UNI IV, the latest Holocene moraine complex, extends ~3 km down-valley from the ice front (Figure 2), covering the present-day forefield. The UNI IV moraine complex includes different types of glacial landforms and structures punctuated by eight moraine ridges.

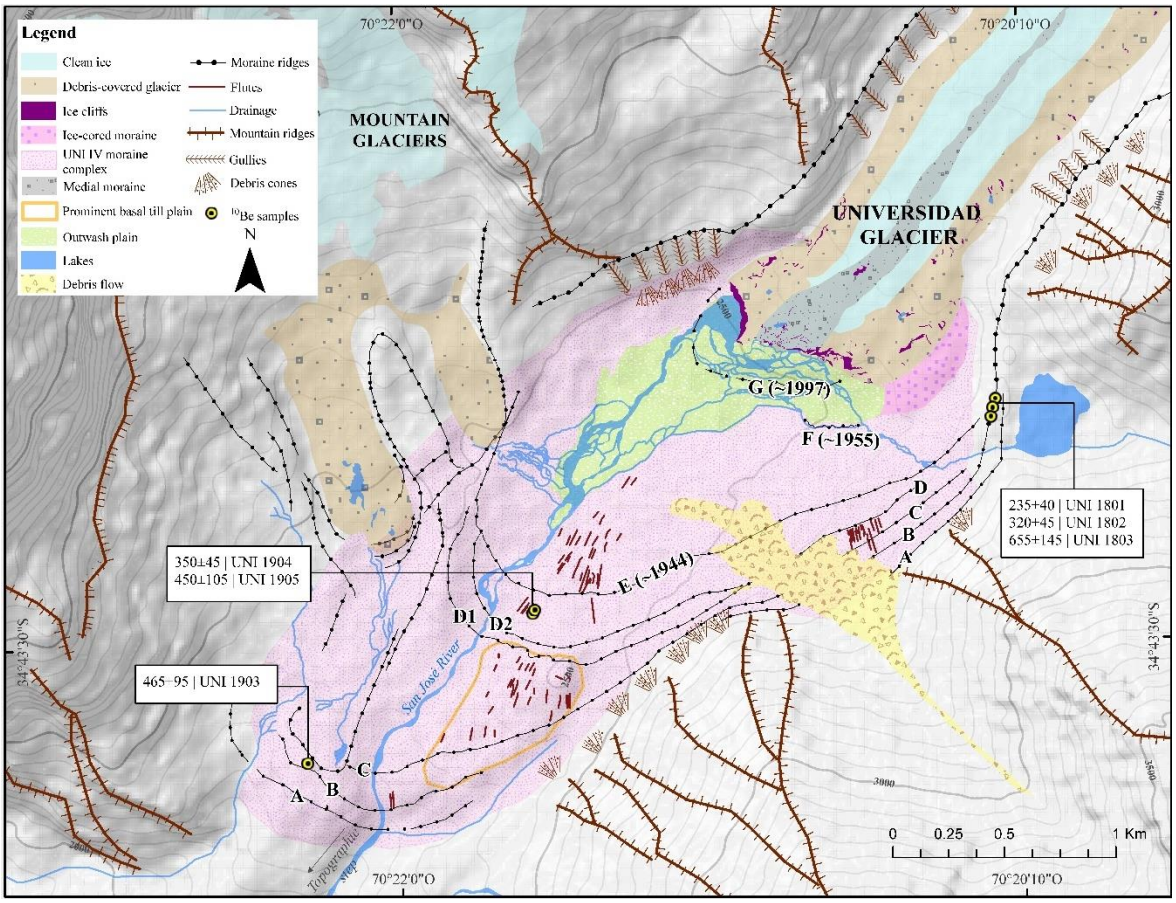


**Figure 2. Glacial geomorphology and geochronology of the Universidad Glacier forefield**. Dotted lines represent the moraine ridges, labeled A–G. On moraine B and between moraines D–E, rock samples were obtained to measure the $^{10}$Be exposure surface dates that offer a temporal frame of the landscape evolution. Moraines A–C represent the outer ice extent of UNI IV moraine complex; $D_1$–E represent the extensive ice, until, at least, the first half of the 20$^{th}$ century; F–G denote much less prominent glacier over the middle and the end of the 20$^{th}$ century. The current glacier front is almost completely covered with debris.

#### 2.4.1.1. Moraine ridges

Eight moraine ridges (A-G from distal to proximal) occur in UNI IV between the current glacier margin and a ~45° steep and ~400 m high topographic step 3 km down-glacier. The outermost frontal moraine A was deposited over gently sloping terrain, where rounded and sub-rounded boulders, some well-faceted and -striated, occur (Figure 3). This diamictic terrain seems to be older than the moraine ridge A.

In some cases, the moraine ridges can be tracked all along the eastern lateral and frontal margins (Figure 2). The moraines in the southwest part of the valley have been crosscut and/or overridden by advances of the mountain glaciers from Cerro El Brujo and their preservation is less clear (Figure 2). The eastern lateral moraines A-D, near the glacier front, exhibit a stepped sequence (Figure 4a). The proximal slopes of these moraines vary between ~15° and ~40°, with the higher angles in the outer moraines A and B. These outer moraines comprise mainly angular and sub-angular, but also sub-rounded boulders. Moraines C and D are formed by matrix-supported diamicts. Some distal sections of the external lateral moraines have been partly covered by colluvial sediment (Figure 4a). Erosive debris flows have interrupted the continuity of the eastern lateral sections of moraines A-D (Figure 2).

The frontal sections of moraines A-D remain well-preserved and are relatively similar in height (~5 m). Their lithologic composition is mostly granodiorite, with a proximal slope angle of 20 to 30° and sub-angular to angular boulder roundness. The frontal margins of moraines A-B are 90—100 m apart from each other. Both ice-marginal positions are separated by a conspicuous deposit of angular basaltic boulders (Figure 3b). Moraine C is located 130 m up-valley from moraine B, which was crosscut by a mountain glacier expansion from Cerro El Brujo (Figure 2). Between moraines B and C, scattered boulders, and patches of sand of varying shapes and sizes make up

an irregular terrain. The largest sandy patch has a basaltic and quartz lithology and is in the central part of the valley in front of moraine C, with a length of ~50 m and a width of ~30 m. The proximal terrain of moraine C reveals a paved surface with flutes (Figure 2) (see section 2.3.1.3).

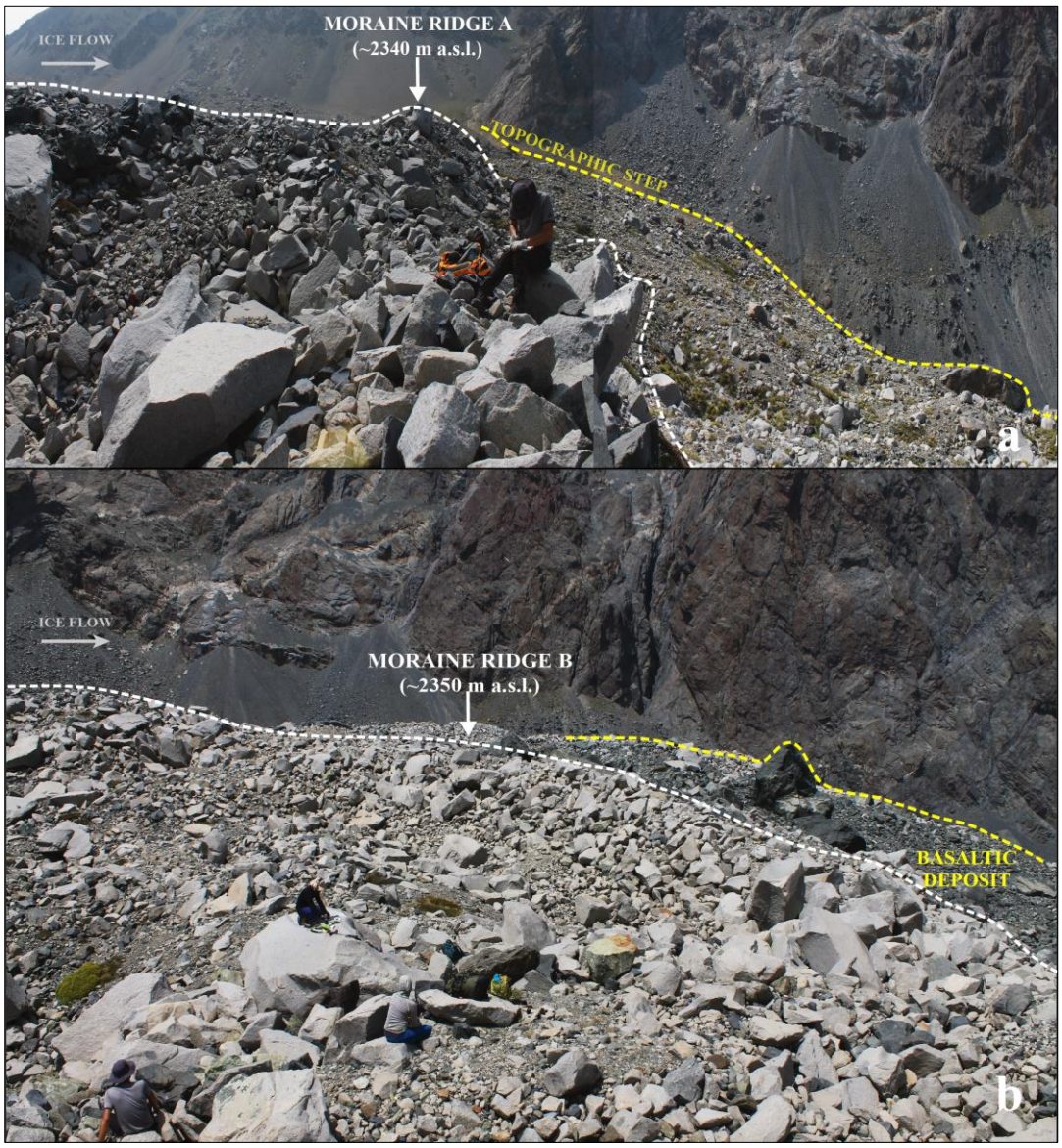


**Figure 3. Frontal ridges of moraines A and B. (a)** The frontal ridge of moraine A is composed mainly of angular boulders. The moraine grades towards a topographic step with striking widespread well-polished boulders that contrast with moraines A-B; **(b)** Intermorainal bouldery hummocky topography of moraines A and B, which includes a basaltic (volcanic) deposit. Ridge of moraine B is also pointed out.

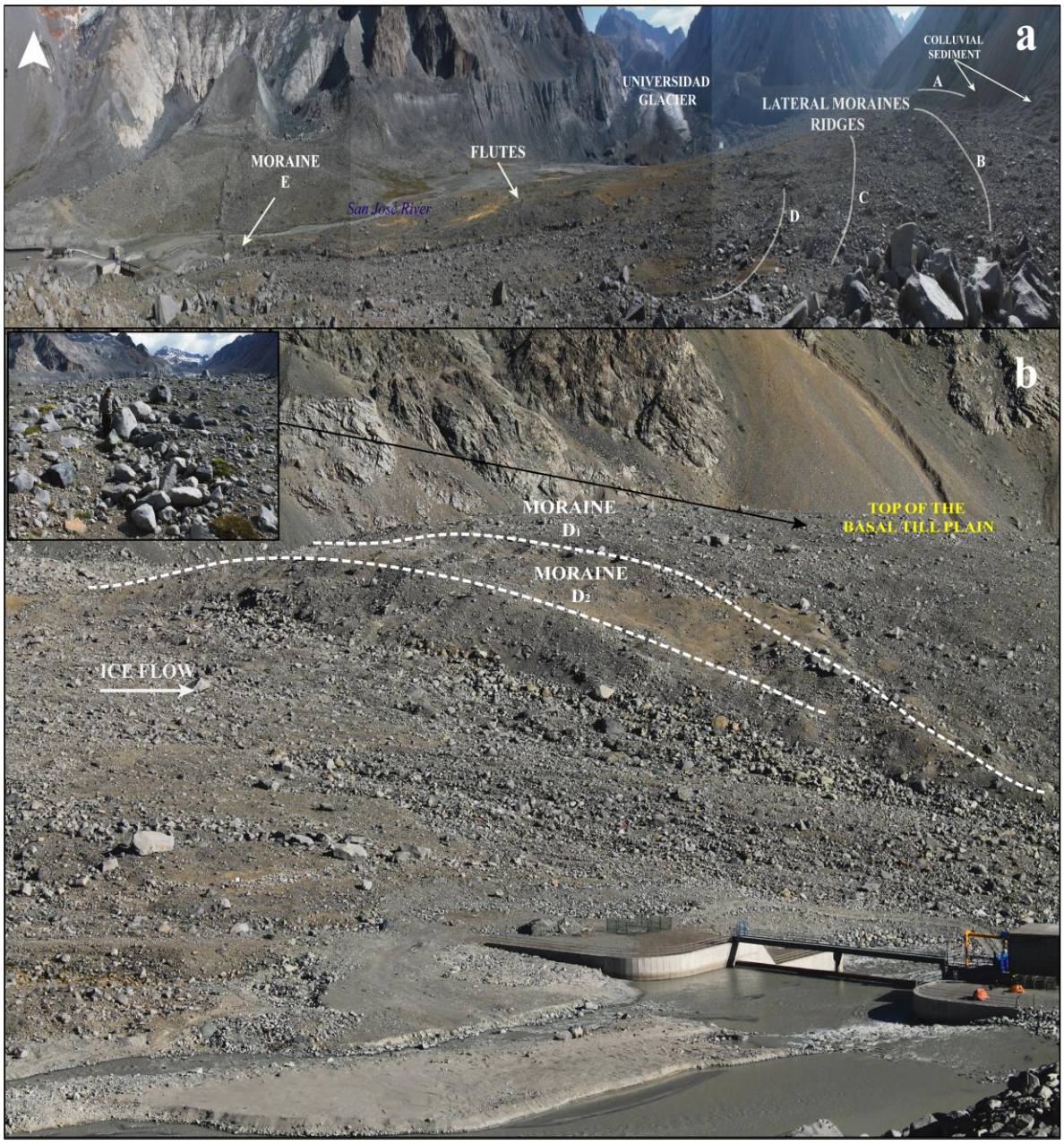


**Figure 4. Overview of the forefield and moraines $D_1$ and $D_2$. (a)** Forefield from the top of basal till plain (oval-shaped landform) with the current glacier in the back. The view is towards the North. Eastern lateral ridges of moraines A-D are arranged in a stepped sequence, representing the outer ice-marginal position. Moraine E, which coincides approximately with the 1944 ice position in Trimetrogon aerial photograph, is a perfectly defined morainic arc. The upper left white arrow indicates the North; **(b)** Frontal moraine D is divided into two ridges ($D_1$ and $D_2$) deposited on the proximal side of the prominent basal till plain on the UNI IV moraine complex. The upper left shows an alignment of debris in the ground on the prominent landform. At the bottom right are two orange tents in the hydropower station infrastructure for scale. The view is to the east.

The frontal section of moraine D is 1.5 km down-valley from the ice margin on the proximal side of a prominent oval-shaped landform (Figure 2). The crest splits into two sinuous ridges, $D_1$ and $D_2$, 10-20 m apart from each other (Figure 4b). The intermorainal depression between moraines $D_1$ and $D_2$ is mainly sand, silt, and abandoned meltwater channels. Both moraine ridges are topped with polished and faceted boulders covered partly by a thin and patchy debris veneer. This debris cover is mainly sub-angular and sub-rounded cobbles. Between moraines $D_2$ and E, there is a set of well-preserved flutes (Figure 2).

Moraine E is found 1.3 km from the ice front. The well-preserved morainic arc is uninterrupted over 2.5 km. It is composed mainly of sub-angular to sub-rounded boulders and cobbles, supporting faceted and striated embedded boulders. Moraine E coincides with the glacier position captured by the 1944 Trimetrogon aerial photograph (Figure 1d). The inboard part of moraine E hosts flutes of different lengths and sizes. Moraine F is a remarkable moraine located ~440 m from the glacier front (Figure 5). It has a height of 7 m and is composed of distinct rounded granodiorite pebbles and boulders. On its top, some of these boulders are striated and faceted. It has a serpentine shape-oriented east-west over 300 m. According to HYCON aerial photography, its position seems to indicate the 1955 latero-frontal ice margin. Lastly, moraine G occurs in patches of no more than 5 m in height on the active outwash plain and spreads out in a sinuous shape. This moraine is 300 m distal to the present glacier front (Figure 5). Moraine G coincides with the 1997 ice front position captured by GEOTEC aerial photography.

In summary, the outer moraines (A, B, and C) are more prominent and well-preserved in their frontal and left lateral margins. They represent the outer ice extents of the UNI IV moraine complex. Moraines $D_1$-E denote the presence of extensive ice until at least the middle of the 20$^{th}$ century. Moraines F and G indicate a much less prominent glacier over the middle and end of the

20th century. Moraines A-G are distinct evidence of significant former marginal positions, except for moraine G, which is primarily mounds being eroded by meltwater streams in the outwash plain (Figure 5).

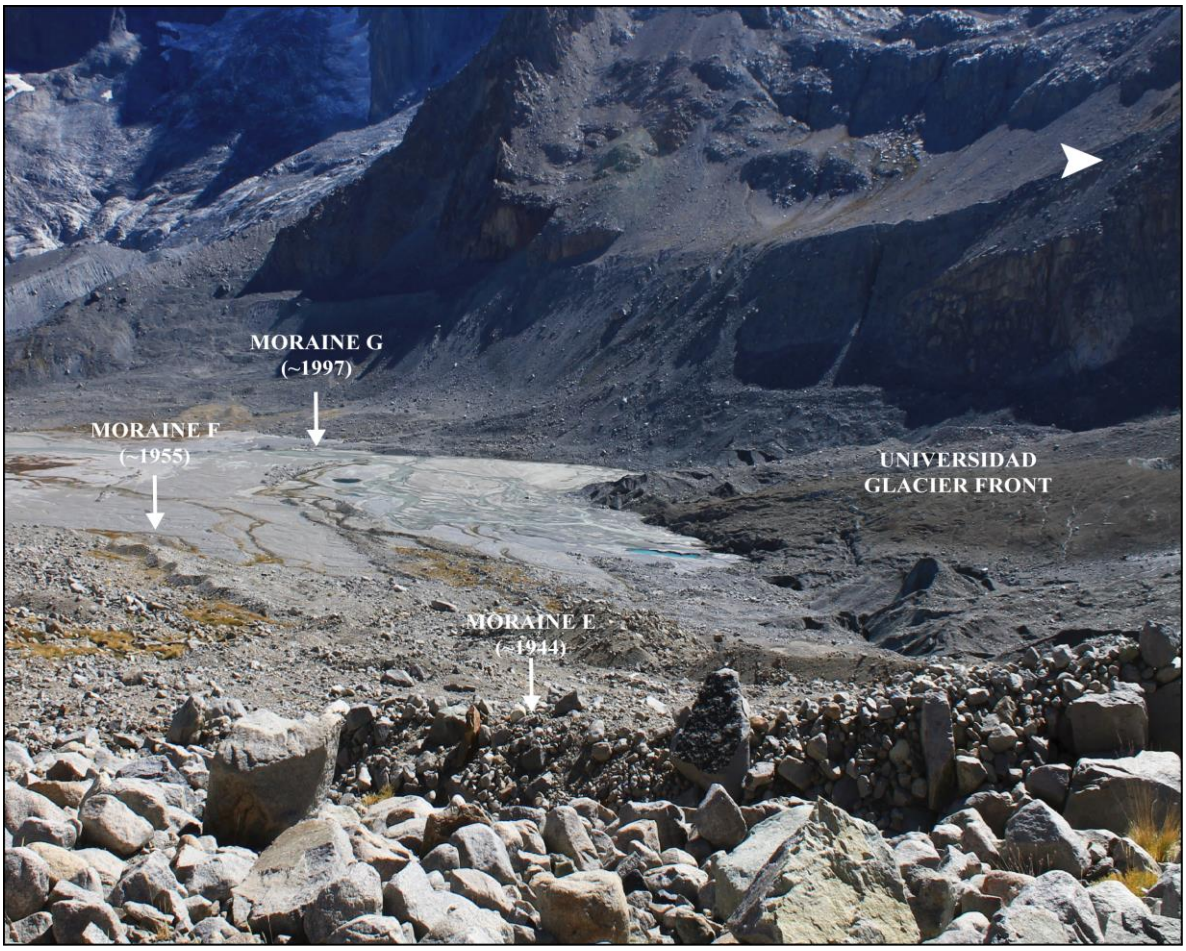


**Figure 5. Universidad Glacier front.** The ice front is totally debris-covered and shows a gentle slope punctuated by ice cliffs and meltwater channels. In the foreground the ridge of moraine E (~1944). In the background, moraine F with a serpentine shape (~1955), and the moraine patches left from the ~1997 moraine (G). The upper right white arrow indicates the North.

#### 2.4.1.2. Hummocky terrain

Moraines A-G are distributed over a massive hummocky terrain that covers most of the forefield, except for the active outwash plain (Figure 2). The hummocky terrain is an irregular complex where the following coexist: i) an irregular bouldery topography; ii) rounded basins with an accumulation of debris at their bottom; iii) debris-filled stripes in the ground; iv) a prominent oval-shaped landform; and v) glacial lineations.

Large angular boulders (>3 m) are piled up between moraines A and C (Figure 6a), while smaller sub-angular debris occurs inboard from moraine C (Figure 6c-e). This produces an overall granulometric gradient along the hummocky terrain. Throughout the hummocky terrain, inactive sinkholes (Schomacker, 2007; Krüger et al., 2010) filled with debris at their bottoms have been identified. The largest sinkholes are in the outer area, with depths of >3 m and widths of >5 m (Figure 6a). Here, recurrent sinkholes, one next to the other and separated by high ground, produce chaotic hummocky relief. In contrast, smaller sinkholes occur inboard to moraine C. The smaller sinkholes are 4-5 m wide and 2 m deep and also have debris accumulation at their bottoms (Figure 6c).

Debris-filled stripes in the ground (Figure 6b) cover most of the hummocky terrain complex, except for the distal area between the moraines A and C, where large piled boulders occur. These sorted debris stripes range from 1to 5 m in length and their depth below the ground varies from a few centimeters to at least 1 m. These debris-filled stripes do not have a prevailing orientation. They spread randomly on the ground and tend to occur on both low and high terrain.

**Figure 6. Geomorphological attributes of hummocky terrain. (a)** Sinkholes in the frontal, distal margin of the UNI IV complex between moraines A-B; **(b)** Sorted debris stripes in the ground and **(c)** sinkholes on the flank of basal till plain; **(d)** Eastern margin of the Universidad Glacier ablation zone; note the wet scars and overall irregular debris-covered ice topography; **(e)** Panoramic view of the forefield near the main active outwash plain. Also, the picture shows, in the background, the main lateral section of moraine B. White arrows point out the North.

A prominent oval-shaped landform stands out ~30 m from the surrounding hummocky terrain. It is ~500 m long, ~450 m wide, and located ~1.5 km from the current glacier front. It is flanked by the two main streams of the valley (Figure 2). Distally, this landform merges with the surrounding topography. On its surface, sub-angular, sub-rounded, and rounded cobbles and boulders occur. Some of these are large boulders embedded in the surface (> 2 m in height), which in turn are faceted and striated. Debris-filled stripes in the ground appear towards the flanks of this prominent landform. These alignments of debris can reach up to 3 m in length (Figure 4) and 1-4 m in width. Debris-filled sinkholes also occur (Figure 6c). Additionally, throughout the landform surface, glacial lineations coincident with the ice flow direction are observed in the satellite images (Figure 2).

#### 2.4.1.3. Flutes

Flutes are ubiquitous in the middle section of the UNI IV moraine complex, where they are superimposed onto the hummocky terrain dominating the forefield. Some of these flutes are distinct and preserved as elongated ridges composed of matrix-supported sub-rounded and rounded granodioritic pebbles (Figure 7a). The flutes are ~1 m in height, decreasing gradually to their distal margin, and their lengths vary from 10 to more than 80 m. Generally, the flutes develop on the lee-side of well-polished and striated boulders (Figure 7b, d). Less well-formed flutes, with discrete conic sediment accumulation on the lee sides of the big boulders, appear covered by a patchy debris veneer on their surface (Figure 7c, e). This debris veneer resembles poorly consolidated melt-out sediment composed of angular to rounded material.

Flutes occur in swaths between moraines B and F (Figure 2). Flutes between moraines C and $D_1$ are spatially distributed in two distinct groups. Group one includes at least twelve flutes near the eastern margin of the forefield. They are no more than 10 m apart and show a 135° azimuth. The second group of flutes occurs over the prominent oval-shaped landform. There are more than thirty flutes spaced 10-30 m apart with a 210° azimuth. While it was not possible to distinguish this last set of flutes during fieldwork, they were identified using satellite imagery, which recorded smooth and narrow flutes of up to 80 m in length (Figure 7f). Another set of flutes occurs between moraines E and F. This set of flutes consists of about thirty units spaced 3-20 m apart. These flutes also have a 210° azimuth and, due to their exceptional preservation, can be identified easily in the field (Figure 7a, b).

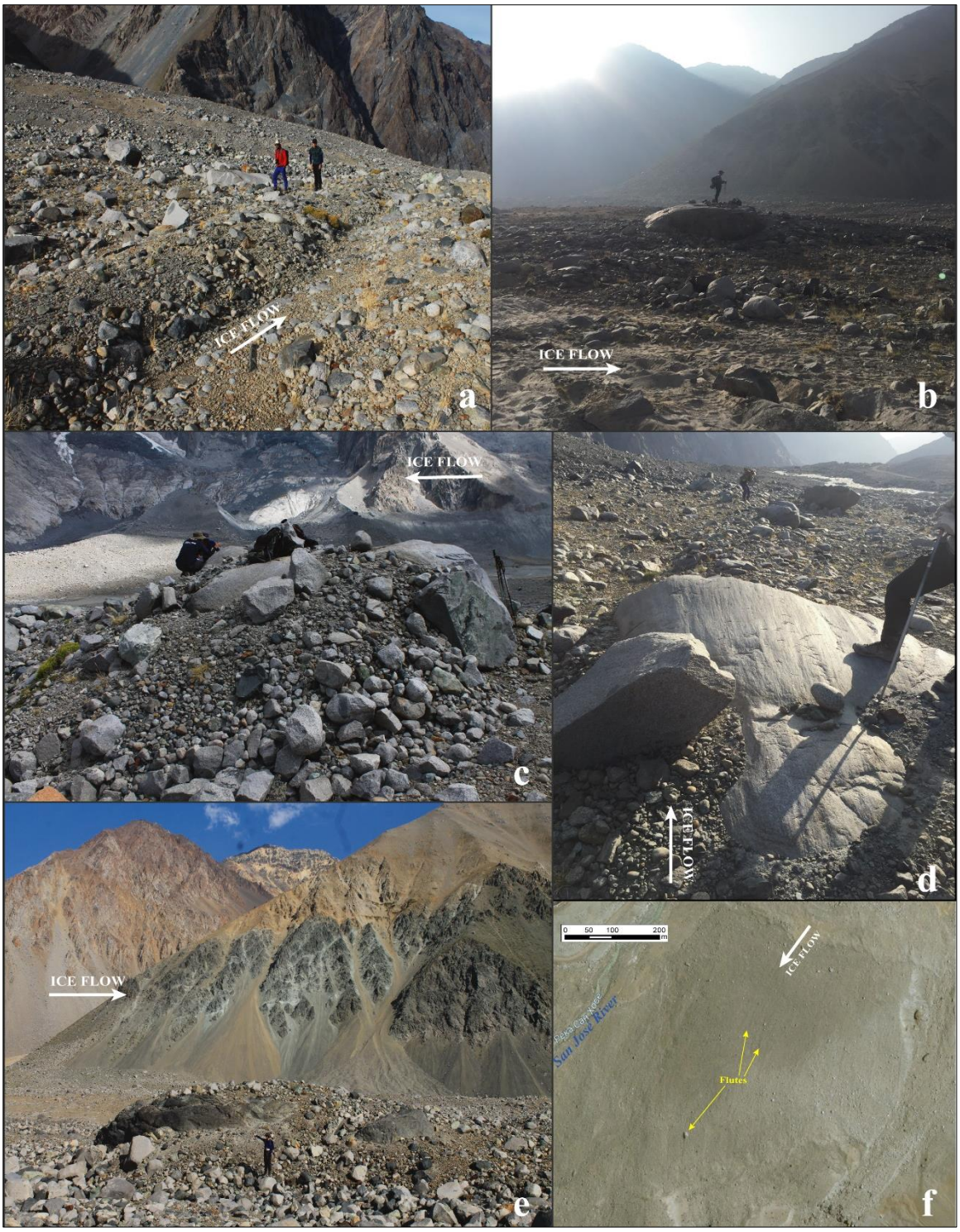


**Figure 7. Different types of glacial flutes on the hummocky terrain. (a)** Flute composed of sub-rounded and rounded granodioritic matrix-supported debris between moraines $D_2$ and E. The view is to the south; **(b)** Profile view of a flute developed on the lee-side of a roche moutonnée boulder; **(c, e)** Large boulders covered with a patchy debris veneer on the surface and with an unconsolidated sedimentary tail; **(d)** Down-glacier view of a flute. The person in the foreground is standing on the flute; **(f)** Aerial view of the flutes overriding the large basal till plain (oval-shaped landform).

#### 2.4.1.4. The debris-covered glacier snout

The Universidad Glacier ablation zone extends from ~3700 to ~2500 m a.s.l. (Bravo et al., 2017). The lower area of the glacier is characterized by extensive debris cover at the margins (Figure 2). This is particularly evident towards the eastern side of the glacier as it approaches the lateral moraines, where debris cover seems thicker. The poorly consolidated debris cover ranges from 0.1-2 m in thickness. A recognizable medial moraine, formed by merging the Manke and Universidad glaciers, emerges over the surrounding ice (Figure 8a). Transversal sediment ridges appear on the glacier surface (Figure 8b). These ridges reach ~3 m in height and are composed of fines and granodiorite rounded and sub-rounded pebbles. Ice cliffs punctuate the whole ablation area near the ice front, as high as 7 m with slopes over 40° (Figure 8c). Stacked granodiorite cobbles are commonly found with boulders, forming gravity cones at the bases of ice cliffs. The accumulated debris includes rounded or sub-rounded shapes with an absence of fine material on the surface, which likely has been washed out. The continuous stacking of debris at the bases of ice cliffs promotes the formation of talus that commonly reaches the tops of the cliffs, covering them totally.

The area close to the eastern lateral moraine exhibits a hummocky topography without visible ice on the surface (Figure 8d). Here, it is possible to recognize debris-filled stripes and sinkholes. Fractures on the slope of the hummocks range from a few cm to ~6 m in length and are not more than 1.5 m wide. Large debris usually falls into the fractures, which are subsequently arranged in linear patterns, embedded in the ground. This process gives, in some cases, a debris-striped ground appearance.

Active supraglacial sinkholes, formed in response to underlying ice melting, occur in the debris-covered glacier snout. They usually have mud and/or water at their bottoms, indicating that the

ice is melting *in-situ*. Overall, these sinkholes reach a width of 3 m and a depth of 3 m into the glacier, and they resemble those described in the hummocky terrain. A common process observed is the sliding of debris (pebble to boulder size) along the slopes of hummocks towards the bottoms of sinkholes. This debris movement produces wet scars on the slopes of the hummocks (Figure 6d).

Small melt-out ponds are scattered over the debris-covered ablation zone. They never exceed a diameter of 5 m or a depth of 1.5 m (Figure 8e). Sandy patches are also common in the ablation zone, probably as a result of the desiccation of these ponds. Turbulent supraglacial meltwater streams occur in the clean ice and reach the subglacial zone and the forefield at some point.

In brief, the geomorphology of the ablation zone is characterized by an extensive debris cover producing a mostly irregular topography near the ice front and towards the lateral moraines A-D (Figure 2). Most of these topographic features have been forming during that last 40 years, as observed in the available remote-sensing imagery. Ice cliffs are frequent and disrupt the local topography. Here, mass wasting, such as the sliding of debris along the slopes of the terrain, occurs. Towards the glacier flanks, no ice is exposed. Debris-filled stripes, debris-filled sinkholes, and dry or water-filled melt-out ponds are present throughout the ice-covered surface.

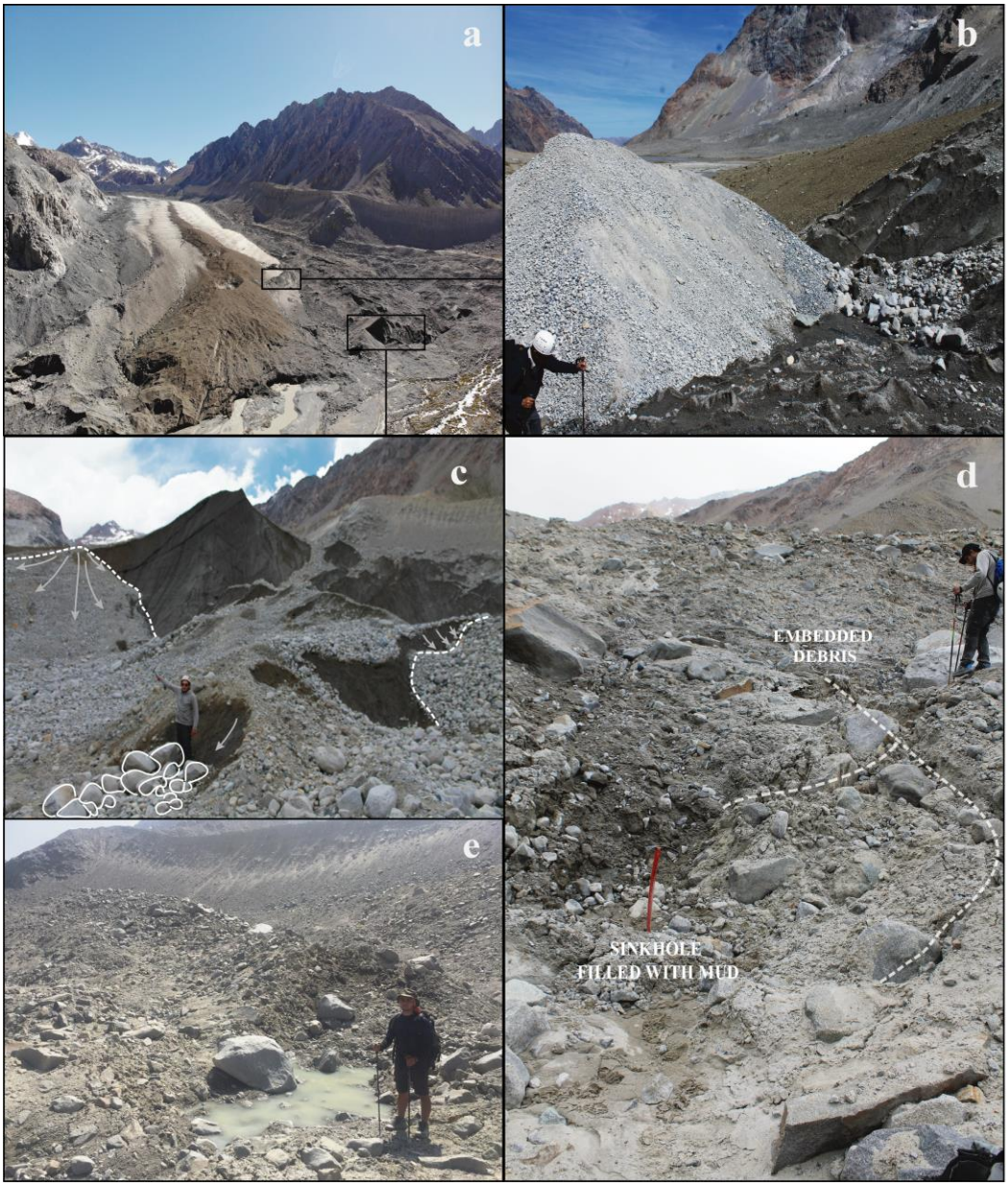


**Figure 8. The debris-covered glacier snout. (a)** Up-glacier view of the ablation zone. The boxes indicate the location of images (b) and (c); **(b)** Crevasse-squeeze ridges on the glacier front; **(c)** Ice cliff and movement of sediment due to backwasting; **(d)** Tension cracks and sinkhole formation where ice is debris-covered; **(e)** Melt-out pond over the glacier debris-covered flank.

### 2.4.2. Geochronology

Four $^{10}$Be-dated erratic boulder samples were obtained from the top of moraine B. Three of them were sampled from the eastern lateral margin (UNI 1801, UNI1802, and UNI1803) and one from the frontal ridge (UNI1903) (Figure 2). Complementarily, two boulders were sampled from the flute field between moraines $D_2$ and E (UNI1904 and UNI1905). The three boulders sampled from the lateral margin of moraine B yielded exposure ages of 235±40, 320±45, and 655±145 years, respectively. The other boulder sampled from the frontal ridge of moraine B yielded an exposure age of 465±95 years. The two samples retrieved from boulders on the flute field between moraines $D_2$ and E yielded exposure ages of 350±45 and 450±105 years (Table 1, Figure 2), respectively.

## 2.5. **Discussion**

In this section, we discuss the morphogenesis and general geochronologic context of landforms studied in the forefield of the Universidad Glacier (i.e., the UNI IV moraine complex). We interpret the geomorphic record to reveal the type of deglaciation that occurred during the latest Holocene period and to provide the context for the interpretation of the present de-icing trend. In order to put our results in a more global context, we analyze our geomorphological interpretations in comparison to work carried out in other regions experiencing glacier recession.

### 2.5.1. Timing of morphogenesis

Taken at face value, the $^{10}$Be exposure dating suggests an overall deglacial trend during the last 655±145 years, interrupted by multiple ice stabilization or re-advance phases. The outer ridges of moraines A-C correspond to the maximum latest Holocene glacier extent. The ice flow that built up moraines $D_1$, $D_2$, and E in the middle of the forefield represents an intermediate glacier extension until the first half of the 20$^{th}$ century. The final ice snout stabilization or re-advance is observed with moraines F and G, which indicate the latest standstill/re-advance of the ice front during the second half and end of the 20$^{th}$ century. Since then, the glacier has only declined.

**Table 1.** Geographical data, analytical data, and exposure ages of 10Be samples of the UNI IV moraine of Universidad glacier

| Sample name | Latitude (DD) | Longitude (DD) | Elevation (m a.s.l.) | Type of sample | Sample height (cm) | Shielding factor | Sample thickness (cm) | Quartz dissolved (g) | $^{9}$Be carrier (mg) | $^{10}$Be/$^{9}$Be ($10^{-12}$) | Error $^{10}$Be/$^{9}$Be ($10^{-12}$) | $^{10}$Be conc. ($10^{4}$) (at/g) | Error $^{10}$Be conc. ($10^{4}$) (at/g) | Age (year) |
|---|---|---|---|---|---|---|---|---|---|---|---|---|---|---|
| **UNI 1801** | -34.715968 | -70.337477 | 2625 | Boulder embedded on lateral moraine B | 124 | 0.977 | 2.6 | 54.34 | 0.2004 | 0.016 | 0.003 | 0.385 | 0.067 | **235±40** |
| **UNI 1802** | -34.715601 | -70.337388 | 2625 | Boulder embedded on lateral moraine B | 118 | 0.977 | 1.9 | 60.67 | 0.1997 | 0.024 | 0.003 | 0.524 | 0.077 | **320±45** |
| **UNI 1803** | -34.715239 | -70.337252 | 2626 | Boulder on lateral moraine B | 90 | 0.976 | 1.8 | 49.60 | 0.1950 | 0.043 | 0.010 | 1.141 | 0.250 | **655±145** |
| **UNI 1904** | -34.723556 | -70.359944 | 2436 | Embedded Boulder on flutes field between moraines D[2] and E | 103 | 0.970 | 1.6 | 55.29 | 0.2005 | 0.021 | 0.003 | 0.514 | 0.067 | **350±45** |
| **UNI 1905** | -34.723694 | -70.360056 | 2430 | Superimposed boulder on flutes field between moraines D[2] and E | 103 | 0.973 | 1.7 | 50.21 | 0.1989 | 0.025 | 0.006 | 0.667 | 0.152 | **450±105** |
| **UNI 1903** | -34.729639 | -70.371167 | 2355 | Boulder on frontal moraine B | 240 | 0.959 | 1.3 | 30.56 | 0.2006 | 0.015 | 0.003 | 0.648 | 0.134 | **465±95** |
| **UNI BI 11** | | | | Chemistry blank | | | | | 0.1997 | 0.010* | 0.001* | | | |
| **UNI BI 12** | | | | Chemistry blank | | | | | 0.1982 | 0.008* | 0.001* | | | |

Note: $^{10}$Be ages in years are calculated using CRONUS-Earth calculator (http://hess.ess.washington.edu/math/) version 3. We use "Lm" ages which is the time-dependent version of Lal/Stone scaling scheme (Lal, 1991; Stone, 2000). All ages are calculated with the production of the local scaled $^{10}$Be production rate for the Southern hemisphere (Kaplan et al., 2011) and "std" atmospheric pressure. The density of rock is 2.65 g cm$^{3}$. Reported $^{10}$Be/$^{9}$Be for 07KNSTD is $2.85 \cdot 10^{-12}$ (Nishiizumi et al., 2007). The $^{9}$Be/$^{10}$Be ratio is corrected to the weighted average of blanks.
* Blank ratios are presented without correction to the weighted average of blanks.

### 2.5.2. Active ice derived landforms

Together with the eight moraine ridges mapped in the Universidad Glacier forefield, the flutes also indicate an actively flowing temperate-based glacier (Boulton, 1976; Gordon et al., 1992; Benn and Evans, 2014). Distinguishing whether moraines represent ice front standstill or re-advances is not possible at this time. Regarding the flutes, we identified two groups parallel to the main valley axis and a third perpendicular to the lateral moraine ridges (D, C, B; Figure 2). Flutes have not been described previously in the literature for the Andes of central Chile, but they have been observed in the forefield of the Juncal Sur Glacier (33º S; J.-L. García, field observations). We mapped two types of flutes with different heights and lengths (Figure 7). Both types occur intercalated, for instance, in the flute field between moraines $D_1$ and F. As the flutes occur superimposed on the massive hummocky terrain, it is assumed that sediments from the latter were reworked into the flutes during active glacier flow. The flutes are composed of glacially polished clasts in the diamict that indicates their subglacial genesis. According to Boulton (1976) and Gordon et al. (1992), flutes accurately indicate the former direction of the ice flow, as they are produced by the abrasion and quarrying of subglacial boulders. Evans (2014) suggested that the glacier-bed coupling should generate similar flute sizes during discrete glacial events. It is possible that the sets of flutes that occur between moraines C—$D_1$ and E-F are linked to different glacial standstill and/or expansion events and, thereby, expose discrete times of active ice flow.

Lliboutry (1958) suggested that there must have been a “glacier flood” of the Universidad Glacier in the first half of the 20$^{th}$ century. The ice field extended 1 km further down-valley in 1944 when compared to 1956. Consequently, some authors started to report glacier surge events in the Andes

of central Chile and Argentina during the mid-20th century, including at the Universidad Glacier (Falaschi et al., 2018; Iturrizaga and Charrier, 2021).

Glacier surges refer to episodes where ice is rapidly transported from an upper reservoir zone to the receiving area in the lower glacier, owing to internal dynamic instabilities (Meier and Post, 1969; Evans and Rea, 1999; Benn and Evans, 2014; Bhambri et al., 2017; Benn, 2021). Surging glaciers are commonly recognizable by their geomorphic signatures. Diagnostic surge landforms summarized by Evans and Rea (1999) and Ingólfsson et al. (2016) include thrust-block moraines and push moraines; crevasse-squeeze ridges on the forefield; concertina ice-cored eskers; long flutes; hummocky moraine belts; pitted outwash; extensive dead ice fields; and drumlins. These landforms alone cannot be attributed to glacier surging without a landsystem approach (Evans and Rea, 1999; Evans et al., 2009; Evans, 2014; Benn, 2021). Surging glaciers have been well documented, particularly in Arctic (Evans and Rea, 1999; Evans et al., 2009; Evans, 2011; Schomacker et al., 2014; Ingólfsson et al., 2016) and alpine environments (Sutherland et al., 2019; Benn, 2021). The UNI IV moraine complex has some of the diagnostic elements of surging ice, such as flutes. However, thrust-block moraines, push moraines, and crevasse-squeeze ridges within the forefield have not been identified. The sinuous shape of moraine F might be interpreted as concertina esker with a subglacial origin. However, this differs from descriptions that suggest englacial and/or supraglacial origins of concertina eskers during a surging event (Evans and Rea, 1999; Schomacker et al., 2014; Ingólfsson et al., 2016). Besides, a concertina ice-cored esker produced by a surging glacier should have poor potential of preservation due to deposition and subsequent melting of dead ice (Evans and Rea, 1999). Additionally, the UNI IV moraine complex does not show hummocky moraine belts or pitted outwash. Therefore, the dead ice present in the glacier margin is not a consequence of a prior surging glacier, but the result of gradual evolution from active to stagnant ice.

The geomorphologic record of putative surging glaciers in the Andes of central Chile and Argentina remains unknown. According to the available literature of surging glaciers and the landforms mapped on the UNI IV moraine complex, surging events are not evident. We recommend further sedimentological analysis of moraine F or the well-preserved flutes of moraine E to establish whether these landforms are associated with a glacier re-advance or surge. Moreover, we consider it necessary to improve our understanding of potential surge events in the central Andes through a regional landsystem approach.

### 2.5.3. Stagnant ice-derived landforms

Deglacial features located between moraines suggest that after a phase of glacial standstill/expansion, a period of mostly *in situ* ice decay took place. The large hummocky terrain contains micro- and meso-scale geomorphologic structures that are best explained by an *in situ* collapse of debris-covered ice (Kjær and Krüger, 2001). Thus, the hummocky terrain is interpreted as the final product of the melting of buried and inactive ice (Benn, 1992; Benn and Evans, 2014). This process implies that after a glacier standstill/advance, the ice front stagnates and becomes debris-covered, leading to geomorphic features associated with dead ice melting. The differential ablation (Eyles, 1979; Mölg et al., 2020) forms the irregular topography that we observe as the hummocky terrain, including the formation of sinkholes and debris-filled stripes. These features have been largely described as a consequence of progressive *in situ* de-icing at present-day glacier margins (Krüger et al., 2010) and of past deglaciation in dead ice topography records (Schomacker, 2007; Crump et al., 2017).

The UNI IV moraine complex exposes irregular topography with 3-4 m relief, particularly toward the frontal margins of the outer moraine ridges (A-C). This chaotic accumulation of debris is punctuated by large depressions that can be best interpreted as inactive sinkholes (Krüger and Kjær, 2000). Morphogenesis of sinkholes in Iceland and the high Arctic is related to dead ice melting (Kjær and Krüger, 2001; Schomacker and Kjær, 2008). According to Kjær and Krüger (2001) and Schomacker and Kjær (2008), the space left by the thaw of the sediment-covered dead ice bodies generates subsidence, producing sinkholes. These hollows are often filled with debris at their bottoms due to sediment gravity flows triggered by the gradual melting of surrounding buried ice. Water or mud deposits at the sinkhole bottoms indicate local water saturation on the ground, originating from the melting of buried ice (Kjær and Krüger, 2001).

The production of sinkholes and melt-out ponds ends when the melting of the buried ice ceases or when water drains through ice fractures during the thawing phase. Sinkholes were also reported in the debris-covered glaciers of the Himalayas, where they were interpreted as resulting from the collapse of englacial conduits (Benn et al., 2017; Dobreva et al., 2017). In the Andes of central Chile, sinkholes are common in present-day debris-covered glaciers and in the latest Holocene glacial geomorphic record (Bodin et al., 2010; García et al., 2014).

The aforementioned fractures are also evidence of *in situ* ice decay. Eyles (1979), Kjær and Krüger (2001), and Schomacker and Kjær (2008) suggested that the gradual decay of buried mostly inactive ice bodies promotes the development of tension cracks above the frozen terrain. Then, pebbles, cobbles, and boulders fill the tension cracks. This process promotes the formation of debris-filled stripes in the ground. The debris-filled stripes vary from place to place depending on the past or present degradation of ice-cored moraines (Eyles, 1979; Kjær and Krüger, 2001). In the UNI IV moraine complex, we found debris-filled stripes that varied from centimeters to meters, suggesting melt-out of dead ice. Debris-filled stripes stand out and are widespread between moraines D-G, denoting progressive *in situ* de-icing. The deglacial geomorphology described here has also been recorded in subpolar and polar regions (Schomacker, 2007; Crump et al., 2017) as a product of the latest Holocene de-icing. The reports match debris-filled stripes with the degradation of ice-cored moraines or the collapse of dead ice bodies (Krüger and Kjær, 2000; Krüger et al., 2010).

The interpretation of the oval-shaped landform in the southwest section of the forefield is more difficult. It may be linked to a prior and longer stagnant phase of the glacier front. During the stagnation phase, the rate of debris accumulation might have been higher than the evacuation to the glaciofluvial system, triggering the vertical deformation of the ice snout. Similar processes

have been described by Eyles and Rogerson (1978) on Austerdalsbreen in Norway; van Woerkom et al. (2019) on Lirung Glacier, a Nepalese debris-covered glacier; and recently by Mölg et al. (2020) on the Zmuttgletscher, a debris-covered glacier in Switzerland. Our interpretation also follows the geomorphological observations made by Iturrizaga and Charrier (2021), who reported the presence of a prominent hummocky terrain deposit in the Chilean Cachapoal Valley (34° S) linked to former dead ice disintegration. According to Iturrizaga and Charrier (2021), that hummocky terrain was overridden by recent re-advances of Cachapoal Glacier. The oval-shaped landform that occurs in the forefield of the Universidad Glacier includes sinkholes and debris-filled stripes in the ground that reflect the de-icing process. Thus, the oval-shaped landform may be part of the relief formed during the development of moraines A-B. After its deposition, this landform was overridden subglacially, similar to what occurred in the Cachapoal Valley.

The top of the overridden till plain has various elongated features. It is possible that some of these features are flutes produced by the ice flow at the time the moraine C was formed. However, other elongated features record the effect of subtle meltwater linear erosion when the ice stood at moraine $D_1$ on the proximal side of this oval-shaped landform. Today, the oval-shaped landform is flanked on both sides by meltwater streams, one of which is the San José River draining the Universidad Glacier. Glaciofluvial erosion has also increased the landform's prominence.

### 2.5.4. Current deglaciation

The Universidad Glacier ablation zone exhibits features of glacier front stagnation and *in situ* degradation of ice under a debris layer, as described in other works in the region (García et al., 2014; Janke et al., 2015). Geomorphic features demonstrate this condition, such as the conspicuous transversal outcrop ridges of sediments composed of rounded pebbles and fines appearing on the ice surface. This sediment is likely to be crevasse-squeeze ridges that attest to shear in the ice margin (Evans and Twigg, 2002; Benn and Evans, 2014). Crevasse-squeeze ridges have been associated with the movement of the upper, active flow of the glacier as it overrides the slow-moving or stagnant ice front (Phillips et al., 2017). This would be connected to the formation of dead ice bodies on the lower section of the glacier during the de-icing process (Kjær and Krüger, 2001). Thus, one deglaciation characteristic is the presence of active (upper-glacier) ice flowing down-valley over stagnant ice that has already separated or started to separate (García et al., 2014).

In addition, the ice cliffs present in the marginal zone might be understood as part of the active/inactive transition of debris-covered glaciers (Watson et al., 2017). The origin of such ice cliffs remains mostly unexplored (Mölg et al., 2020), although some authors suggest that their formation is linked to the overriding dynamics of active ice over inactive ice (Krüger et al., 2010). The ice cliffs are melting chiefly through backwasting, the principal ablation factor of debris-covered glaciers (Krüger and Kjær, 1999; Sakai et al., 2000; Schomacker and Kjær, 2008; Reid and Brock, 2014; Ewertowski and Tomczyk, 2015). Backwasting consumes the vertical clean ice, triggering two results: remobilization of debris and more irregular topography (Krüger et al., 2010; Mölg et al., 2020). Therefore, the presence of ice cliffs in the ablation zone is another feature reflecting the current deglaciation of the stagnant Universidad Glacier snout.

According to Eyles (1979) and Krüger et al. (2010), sinkholes are associated with the presence of ice bodies below a reworked supraglacial till. Local melting of isolated and buried ice cores triggers ground subsidence (Krüger and Kjær, 2000). Sinkholes and melt-out ponds can be considered landforms inherited from the current deglaciation. Ultimately, debris-filled stripes in the ground denote debris-filled tension cracks formed during the de-icing of the stagnant ice (Kjær and Krüger, 2001). The surface lowering due to ice melting produces other topographic features, including wet scars on the hummocks' slopes. The geomorphic record in the Universidad Glacier's ablation zone indicates that the *in situ* ice-decay is associated with a stagnant ice front that best characterizes the present-day response to climate warming and drying (García et al., 2014; Janke et al., 2015; Charrier et al., 2019; Iturrizaga and Charrier, 2021).

### 2.5.5. De-icing conceptual model

The geomorphological record of the Universidad Glacier is associated with glacier standstills/advances, glacier front stagnation, the transition to debris-covered ice, and finally, degradation into ice-cored moraines. Thus, the melting of isolated dead ice bodies leads to the dead ice moraine (*sensu* Kjær and Krüger, 2001; Schomacker and Kjær, 2007; Krüger et al., 2010) with a massive ice-free hummocky topography that is preserved along this upper Andean catchment (Janke et al., 2015; Charrier et al., 2019; Iturrizaga and Charrier, 2021). Based on our findings, we develop the following de-icing model for the Universidad Glacier, which also represents other glaciers of the region (Figure 9):

- After an ice advance (Figure 9a), long periods of negative mass balance trigger the glacier front to stagnate, be covered by debris, and downswaste (Figure 9b). The movement of active ice onto the inactive glacier front triggers intense shearing in the transitional zone. This produces crevasse-squeezed ridges and ice cliffs. The supraglacial sediment layer gets thicker as ice-downwaste sediment emerges through thrust planes. Mass wasting on the valley's sides and lateral moraines also occurs (Curry et al., 2006; Janke et al., 2015). Once the local exposed ice, such as in ice cliffs, is completely debris-covered, the supraglacial layer thickness determines the de-icing progress and resultant geomorphology.
- The debris-covered ice snout becomes an ice-cored moraine detached from the active glacier (Figure 9c). The ice-cored terrain degradation produces identifiable landform features such as i) hummocky topography; ii) sinkholes with their bottoms filled by debris; iii) tension cracks in the inner slopes; iv) debris-filled stripes in the ground; and v) meltwater in melt-out ponds. These features have been described as part of the

disintegration of ice-cored moraines (Kjær and Krüger, 2001; Schomacker and Kjaer, 2007) following a stagnant phase of debris-covered ice. We observe these features at different locations, such as between moraines A-D. The geomorphological features described above were also observed in the degradation of dead-ice bodies by García et al. (2014) in the Andes of central Chile; Krüger et al. (2010) in subpolar environments; and Benn et al. (2017) in the Himalayas.

- After de-icing of buried ice has ended, the ice-free hummocky terrain or dead-ice moraine is produced and remains as the deglacial record. The ice-free hummocky topography has been described as part of the geomorphology of the upper catchment in the Andes of central Chile and Argentina (Wayne and Corte, 1983; Bodin et al., 2010; García et al., 2014; Janke et al., 2015; Charrier et al., 2019; Iturrizaga and Charrier, 2021), but without the morphogenetic interpretation we provide here.

The deglaciation process of the Universidad Glacier has not been linear during the last 655±145 years, but interrupted by ice standstills/re-advances until very recently. Flutes within moraines C and D are evidence of active flowing ice. Glacier activity near the mid-20$^{th}$ century, represented by moraine E, also left flutes. Since then, the ice has collapsed, and the glacier has had short standstills or pulses (moraines F and G). Therefore, a complete deglaciation model for the latest Holocene period needs to include this dynamic nature of active and inactive ice phases in the Andes of central Chile (Figure 9d-e).

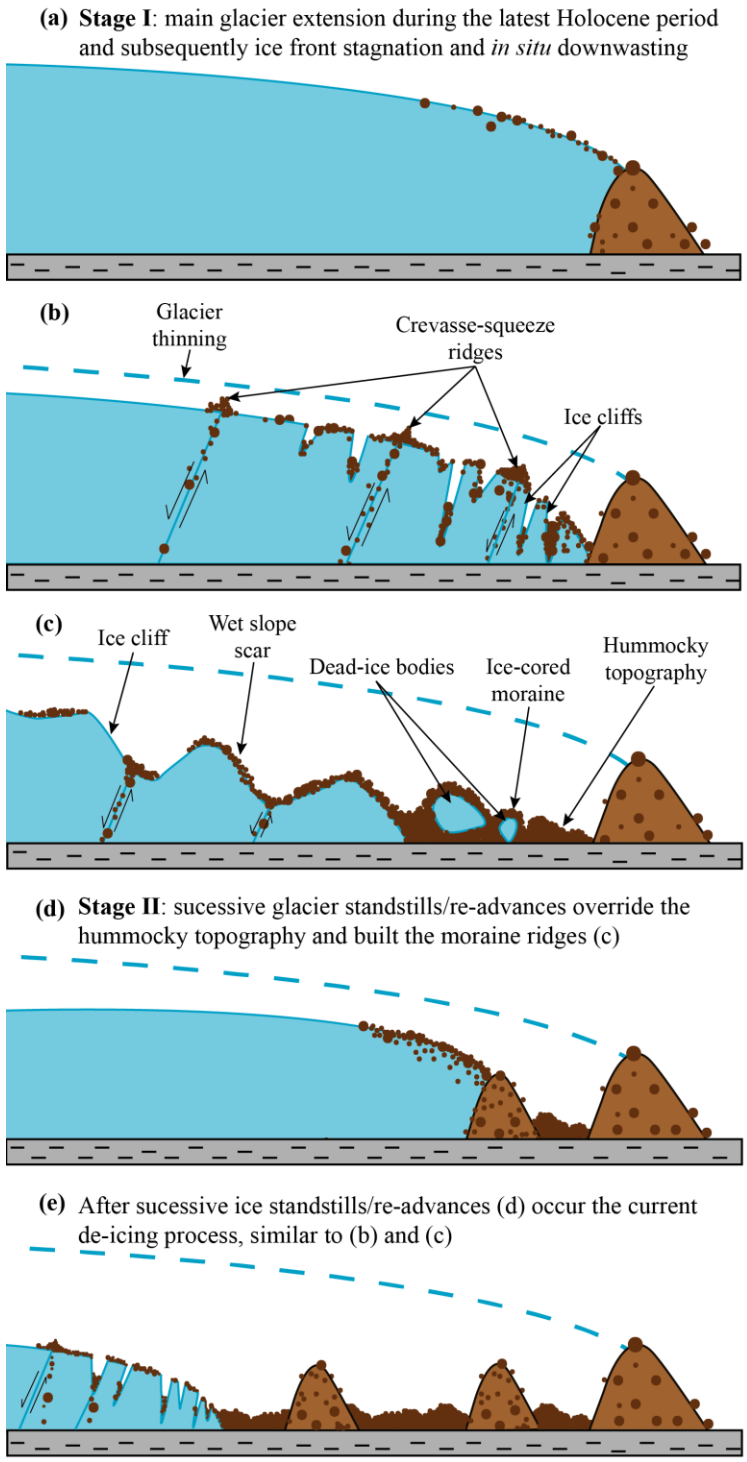


**Figure 9. De-icing model for the Universidad Glacier. Stage I**: **(a)** main glacier extension during the latest Holocene period; **(b)** During the de-icing process, the glacier front becomes stagnant and thinner. As a result, the ice surface is covered with debris; **(c)** The debris-covered glacier front undergoes differential ablation and ice-cored moraines are developed; **Stage II (d)** successive glacier standstills/re-advances override the forefield; **Stage III (e)** current de-icing. The main implication of the landsystem including glacial and deglacial features is that the current de-icing process seems to be mimicking what occurred after the main late Holocene advance (moraines A-B).

## 2.6. **Conclusions**

The geomorphology of the forefield of the Universidad Glacier is a mosaic of glacial and deglacial landforms, that exposes a juxtaposition of morphogenetic ice processes acting over the past 655±145 years. The main geomorphic deglacial features we observe are sinkholes and debris-filled stripes in the ground within a bouldery, hummocky relief surface. These features, along with ice cliffs, crevasse-squeeze ridges, melt-out ponds, and debris-infilled sinkholes, indicate an inactive ice phase we observe in present-day Universidad Glacier. On the other side, we identified eight moraine belts and flutes that emerge from the UNI IV moraine complex, evidence of active ice flow and sediment transport/rework during the overall ice decay period until very recently (the end of the 20$^{th}$ century).

A debris-rich environment such as the Andes of central Chile affects the ice front during warming climate conditions: a stagnant buried ice body evolves. The transition from active ice to inactive buried ice during deglaciations is expected to occur each time the climate warms and dries, as we observe today at the Universidad Glacier. Intercalated colder and wetter climate regimes will promote a composite geomorphic record like that recorded by the UNI IV moraine complex.

A heuristic model for the latest Holocene glacial and deglacial phase for the Universidad Glacier, and likely other glaciers in the Andes of central Chile, includes three stages: (I) main glacier expansion within the last 655±145 years (moraine A) and subsequent ice front stagnation associated with a rich debris cover leading to the development of ice-cored and finally dead-ice moraines; (II) glacier front retreat interrupted by multiple standstill/re-advances that overrode and reworked former glacial deposits, producing landforms such as flutes and inner moraine ridges; and (III) the current deglaciation, which repeats the de-icing process described in Stages I and II.

Under the current warming and drying trends in the Andes of central Chile (Barcaza et al., 2017; Garreaud et al., 2020), a negative mass balance of glaciers will continue to result in increased debris coverage and gradual loss of ice under a thick debris mantle. The relevance of these glaciers as essential water resources in the Andes of central Chile contrasts with the lack of work dedicated to the Andean cryosphere. We thus suggest that further studies associated with the depth, volume, rate, and manner of deglaciation in the Andes of central Chile are urgently needed to build a comprehensive regional understanding of glacier-climate interactions. The Universidad Glacier can be a starting point for interpreting the latest Holocene de-icing dynamics of the other glaciers in this region. Furthermore, additional sedimentological investigations would improve our understanding of standstill/advance periods and their relationship to the presence or absence of surge-type glaciers.

## 3. FLUCTUATIONS OF THE UNIVERSIDAD GLACIER IN THE ANDES OF CENTRAL CHILE (34° S) DURING THE LATEST HOLOCENE DERIVED FROM A 10BE MORAINE CHRONOLOGY

Este tercer capítulo se presenta como artículo científico y por ese motivo está escrito en inglés. El artículo está publicado en la revista Quaternary Science Reviews: Fernández-Navarro, H., García, J.L., Nussbaumer, S.U., Tikhomirov, D., Pérez, F., Gärtner-Roer, I., Christl, M., Egli, M., 2023. Fluctuations of the Universidad Glacier in the Andes of central Chile (34° S) during the latest Holocene derived from a 10Be moraine chronology. Quaternary Science Reviews 300. El acceso al artículo puede realizarse a través del siguiente enlace: doi.org/10.1016/j.quascirev.2022.107884. La numeración de figuras y tablas es correlativa a toda la tesis doctoral, por lo cual las figuras y tablas expuesta aquí no guardan exclusiva relación con este capítulo.

## 3.1. **Introduction**

Long-term glacier changes are modulated by the balance between accumulation and ablation of ice and mostly reflect climate variations (Oerlemans, 1994; Benn and Evans, 2014; Huston et al., 2021). Mapping and dating of well-preserved latest Holocene (<1000 years) glacial landforms, such as moraines, are then suitable for reconstructing former fluctuations of glaciers and climate (Mackintosh et al., 2017). Moreover, unveiling the glacier changes over the latest Holocene provides a broader temporal context for current climate change (Jomelli et al., 2009; Masiokas et al., 2009; Solomina et al., 2016; Kaplan et al., 2016; Huston et al., 2021). The Holocene glacial landscape is well-preserved in the Andes of central Chile (30—35° S; García et al., 2014; Sagredo et al., 2017; Charrier et al., 2019; Iturrizaga and Charrier, 2021; Fernández et al., 2022), but the magnitude, timing, and cause of the associated ice variations remain mostly unknown. The lack data retrieved from the Andes of central Chile has precluded regional glacial geochronologies and the forcing mechanisms behind climate change for the latest Holocene (Bradley et al., 2003; Masiokas et al., 2009; Solomina et al., 2016). Few works have established the dating of the glacial landforms in the Andes of central Chile and Argentina (Röthlisberger, 1986; Espizua, 2005; Espizua and Pitte, 2009; Sagredo et al., 2017; Price et al., 2022). Hence the correlations between glacial fluctuations and climate changes of southern mid-latitudes on a millennial-to-centennial time scale remain unclear. In this study, we aim to reconstruct the fluctuations of the Universidad Glacier over the past millennium using $^{10}$Be dating of glacial landforms. We propose a chronology of glacier fluctuations based on twenty-two $^{10}$Be ages to analyze: When did the main glacial advances occur over the latest Holocene? Which climate setting forced these glacier fluctuations? Do we observe a southern mid-latitude climate signal in the record from the Universidad Glacier?

South of the Atacama Desert and north of Patagonia, the Andes of central Chile are suitably located to reconstruct the migration of the northern border of the Southern Westerly Winds (SWW), which is interlinked with the southern margin of the Subtropical Pacific Anticyclone (SPA) (Figure. 10a; Garreaud, 2009; Flores-Aqueveque et al., 2020). During the austral summer, the SPA blocks the northward migration of the SWW, causing relatively dry and warm conditions in the region. Conversely, during the austral winter, the SPA becomes weaker, allowing the SWW to bring along higher amounts precipitation (Escobar and Aceituno, 1998; De Jong et al., 2013) and colder conditions in the Andes of central Chile (Flores-Aqueveque et al., 2020). The highest peaks in the Andes of central Chile and Argentina reach near 7000 m a.s.l (Figure 10b), which makes this mountain range very sensitive to climate variations due to orographic effect (Garreaud, 2009). By determining past Universidad Glacier fluctuations, we aim to reconstruct the past changes of the SWW in a region where few studies and limited records have precluded paleoclimate reconstructions and, thus, implications for near-future climate projections (Araneda et al., 2009; Magrin et al., 2014; Sagredo et al., 2017).

The decadal to interdecadal variability in the latitudinal position of the SWW in mid-latitudes (including the Andes of central Chile) has been associated with both the Pacific Decadal Oscillation or Interdecadal Pacific Oscillation (PDO/IPO; hereafter PDO; Carrasco et al., 2005; Masiokas et al., 2012; Quintana and Aceituno, 2012; Barria et al., 2019; Garreaud et al., 2020) and the Southern Annular Mode or Antarctic Oscillation (SAM/AAO; hereafter SAM; Christie et al., 2011; Villalba et al., 2012; Garreaud et al., 2020; Morales et al., 2020). The PDO is a multi-decadal (20-30 years) pattern of variability of North Pacific (north of 20° N) monthly sea surface temperatures (Mantua et al., 1997; Mantua, 2002; Garreaud et al., 2009), which triggers precipitation anomalies in northern South America (Johnson et al., 2020). The positive (negative) phase of the PDO has been associated with the increased frequency of El Niño (La Niña) events

in the Andes of central Chile (Garreaud et al., 2009; Rabatel et al., 2010; Quintana and Aceituno, 2012). The positive phase of the PDO in subtropical latitudes involves the increased frequency of wet years linked with the arrival of storms from the Pacific (Quintana and Aceituno, 2012) in a context where the mean air temperature is higher (Garreaud, 2009). Conversely, the negative phase of the PDO is related to drier conditions linked to colder temperatures and an enhanced SPA that blocks storm systems sourced in the Pacific. The PDO has been identified as a potential influence on the low-frequency modes of variability of precipitation in the Andes of central Chile (Montecinos and Aceituno, 2003; Carrasco et al., 2005; Masiokas et al., 2010, 2012; Quintana and Aceituno, 2012; Barria et al., 2019). Thus, some studies have linked years with positive (negative) mass balance of glaciers to positive (negative) phases of the PDO (Rabatel et al., 2011; Barria et al., 2019; Farías-Barahona et al., 2019).

On the other hand, the SAM is considered the leading principal component of climate variability in the Southern Hemisphere south of 20° S (Thompson and Wallace, 2000; Flores-Aqueveque et al., 2020; Morales et al., 2020; Wachter et al., 2020). The SAM is inferred by the geopotential height or the zonal mean atmospheric pressure difference between southern mid- and high-latitudes (Thompson and Wallace, 2000; Abram et al., 2014; Dätwyler et al., 2018). During positive phases of the SAM, the Hadley Cell (and consequently the SPA) shift south, provoking the poleward migration and contraction of the SWW. The latter results in dry and warm conditions in the mid-latitudes (Marshall, 2003; Abram et al., 2014; Dätwyler et al., 2018, 2020; Fogt and Marshall, 2020), as it is currently occurring in central Chile (Garreaud, 2009; Boisier et al., 2018; Garreaud et al., 2020; Morales et al., 2020). Conversely, during the negative phases of the SAM, the position of the storm tracks is moved towards the Equator (Dätwyler et al., 2018), resulting in weaker circumpolar SWW but wetter and cooler conditions bringing enhanced snow conditions to the Andes of central Chile and Argentina (Villalba et al., 2012; Morales et

al., 2020). Linked SAM-like conditions and glacier fluctuations have been suggested for Patagonia (49°—51° S; Kaplan et al., 2016; Reynhout et al., 2019; García et al., 2020) and recently for the Andes of south-central Chile (38° S; Price et al., 2022). Here, we use our new $^{10}$Be record at 34º S to test causal links between SWW migrations, former SAM-like conditions, and glacier fluctuations.

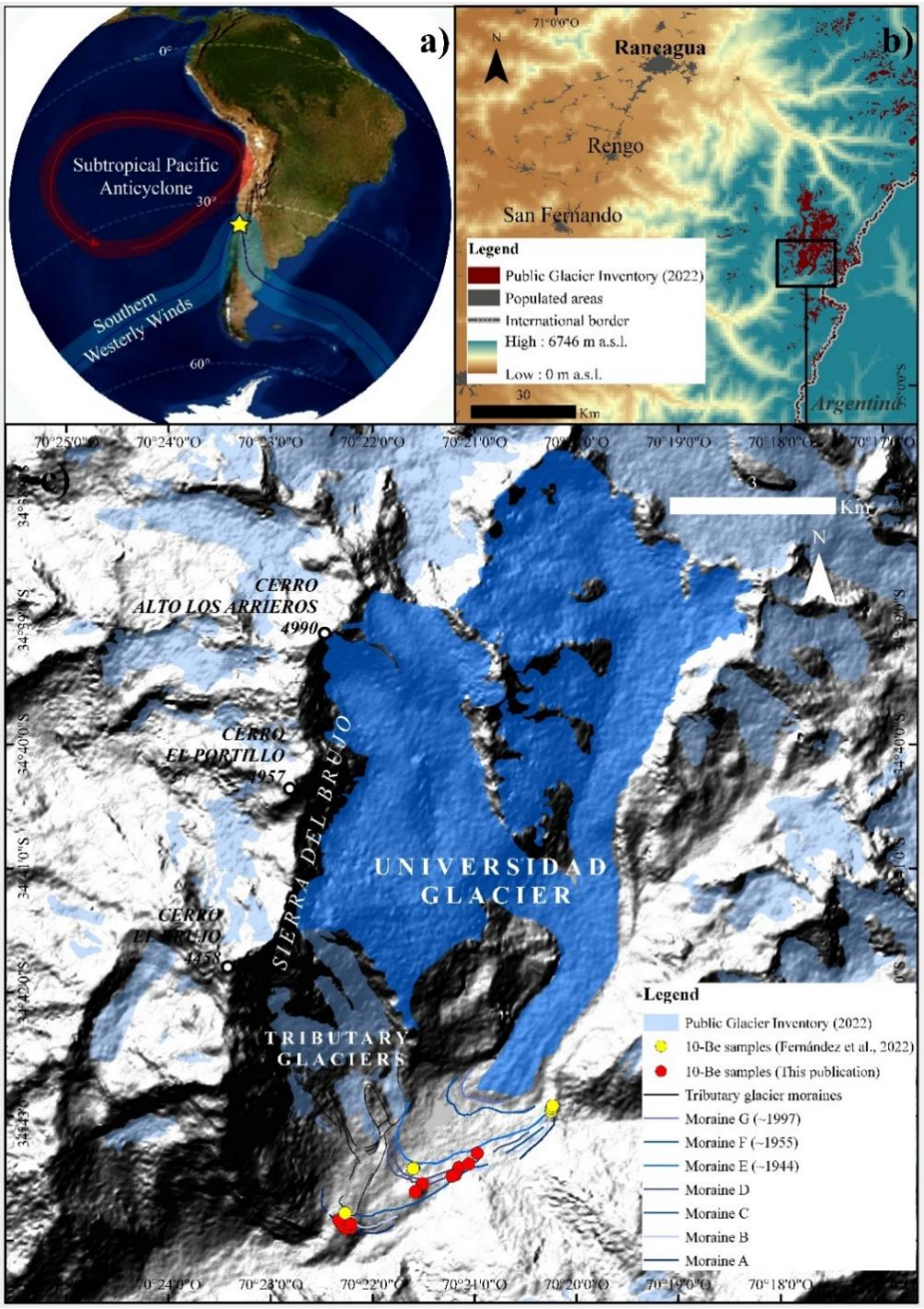


**Figure 10. Location of the study area in the Andes of central Chile**. **(a)** Study area (yellow star) in South America and central Chile; **(b)** glaciers as mapped (red) in the national glacier inventory (Dirección General de Aguas, 2022b) with nearest populated areas. **(c)** Universidad Glacier and its mountain environment: Universidad Glacier and the latest Holocene moraines (A-G) and moraine ridges associated with tributary glaciers (black lines). $^{10}$Be exposure ages represented in yellow dots were published by Fernández et al. (2022). $^{10}$Be exposure ages in red dots are presented in this work for first time.

## 3.2. **Study area**

The Andes of central Chile comprise a rugged topography characteristic of active tectonic uplift, volcanism, and incised glacial basins (García et al., 2014; Charrier et al., 2019). Their altitude and physical setting promote different sizes and types of glaciers (Lliboutry, 1956, 1998), such as glaciers with a clean ice surface, glaciers with debris-covered snouts, and debris-covered glaciers. Glaciers with a clean ice surface and debris-covered glaciers are more abundant south of 33° S. Rock glaciers are the dominant cryo-landform from 33° S to the north (Azócar and Brenning, 2010; Azócar et al., 2017).

The glaciated area has been declining at least since the mid-20$^{th}$ century (Malmros et al., 2016), and the negative glacier mass balance trend has been accelerated over the past two decades (Dussaillant et al., 2019; Hugonnet et al., 2021). Since the year 2010 central Chile has been affected by the Mega Drought (MD), one of the longest and driest periods of the last millennium (Garreaud et al., 2020). The MD represents a precipitation deficit of 20-40%, which is linked with deep tropospheric anticyclone anomalies over the subtropical Pacific and cyclonic anomalies over the Antarctic Sea (Garreaud et al., 2020). The MD has influenced the decrease in the glacier albedo (Shaw et al., 2021) and has led to an unprecedented loss of ice-covered areas of some of the largest glaciers in the Andes of central Chile (Dirección General de Aguas, 2022a).

The Andes of central Chile are situated south of the Pacific side of the Arid Diagonal (Abraham et al., 2020). In this region, precipitation is associated with the passage of frontal systems moving eastward from the Pacific (Garreaud, 2009); 80% of the annual precipitation occurs between May and August, mainly in the form of snow. According to regional climate data from the Embalse El Yeso station (33° 40' S, 70° 5' W, ~2400 m a.s.l.), the mean annual air temperature is 8.3 °C and the mean annual precipitation amounts to 515 mm (Barcaza et al., 2017). The local climate

defines the glaciers' equilibrium line altitude (ELA) at 4300- 4400 m a.s.l. at 32° S, declining gradually to 3700 - 3800 m a.s.l. at 34° S (Azócar and Brenning, 2010).

Universidad Glacier (Figure 10c; 34° 42' S, 70° 20' W) is situated in the southern part of the Andes of central Chile and spans an altitudinal range from ~4540 to 2500 m a.s.l. Louis Lliboutry named the Universidad Glacier after his visit in 1956. Nevertheless, there is evidence that this glacier was locally called "Resurrección" (Kuhn, 1930). Here, we use the given name by Lliboutry, which is the current official name of this glacier (Dirección General de Aguas, 2022b). High summits surround the Universidad Glacier (Figure 10c). The highest peaks on the west side of the catchment area include Cerro Alto Los Arrieros (4990 m a.s.l.), El Portillo (4957 m a.s.l.), and Cerro El Brujo (4458 m a.s.l.). All together those peaks are known as “La Sierra del Brujo” (“The Sorcerer’s mountain range”). To the east, the highest peaks include the volcano El Palomo (4860 m a.s.l.) and other peaks at ~3500 m a.s.l. El Palomo has no recent volcanic activity recorded. The main lithologies surrounding the Universidad Glacier are granodiorites, rhyolites, and andesites (Charrier and Lillo, 1973).

The mountain range surrounding the Universidad Glacier also hosts three other glaciers that cover an area of ~70 $km^2$ (Dirección General de Aguas, 2022b): the Cipreses Glacier to the northwest, the Cortaderal Glacier to the east, and the Palomo Glacier to the north. The Universidad Glacier has the largest surface area in the Andes of central Chile that amounts to 26 $km^2$ (Dirección General de Aguas, 2022b), and a length of ~10 km. Aerial photographs available since 1944 allow the determination of the ice front evolution since then. In the 1944 Trimetrogon aerial photographs, the ice front was ~1.5 km further down-valley than at present. Between 1944 and 1955, the ice front retreated ~1 km (HYCON flight, 1955; Lliboutry, 1958). Since 1955, the ice front has retreated about 550 m. Fernández et al. (2022) recognized four distinct moraine belts

within 20 km from the actual glacier margin between ~1100 and 2500 m a.s.l (Figure 11a). The authors labeled these moraines as UNI I to UNI IV from outer to inner position, with moraine UNI IV being the youngest Holocene moraine complex we $^{10}$Be date in this paper. The UNI IV complex is a massive dead-ice moraine punctuated for eight moraines ridges (A-G), and other glacial features such as flutes (Fernández et al., 2022).

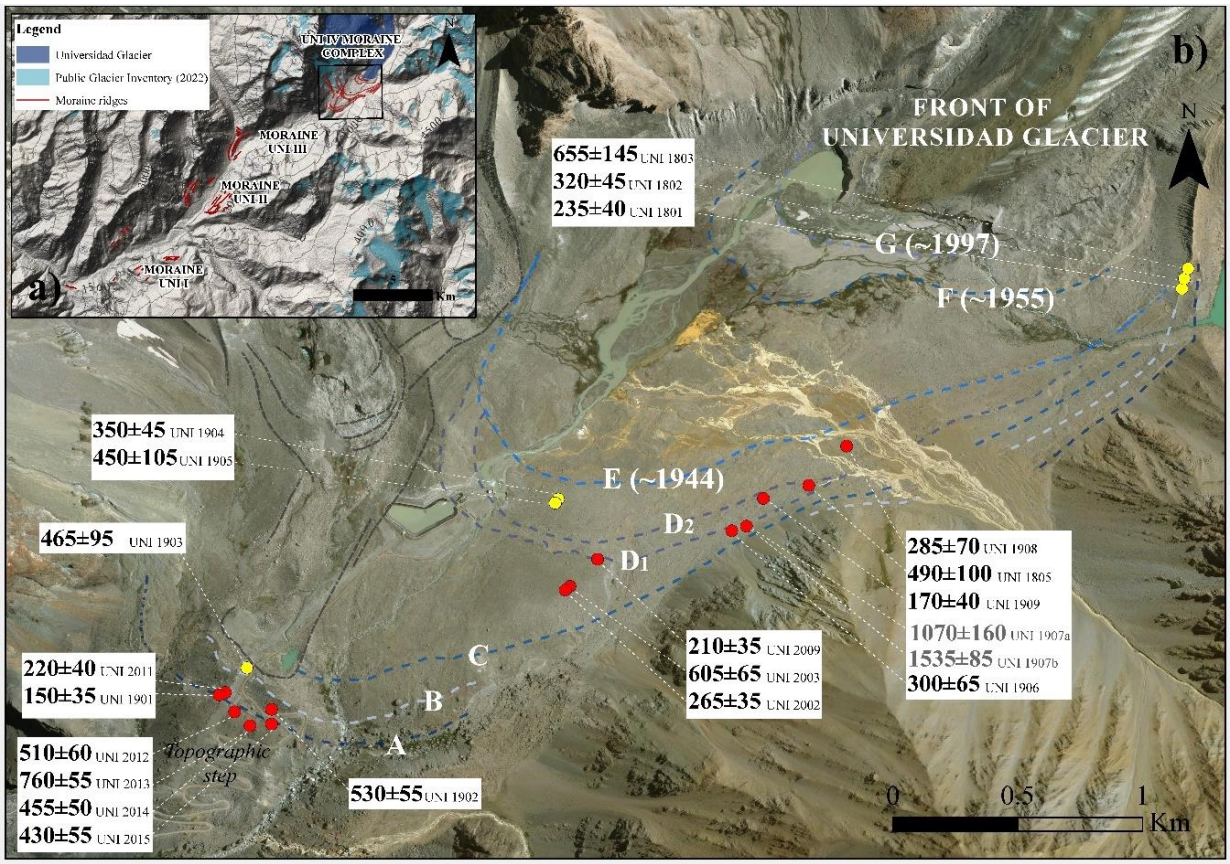


**Figure 11. $^{10}$Be geochronology of the UNI IV moraine complex at the Universidad Glacier (ages in years ago). (a)** Moraines mapped along the Universidad Glacier valley. UNI IV moraine is marked in a box; **(b)** Moraine ridges A-C represent the outermost ice extent during the latest Holocene. The moraines ridges $D_1$-E represent less extensive ice preserved until the first half of the 20$^{th}$ century; F-G small ridges denote a much less prominent glacier towards the end of the 20$^{th}$ century. Red dots represent the exposure ages presented in this paper. Yellow dots show exposure ages published by Fernández et al. (2022). The mapping was made on ESRI ArcGIS imagery of 2020.

## 3.3. **Material and methods**

### 3.3.1. Geomorphological mapping

Our geomorphological mapping is based on the interpretation of satellite images, stereoscopic aerial photographs, and field observations. We analyzed aerial photographs from 1997 (1:50,000, produced by GEOTEC flight, Servicio Aerofotogramétrico (SAF), Chile) and 1955 (1:70,000, produced by HYCON flight, SAF, Chile) to map the glacial geomorphology. In addition, we composited a Digital Elevation Model (DEM) with 12.5 m resolution from the ALOS-PALSAR data mission from 2006-2011 (https://vertex.daac.asf.alaska.edu/). Finally, we conducted four fieldwork campaigns in 2019 and 2020 to verify the landform interpretation of remote sensing data. In the field, we used a handheld GPS device with ± 3 m horizontal accuracy to document the $^{10}$Be sample and landform locations. To produce geomorphic maps, we used ESRI ArcGIS (Version 10.8.1).

### 3.3.2. Geochronology

During fieldwork, we collected sixteen new rock samples (>1.5 kg) from the top (upper <3.6 cm) of fifteen granodiorite boulders (Table 2) distributed on the UNI IV moraine complex in the present-day forefield of the Universidad Glacier. In addition, we include in our analysis six $^{10}$Be exposure ages from the same UNI IV moraine reported recently by Fernández et al. (2022).

We followed the standard procedures for *in situ* Terrestrial Cosmogenic Nuclides ($^{10}$Be) dating (TCN) (Gosse and Phillips, 2001) to sample boulders resting on moraine ridges, flute fields and other glacial landforms, all within the UNI IV moraine complex. The sampling focused on boulders ranging in height between 51-390 cm above the surrounding surface and showing

minimal surface weathering, fractures, or evidence of gravitational movement or post-deposition exhumation (Figure 12a-f). In order to minimize previous surface-exposure inheritance, we targeted glacially-polished boulders most of them preserving glacial striations, thus denoting significant ice erosion. We used a hammer and chisel, blasts, and a handheld circular saw to collect the rock samples.

Clean quartz was extracted in the Cosmogenic Isotope Laboratory at the Pontificia Universidad Católica de Chile. Beryllium was isolated at the Surface Exposure Lab at the University of Zurich, following standard procedures (Kohl and Nishiizumi, 1992). All $^{10}Be/^{9}Be$ ratios were measured at the ETH Zurich on the TANDY (in 2019) and MILEA (in 2021) AMS systems (Christl et al., 2013; Maxeiner et al., 2019) and normalized to the ETH in-house AMS standards S2007N and S2010N ($^{10}Be/^{9}Be = 28.1 \cdot 10^{-12}$ and $3.3 \cdot 10^{-12}$, respectively), which were calibrated to the ICN 01-5-1 standard (Nishiizumi et al., 2007). All AMS standards are associated with a $^{10}Be$ half-life of 1.387±0.012 Myr (Chmeleff et al., 2010; Korschinek et al., 2010). Because the samples were prepared and measured in two separate batches in 2019 and 2021, the $^{10}Be/^{9}Be$ sample ratios of each batch were corrected to its blanks (Table 2). We calculated $^{10}Be$ exposure ages with the CRONUS-Earth online calculator (http://hess.ess.washington.edu/math/) version 3 (Balco et al., 2008). We used the calibration dataset developed by Kaplan et al. (2011) to obtain the $^{10}Be$ production rate for southern South America. Age calculation was done with the assumption of zero rock erosion and zero snow cover. In our research we rely on time-dependent scaling scheme (Lm) after Lal (1991) and Stone (2000) (Table 3). We also discuss previously reported radiocarbon dates, here calibrated using Calib 8.2 software and the SHCal20 curve (http://calib.org/calib/; Stuiver and Reimer, 1993). Calibrated ages are reported as mean ages with 2 sigma error.

## 3.4. **Results**

### 3.4.1. Geochronology of the UNI IV moraine complex

Analytical details of our new sixteen $^{10}$Be samples plus samples reported by Fernández et al. (2022) retrieved across the UNI IV moraine complex are shown in Table 2. Figure 11b summarizes all the $^{10}$Be exposure ages and 1 sigma errors in the moraine UNIV IV geomorphic context.

Following, we describe all exposure $^{10}$Be ages based on their position within the UNI IV moraine complex, from distal to proximal locations. Four $^{10}$Be samples (UNI 2012, UNI 2013, UNI 2014, and UNI 2015) were obtained from faceted and striated boulders on a till surface grading from the frontal ridge A (Figure 12a). They yielded exposure ages of 760±55, 510±60, 455±50, and 430±55 years ago. Moraine ridge A, ~3 km from the present ice-front, is composed mainly of angular and sub-angular boulders. A pair of glacially polished boulders were sampled from the top of this ridge (UNI 1901 and UNI 2011), yielding exposure ages of 150±35 and 220±40 years ago, respectively. The frontal moraines ridges A-B are separated by 100 m of intermorainic basaltic bouldery topography. One large boulder in this intermorainic depression indicated an exposure age of 530±55 years ago (UNI 1902; Figure 12b). Fernández et al. (2022) retrieved four samples from the top of the moraine B. One of them (UNI 1903) was collected from the frontal ridge and yielded an exposure age of 465±95 years ago. The other three boulders (UNI 1801, UNI 1802, and UNI 1803) were sampled side-by-side in this main left lateral ridge and yielded exposure ages of 235±40, 320±45, and 655±145 years ago, respectively.

Between the frontal C and D moraines, a basal till plain punctuated by glacial flutes and abandoned meltwater routes occurs about 30 m above the surrounding topography. We recovered

two $^{10}$Be samples from faceted boulders embedded in glacial flutes, which yielded exposure ages of 605±65 and 265±35 years ago (UNI 2002 and UNI 2003).

The frontal section of moraine D is ~1.8 km down-valley from the present-day ice margin. The D crest splits into two smooth and sinuous ridges, $D_1$ and $D_2$, separated 10–20 m from each other. These two ridges are joined up-valley, conforming to one single moraine crest D (Figure 11b). We obtained four samples from three boulders on the top of the frontal and lateral sections of moraine ridge $D_1$ (UNI 2009, UNI 1906, UNI 1907a, and UNI 1907b). Boulders UNI 2009 and UNI 1906 yielded exposure ages of 210±35 and 300±65 years ago, respectively (Figure 12c). Samples UNI 1907a and UNI 1907b were obtained from the same boulder top surface separated by 45 cm (Figure 12d), and they yielded exposure ages of 1535±85 and 1070±160 years ago, respectively. The lateral moraine $D_2$ was also sampled (UNI 1805 and UNI 1909). These two samples obtained here gave exposure ages of 490±100 and 170±40 years ago (Figure 12e). We retrieved one sample from an embedded boulder on the intermorainic depression between moraines $D_2$ and E (UNI 1908) that yielded an exposure age of 280±70 years ago (Figure 12f). Previously Fernández et al. (2022) recovered two samples (UNI 1904 and UNI 1905) from intermorainic depression between moraines $D_2$ and E that yielded exposure ages of 350±45 and 450±105 years ago. Moraines E, F, and G represent moraine landforms deposited between about 1944 and 1997 and situated within 1.5 km from glacier margin.

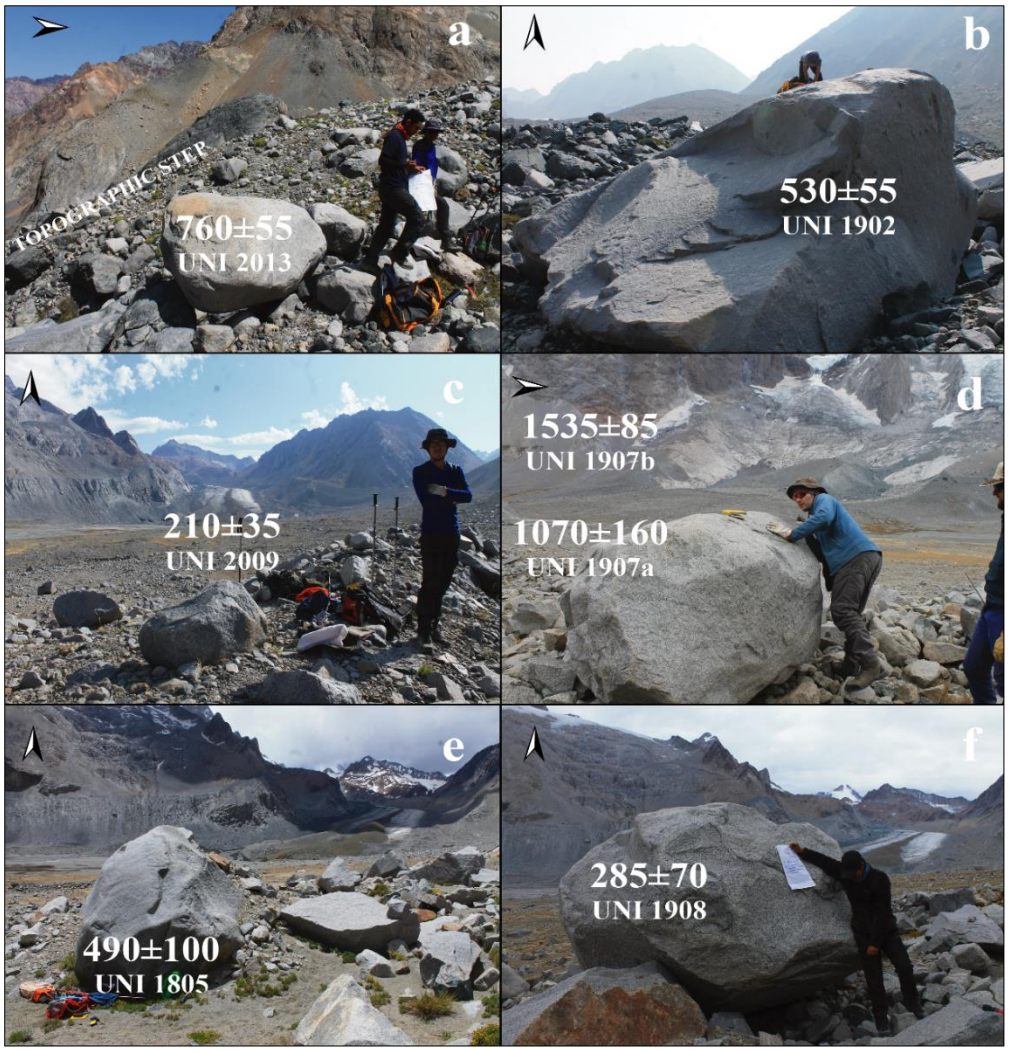


**Figure 12. Sampled boulders within the UNI IV moraine complex and their ages in years ago. (a)** Sample UNI 2013 was obtained from a perched and striated boulder on the till surface distal to moraine ridge A; **(b)** UNI 1902 was recovered from a large boulder located between moraine ridges A and B; **(c)** Sample UNI 2009 was retrieved from an embedded boulder resting on the frontal moraine ridge $D_1$; **(d)** Samples UNI 1907a and UNI 1907b were collected from a boulder with striated surface and stable position on lateral moraine ridge $D_1$. The exposure ages of UNI 1907 "a" and "b" are much older than all other samples reported in this paper. Therefore, they were considered as outliers due to their $^{10}$Be inheritance; **(e)** Sample UNI 1805 was retrieved from a stable boulder on the ridge of moraine $D_2$ and is characterized for a well-striated surface; **(f)** Sample UNI 1908 was recovered from a boulder located between lateral moraine ridges $D_2$ and E. Arrows point out the North.

## 3.5. **Discussion**

### 3.5.1. Geochronology

There is no obvious spatial organization of $^{10}$Be ages within the moraine UNI IV (Figure 11b). For instance, older and younger ages can occur nearby each other, either on the outermost or innermost landforms comprising the UNI IV moraine complex. This occurs between the distal till surface and the outermost morainic ridge A, where ages range from 760 to 150 years ago. In the main outermost left moraine (A-B) ages of three boulders range from 655 to 235 years ago. Also, nearby boulders on the basal till plain yielded ages of 605 and 265 years ago.

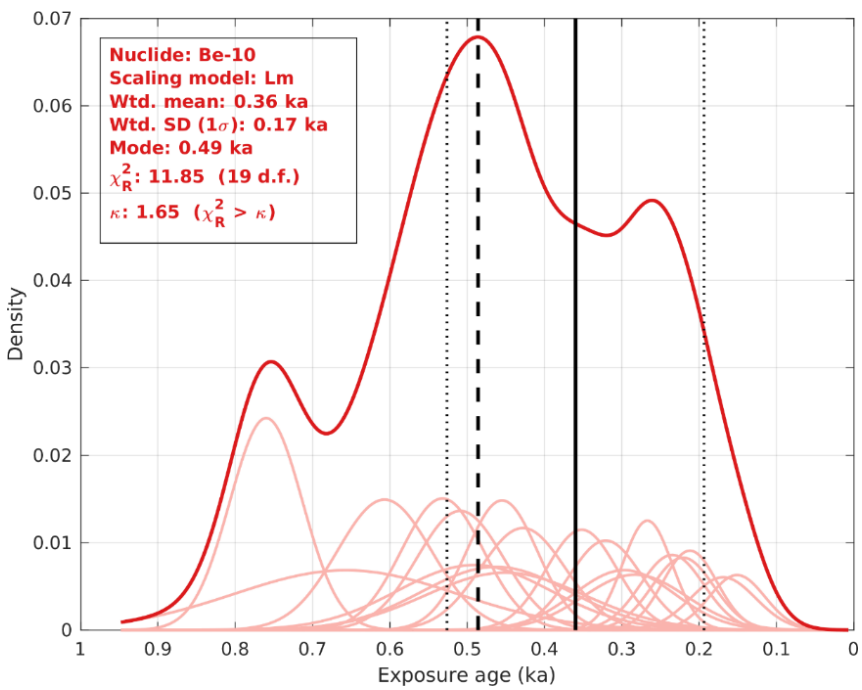


**Figure 13. Probability density of exposure ages for the UNI IV moraine complex (=20).** Graph based on the exposure ages as discussed in this work**.** The two outliers (UNI 1907a and UNI 1907b) were not considered. The mode (dashed black line), weighted mean (solid black line), and weighted standard deviation (dotted black line) are presented. Graphs were made using the online calculator *iceTEA* (ice-tea.org/en/; Jones et al., 2019).

We propose that the UNI IV moraine complex was deposited (and reworked) by more than one glacier expansion within the last 1000 years, making up a morainic deposit between about 760 and 150 years ago (Figure 13). In this scenario different glacier expansions incorporated boulders from the recently deglaciated landscape (century-scale) without resetting their cosmogenic $^{10}$Be clock. Thus, the range of exposure ages between the distal till surface and the moraine ridges A through D denotes the timing of the whole UNI IV moraine complex deposition.

In order to interpret the timing of specific glacial advances that produced this moraine complex we then apply a cluster $^{10}$Be approach (e.g., Stroeven et al., 2011). These authors suggested that if the dispersion of ages obtained from an assemblage of glacial-derived landforms has certain clusters or subpopulations, these may indicate distinct glacial events. We analyzed the frequency of all $^{10}$Be exposure ages and found two main clusters (Figure 14) ranging from 530 to 430 years ago (n=7) and 350 to 150 years ago (n=10). According to this approach, the glacier expansions ended first by the late 16$^{th}$ century and then by early to mid-19$^{th}$ century. Another possible expansion of the Universidad Glacier could have occurred by the early 18$^{th}$ century.

Against our interpretation , it could be argued that the size of the boulders conditioned their exposure age due to snow shielding or exhumation (Gosse and Phillips, 2001; Dunai, 2010). Nevertheless, we see no obvious relation between size and age. A particular case is boulder UNI 1907, from which we obtained two samples, "a" and "b," side-by-side that yielded exposure ages of 1070±160 and 1535±85 years ago (Figure 12d), respectively. These two exposure ages are significantly older than all the other exposure ages obtained from the moraine UNI IV. We interpret these ages as evidence of inheritance in this boulder from exposure before the build-up of the UNI IV moraine complex, so considered as outliers.

Taken at face value, the $^{10}$Be ages from the distal till surface and the frontal moraine A suggest the Universidad Glacier reached approximately the same ice extent first at 760±55 to 430±55 years ago (n=4) and then at 220±40 to 150±35 years ago (n=2). The older exposure ages were collected from the most distal till surface, while the younger exposure ages were obtained from boulders resting on the top of the moraine A, the outermost morainic ridge (Figure 11b). We thus interpret that the Universidad Glacier reached about the same maximum extent two times during the last 1000 years: first by the late 16$^{th}$ century and then again by the early to mid-19$^{th}$ century. These findings are consistent with our above interpretation of the chronology of two main glacial expansions based on the cluster approach. The prominent A-B left lateral moraine illustrates this long-term morainic production. The $^{10}$Be samples collected side-by-side from the top of this lateral include three different exposure ages (235±40, 320±45, and 655±145 years ago; Fernández et al. 2022), suggesting that this moraine is a composite landform (cf. Kirkbride and Winkler, 2012) where the Universidad Glacier recurred several times during the latest Holocene. The same could be proposed for the basal till plain where nearby boulders yielded exposure ages of 605±65 and 265±35 years ago.

In summary, our best interpretation of the geomorphic and $^{10}$Be data is that the latest Holocene maximum glacial advance culminated first by the late 16$^{th}$ century and then again by the early to the mid-19$^{th}$ century, reaching the same extent in both times. During the latest main glacial advance, the glacier built the moraine A. After this, we interpret a continuous active glacier retreat trend interrupted by multiple ice readvances or stillstands that built the moraine ridges B-G and reworked boulders from previous glacial expansions into the newly formed landforms, including flutes.

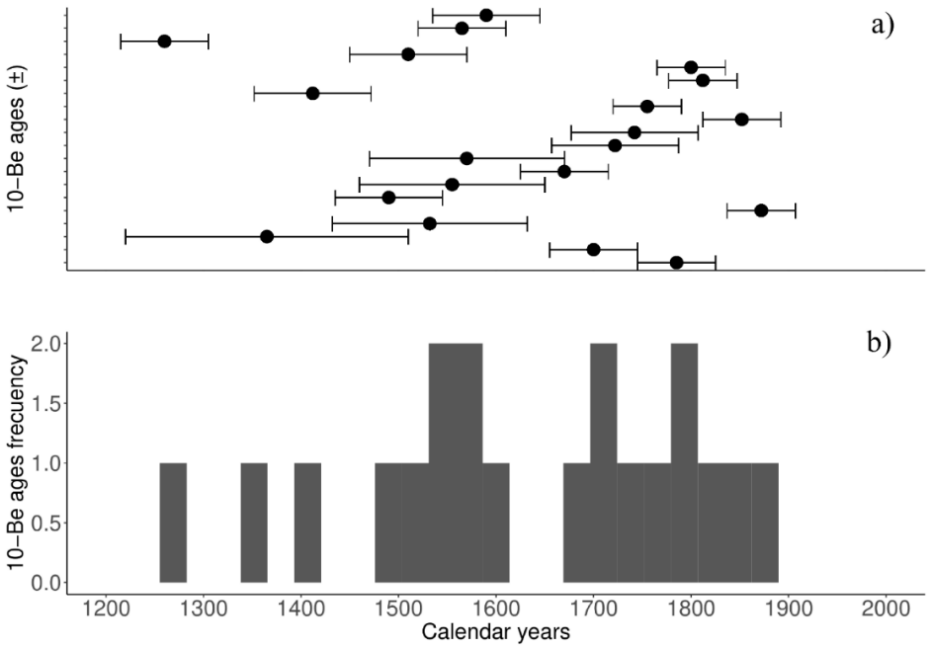


**Figure 14. Frequency of $^{10}$Be exposure ages available for the UNI IV moraine complex represented in calendar years (n=20). (a)** $^{10}$Be exposure ages with their corresponding 1 sigma bar; **(b)** Graph shows two main clusters of $^{10}$Be exposure ages that we interpret as the timing of the two main glacial advances. The three older boulders yielded a range of 760±55 to 605±65 years ago may indicate a previous glacier advance. The first group of seven exposure ages is between 530±55 and 430±55 years ago. The second group of ten boulders yielded exposure ages from 350±45 to 150±35 years ago. The outliers (UNI 1907a and UNI 1907b) were not considered in (a) and (b). The surface exposure ages presented in this work refer to the year 2020.

**Table 2.** Analytical data used for age calculation of the samples of the UNI IV moraine complex of the Universidad Glacier

| Sample name | Latitude (DD) | Longitude (DD) | Elevation (m a.s.l.) | Shielding factor | Sample thickness (cm) | Quartz dissolved (g) | $^{9}$Be carrier (mg) | $^{10}$Be/$^{9}$Be ($10^{-12}$)* | $^{10}$Be conc. ($x10^{4}$) (at/g) | Error (%)* |
|---|---|---|---|---|---|---|---|---|---|---|
| **Samples of the current study collected in 2020, prepared and measured in 2021** | | | | | | | | | | |
| UNI 2013 | -34.731722 | -70.371056 | 2324 | 0.954 | 3.1 | 61.20 | 0.2083 | 0.048 | 1.088 | 6.2 |
| UNI 2012 | -34.731222 | -70.371611 | 2331 | 0.957 | 2.1 | 52.84 | 0.2076 | 0.027 | 0.699 | 11 |
| UNI 2014 | -34.731722 | -70.371056 | 2324 | 0.955 | 2.3 | 61.53 | 0.2078 | 0.027 | 0.616 | 10.2 |
| UNI 2015 | -34.731667 | -70.370278 | 2335 | 0.959 | 3.6 | 57.30 | 0.2081 | 0.024 | 0.579 | 12.7 |
| UNI 2011 | -34.730528 | -70.371944 | 2342 | 0.959 | 1.9 | 57.97 | 0.2074 | 0.013 | 0.302 | 17.8 |
| UNI 1902 | -34.731139 | -70.370278 | 2336 | 0.960 | 2 | 39.87 | 0.2081 | 0.021 | 0.738 | 9.8 |
| UNI 2002 | -34.726833 | -70.359694 | 2472 | 0.973 | 1.7 | 56.99 | 0.2069 | 0.016 | 0.398 | 11.8 |
| UNI 2003 | -34.726694 | -70.359528 | 2477 | 0.974 | 1.7 | 61.51 | 0.2083 | 0.042 | 0.953 | 10.0 |
| UNI 2009 | -34.725722 | -70.358528 | 2471 | 0.971 | 2.9 | 60.57 | 0.2085 | 0.014 | 0.315 | 16.5 |
| UNI 1907b | -34.724528 | -70.353167 | 2503 | 0.969 | 3 | 57.02 | 0.2090 | 0.1135 | 2.782 | 4.2 |
| Preparation blank Bl 24 | | | | | | | 0.3081 | 0.011** | | 8.6** |
| **Samples of the current study collected, prepared and measured in 2019** | | | | | | | | | | |
| UNI 1901 | -34.730611 | -70.372167 | 2342 | 0.967 | 1.7 | 56.32 | 0.2005 | 0.009 | 0.211 | 23.5 |
| UNI 1906 | -34.724694 | -70.353694 | 2494 | 0.966 | 2.7 | 52.08 | 0.1980 | 0.017 | 0.441 | 21.9 |
| UNI 1907a | -34.724528 | -70.353167 | 2503 | 0.969 | 1.8 | 38.97 | 0.2017 | 0.055 | 1.907 | 14.6 |
| UNI 1805 | -34.723056 | -70.350917 | 2500 | 0.969 | 2 | 45.38 | 0.2001 | 0.026 | 0.756 | 20.3 |
| UNI 1909 | -34.723528 | -70.352556 | 2485 | 0.963 | 2.7 | 41.99 | 0.1993 | 0.008 | 0.253 | 24.9 |
| UNI 1908 | -34.721639 | -70.349556 | 2492 | 0.965 | 2.6 | 47.70 | 0.1834 | 0.016 | 0.420 | 23.7 |
| **Samples published in Fernández et al. (2022), collected, prepared and measured in 2019** | | | | | | | | | | |
| UNI 1801 | -34.715968 | -70.337477 | 2625 | 0.977 | 2.6 | 54.34 | 0.2004 | 0.016 | 0.385 | 17.3 |
| UNI 1802 | -34.715601 | -70.337388 | 2625 | 0.977 | 1.9 | 60.67 | 0.1997 | 0.024 | 0.524 | 14.6 |
| UNI 1803 | -34.715239 | -70.337252 | 2626 | 0.976 | 1.8 | 49.60 | 0.1950 | 0.043 | 1.141 | 21.9 |
| UNI 1904 | -34.723556 | -70.359944 | 2436 | 0.970 | 1.6 | 55.29 | 0.2005 | 0.021 | 0.514 | 13.1 |
| UNI 1905 | -34.723694 | -70.360056 | 2430 | 0.973 | 1.7 | 50.21 | 0.1989 | 0.025 | 0.667 | 22.9 |
| UNI 1903 | -34.729639 | -70.371167 | 2355 | 0.959 | 1.3 | 30.56 | 0.2006 | 0.015 | 0.648 | 20.7 |
| Preparation blank BI 11 | | | | | | | 0.1997 | 0.010** | | 11.6** |
| Preparation blank BI 12 | | | | | | | 0.1982 | 0.008** | | 18.3** |

* The ratios are corrected to the background of the blank samples. The errors include the error of the blanks and AMS standards. Blank Bl24 was used to correct ratios of UNI 2013-2009, 1902 and 1907b samples. A weighted average of blanks BI 11 and 12 was used to correct ratios of UNI 1801-1803, 1805, 1901, 1903-1906, 1907a, 1908 and 1909 samples.

** Blank ratios and errors are presented without background correction.

**Table 3.** Geomorphic context and $^{10}$Be exposure ages of the samples of the UNI IV moraine complex of the Universidad Glacier. The samples are arranged according to their morphostratigraphical position

| Sample name | Type of sample | Elevation (m a.s.l.) | Sample height (cm) | **Exposure age (St) (year)** | **Exposure age (Lm) (year)** | **Calendar year (Lm)**** | **Exposure age (LSDn) (year)** |
|---|---|---|---|---|---|---|---|
| UNI 2013 | Boulder on till surface distal to moraine ridge A | 2324 | 120 | 620±45 | **760±55** | **1260±55** | 800±55 |
| UNI 2012 | Boulder on till surface distal to moraine ridge A | 2331 | 110 | 395±45 | **510±60** | **1510±60** | 545±60 |
| UNI 2014 | Boulder on till surface distal to moraine ridge A | 2324 | 99 | 350±40 | **455±50** | **1565±50** | 490±50 |
| UNI 2015 | Boulder on till surface distal to moraine ridge A | 2335 | 134 | 330±45 | **430±55** | **1590±55** | 460±60 |
| UNI 2011 | Boulder on frontal moraine ridge A | 2342 | 158 | 170±30 | **220±40** | **1800±40** | 245±45 |
| UNI 1901 | Boulder on frontal moraine ridge A | 2342 | 135 | 115±30 | **150±35** | **1870±35** | 170±40 |
| UNI 1902 | Boulder between frontal ridges of moraines A and B | 2336 | 390 | 410±45 | **530±55** | **1490±55** | 565±60 |
| UNI 1801 | Boulder embedded on lateral moraine ridge B | 2625 | 124 | 175±30 | **235±40*** | **1785±40** | 255±45 |
| UNI 1802 | Boulder embedded on lateral moraine ridge B | 2625 | 118 | 240±35 | **320±45*** | **1700±45** | 345±50 |
| UNI 1803 | Boulder on lateral moraine ridge B | 2626 | 90 | 520±115 | **655±145*** | **1365±145** | 690±155 |
| UNI 1903 | Boulder between frontal moraine ridges B and C | 2355 | 240 | 355±75 | **465±95*** | **1555±95** | 495±105 |
| UNI 2002 | Boulder on flute between latero-frontal moraine ridges C and $D_1$ | 2472 | 148 | 200±25 | **265±35** | **1755±35** | 290±35 |
| UNI 2003 | Boulder on flute between latero-frontal moraine ridges C and $D_1$ | 2477 | 81 | 480±50 | **605±65** | **1415±65** | 640±65 |
| UNI 2009 | Boulder on frontal moraine ridge $D_1$ | 2471 | 51 | 160±25 | **210±35** | **1810±35** | 235±40 |
| UNI 1907b | Boulder on lateral moraine ridge $D_1$ | 2503 | 120 | 1395±75 | 1535±85 | 485±85 | 1605±85 |
| UNI 1906 | Boulder on lateral moraine ridge $D_1$ | 2494 | 283 | 220±50 | **300±65** | **1720±65** | 320±70 |
| UNI 1907a | Boulder on lateral moraine ridge $D_1$ | 2503 | 120 | 955±145 | 1070±160 | 950±160 | 1100±165 |
| UNI 1805 | Boulder on lateral moraine ridge $D_2$ | 2500 | 200 | 375±75 | **490±100** | **1530±100** | 525±105 |
| UNI 1909 | Boulder on lateral moraine ridge $D_2$ | 2485 | 113 | 130±30 | **170±40** | **1850±40** | 185±45 |
| UNI 1908 | Boulder between lateral moraine ridges $D_2$ and E | 2492 | 236 | 210±50 | **285±70** | **1735±70** | 310±75 |
| UNI 1904 | Embedded boulder on flutes field between moraine ridges $D_2$ and E | 2436 | 103 | 265±35 | **350±45*** | **1670±45** | 380±50 |
| UNI 1905 | Superimposed boulder on flutes field between moraine ridges $D_2$ and E | 2430 | 103 | 345±80 | **450±105*** | **1570±105** | 485±110 |

The exposure ages are calculated using CRONUS-Earth calculator (http://hess.ess.washington.edu/math/) version 3 for three different scaling schemes (St, Lm, LSD; Lal, 1991; Stone, 2000; Balco et al., 2008; Lifton et al., 2014). The exposure ages calculated with "Lm" time-dependent scaling scheme and standard atmospheric pressure are used for discussion and result presentation (Lal, 1991; Stone, 2000). All ages are calculated with the local $^{10}$Be production rate for southern South America of 3.71±0.11 atoms/g/yr (Kaplan et al., 2011). We use a sample rock density of 2.65 g/cm$^3$ and apply no erosion correction. Reported $^{10}$Be/$^{9}$Be for 07KNSTD is $2.85 \cdot 10^{-12}$ (Nishiizumi et al., 2007).

* The result is originally published in Fernández et al. (2022).

### 3.5.2. Glacier records for the central Andes of Chile and Argentina

Previous studies carried out in the present-day glacier forefields on the western and eastern slopes of the Andes at this latitude have also reported glacier advances during the latest Holocene. Sagredo et al. (2017) mapped four moraine belts arranged between 1730 to 2000 m a.s.l. and used TCN ($^{10}$Be) dating to conclude that the Chilean Cipreces Glacier was expanded between ~950 and 550 years ago. Earlier, Röthlisberger (1986) obtained a radiocarbon age of 625±155 years BP for a paleosol buried by the inner lateral moraine in the Río Cipreses valley, which led him to conclude that this glacier advanced at that time. Sagredo et al. (2017) distinguished three to four moraine ridges at 4420 and 4620 m a.s.l. in the foreland of the El Tapado Glacier further north (30° S). Using $^{36}$Cl, they inferred a period from 1000 to 500 years ago when moraines were deposited. More recently, Price et al. (2022) obtained $^{36}$Cl age of ~450 to 280 years ago for nested moraines at 1700 m a.s.l. in the Monte Sierra Nevada (38° S). In Argentina, Espizua (2005) mapped four moraines in the El Azufre valley (35° S) and $^{14}$C dated two basal peats below the inner moraine in 400±100 cal years BP and 390±100 years cal BP. Espizua and Pitte (2009) identified three moraines in the forefield of El Peñon Glacier (35° S) and established a minimum radiocarbon age of <280 cal years BP for the inner moraine. Moreover, they mapped a hummocky moraine at 2950 m a.s.l. in the valley of Las Damas Glaciers (34° S), 3 km from the present-day ice front. This hummocky moraine was dated with minimum $^{14}$C ages of 390±80 and <320 cal years BP. In summary, most of the available data show that glaciers in the Andes of central Chile and Argentina fluctuated over its maximum latest Holocene between the 14$^{th}$ and 19$^{th}$ centuries.

### 3.5.3. Paleoclimate context

Together with glaciers, ecological and sedimentological proxies evidence a distinct wetter and colder climate between about the 13th to 19th centuries in central Chile. Veit (1996) used samples of paleosols of the Norte Chico (27°—33° S) to identify an overall wetter period between the 14th to 19th centuries. In fact, analysis of pollen demonstrated an increase in humidity during the 14th century (Maldonado and Villagrán, 2002). Jenny et al. (2002), based on sediment accumulating in the former Laguna de Aculeo (33° S, at 350 m a.s.l.), interpreted a high frequency of flood events between the 14th to 18th centuries, with a peak around the 15th to 17th centuries associated to a wetter climate in central Chile. Similar conclusions were obtained from pollen in the same site (Villa-Martínez et al., 2004). In the high Andes, pollen analysis of lake sediments (32° S, at 3050 m a.s.l.) revealed that cooler summers and extended ice cover occurred first around the early 16th and 19th centuries and again during the second half of the 19th century (Martel-Cea et al., 2016). Also, Masiokas et al. (2012), based on tree-ring and historical records, made regression models to derive extremely snowy conditions over the last millennium in the Andes of central Chile and Argentina during the first half of the 13th century, by the mid-15th century, end of the 16th century, and mid-17th and 18th centuries. Altogether, these data confirm a generalized cold and humid period mostly between the 14th and 19th centuries. Nonetheless, paleoclimatic modeling based on tree rings, pollen, and historical records suggest that central Chile has had a high climate variability over the last 1000 years (Villalba, 1994; Le Quesne et al., 2006, 2009; Masiokas et al., 2012; Dätwyler et al., 2018; Morales et al., 2020). The atmospheric variability in interannual, interdecadal, and centennial timescale challenges the interpretation of climate forcing.

### 3.5.4. Paleoclimate forcing

In order to assess the climate mechanisms for past glacier/climate change, we compared the frequency of the Universidad Glacier $^{10}$Be exposure ages with reconstructions of the IPO Index (Porter et al., 2021) and the summer (DJF) SAM Index (Dätwyler et al., 2018) and test the link between glacier changes and these oceanic-atmospheric indexes during the latest Holocene (Figure 15). The IPO shares a similar sea surface temperature signature with the PDO, and several authors suggested that they are comparable in describing tropical and subtropical climate variability (Folland et al., 2002; Dong and Dai, 2015; Porter et al., 2021). This reconstruction of the IPO/PDO Index over the past ~550 years (1450-1996 CE) was based on ice core records from tropical South America, the Tibetan Plateau, the Antarctic Peninsula, and southeast Alaska, which exhibit Pacific climate variability on an interannual and decadal time scale (Porter et al., 2021). The lack of reconstructions of older IPO/PDO conditions preclude comparisons with our oldest set of $^{10}$Be exposure ages. The SAM Index by Dätwyler et al. (2018) was reconstructed based on proxy data including tree-ring and ice core records obtained from western South America (including central Chile and Patagonia), Australia, New Zealand, and Antarctica.

As shown in Figure 15a, the reconstructed SAM Index remains mostly negative from the early 15$^{th}$ century to the mid-19$^{th}$ century, indicating cold and wet conditions associated with the northward shift of the SWW (Villalba et al., 2012; Morales et al., 2020). Around the mid-15$^{th}$ century, the values of the SAM were very low until about the late-16$^{th}$ century, when the first maximum advance of the Universidad Glacier occurred. Again, the SAM Index shows a second distinct negative phase between the mid-18$^{th}$ century and the mid-19$^{th}$ century, during the second maximum advance of the Universidad Glacier. In the mid-20$^{th}$ century, the SAM returned to negative values when the Universidad Glacier had one of its last minor readvances, according to

our mapping (Figure 11b) and Lliboutry's report (1958). In other words, the deposition of the UNIV IV moraine complex by the Universidad Glacier occurred mainly in a phase dominated by a negative SAM.

During the mid-15$^{th}$ century and the end of the 19$^{th}$ century, the period that cover most of the UNI IV moraine complex formation, the IPO/PDO Index (Figure 15b) remained mostly negative, implying concurrent La Niña-like conditions (Porter et al., 2021). These conditions are inconsistent with positive glacier mass balance and advances recorded in the Andes (Rabatel et al., 2010; Barria et al., 2019). Thus, a more consistent link between SAM and glacier fluctuations seems to have operated during the last millennium in the Andes of central Chile. This conclusion seems to contradict recent studies relating positive glacier mass balances with El Niño conditions during the second half of the 20$^{th}$ century (Espizua and Pitte 2009; Farías-Barahona et al., 2019). We argue that in order to produce significant ice expansion and to build massive moraines in the Andes of central Chile, such as UNI IV moraine complex, a sustained climate condition is needed over long-time, rather than short-term individual years characterized by positive glacier mass balance.

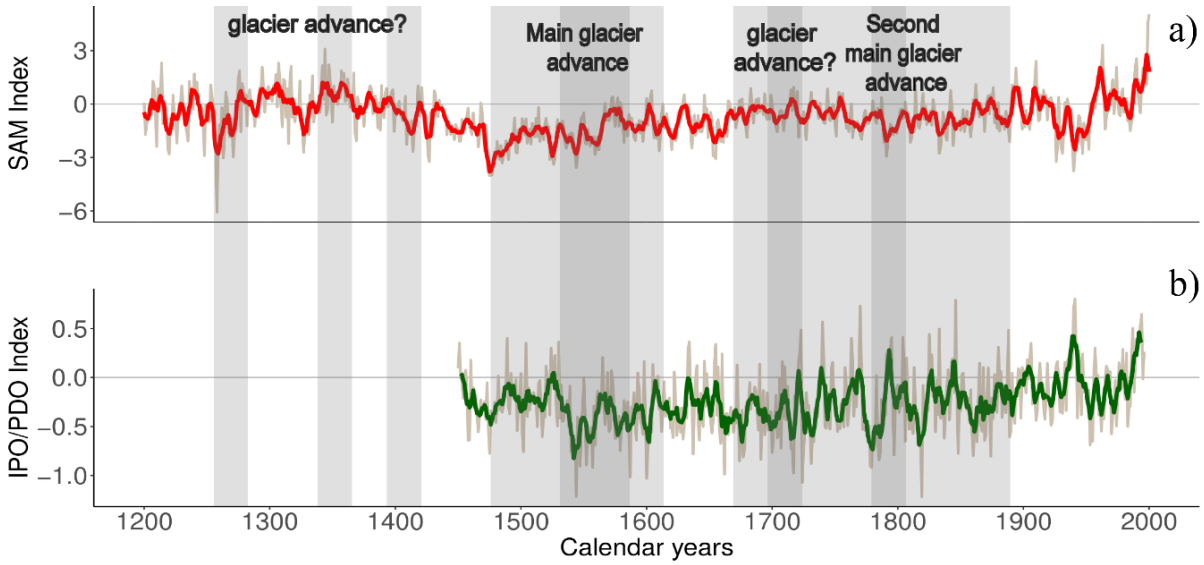


**Figure 15. Universidad Glacier $^{10}$Be chronology (in gray) compared to climate indexes for the latest Holocene. a)** Reconstruction of the Southern Annular Mode (SAM) Index over the last millennium during the austral summer (DJF) (Dätwyler et al., 2018); **b)** reconstruction of the Interdecadal Pacific Oscillation (IPO/PDO) (Porter et al., 2021). The moving average for the SAM and IPO/PDO was calculated for a 5-year window. The grey areas indicate the distribution of $^{10}$Be exposure ages available for the UNI IV moraine complex. Darker grey bars are detected in clusters of $^{10}$Be exposure ages.

### 3.5.5. Wider implications at regional and hemispheric scale

From a broad perspective, our geochronological data show an overlap with other glacial reconstructions carried out in the tropical and southern latitudes of the Southern Hemisphere, denoting a similar climatic behavior during the latest Holocene. To the north of our study area, ice expansion by the 19$^{th}$ century was also recorded in the Tropical Andes (13°—16° S; Rabatel et al., 2005; Licdardi et al., 2009; Stroup et al., 2014). In Patagonia, glaciers between 49° and 51° S first expanded between the 15$^{th}$ and 17$^{th}$ centuries and a second after the early 19$^{th}$ century (Reynhout et al., 2019; García et al., 2020). Similarly, glacier advances in New Zealand (39°—43° S) were recorded from the 15$^{th}$ century to the mid-to-late 19$^{th}$ century by Schaefer et al. (2009). Also in New Zealand, Eaves et al. (2019) demonstrated glacier variations from the 16$^{th}$ century to the mid-to-late 19$^{th}$ century. Glacier fluctuations reported from the Andes and the New Zealand Alps thus denote similar timing and indicate a hemispheric-wide glacier expansion at both sides of the South Pacific Ocean first during the 15$^{th}$ and 16$^{th}$ centuries, and then by the 19$^{th}$ century. These extratropical glacier fluctuations evidence periods of stronger and northward shifted SWW.

## 3.6. **Conclusions**

We provide a new $^{10}$Be exposure age chronology to constrain the Universidad Glacier fluctuations during the latest Holocene (<1000 years ago) in the Andes of central Chile, and its associated climate implications. The $^{10}$Be chronology suggests that the Universidad Glacier had two main advances during the last millennium: the first culminated by the end of the 16$^{th}$ century, and the second by the early to mid-19$^{th}$ century. Both advances reached approximately the same maximum extent (~3 km from present day glacier front). We cannot rule out other glacier advances by the 13$^{th}$ and early 18$^{th}$ centuries. The timing of these glacier advances and the overall timeframe of the UNI IV moraine complex deposition occurred alongside with persistent reconstructed negative values of the Southern Annular Mode (SAM). Thus, cold and wet conditions in response to a northward migration of the Southern Westerly Winds (SWW) during a negative SAM phase triggered extended glaciers in central Chile between about the 13$^{th}$ century to the mid-19$^{th}$ century. Our data do not support cold and dry conditions for central Chile as suggested by the reconstructed IPO/PDO negative phase between the mid-15$^{th}$ century until the mid-19$^{th}$ century. Near-synchronous glacier advances in the southern extratropics at both sides of the Pacific Ocean can be explained by a reinforced SWW circulation in the southern middle latitudes as far north as 34ºS during the latest Holocene.

# 4. EVIDENCE OF LAST GLACIAL MAXIMUM AND A LATE GLACIAL ADVANCE IN UNIVERSIDAD GLACIER VALLEY (34° S), ANDES OF CENTRAL CHILE: PALEOCLIMATE IMPLICATIONS

Este cuarto capítulo se presenta como artículo científico y por ese motivo está escrito en inglés. Este capítulo prontamente será enviado a una revista científica internacional para su evaluación y publicación. La numeración de figuras y tablas es correlativa a toda la tesis doctoral, por lo cual las figuras y tablas expuesta aquí no guardan exclusiva relación con este capítulo.

## 4.1. **Introduction**

The Last Glacial Maximum (LGM; 16 to 26.5 ka; Clark and Mix, 2002; Clark et al., 2009) and the Last Glacial Termination (LGT; 11 to ~18 ka; Denton et al., 2010) are two of the most studied climate events at the end of the last glacial period (Mercer, 1984; Broecker, 1998; Broecker and Denton, 1990; Denton et al., 1999a, 1999b, 2021; McCulloch et al., 2000; Yokoyama et al., 2000; Monnin et al., 2001; Harrison, 2004; Otto-Bliesner et al., 2006; Schaefer et al., 2006; Barker et al., 2009; Rojas et al., 2009; Liu et al., 2009; Otto-Bliesner and Brady, 2010; Menviel et al., 2011; Chavaillaz et al., 2013; Hughes and Gibbard, 2015; Fogwill et al., 2017; Soteres et al., 2022). The LGM refers to the most recent maximum of terrestrial global ice volume linked to a minimum in the northern hemisphere summer insolation (Mix et al., 2001; Clark et al., 2009). This orbital-controlled condition allowed ice to remain in the ablation season, provoking positive feedback leading to the glacier's growing process (Ruddiman, 2006). The LGT refers to the abrupt end of the last glacial period and the transition from the LGM toward the present interglacial period (Osman et al., 2021). Massive global glacier retreat has been associated with the rising of northern middle-latitude summer insolation and northern ice sheet's oversized instability, a southern shift of main tropical and extratropical ocean and climate regimes, and Southern Ocean ventilation of $CO_2$ (Denton et al., 2010). The trigger of this global warming trend is still debated, but the role of the Southern Westerlies circulation shifts seems critical (e.g., Toggweiler et al., 2006; Denton et al., 2021).

The Milankovitch theory (Milankovitch, 1941) is the most accepted model for the origin and the end of the ice ages. Milankovitch postulated that variations in summer insolation received at 65° N at the 23 ka periods of precession and the 41 ka period of Earth rotation-axis obliquity should

be key to the growth and decay of ice sheets (Huybers and Wunsch, 2005). According to this, the variation of summer insolation in the high northern latitudes determines long-term planetary (orbital scale), or at least hemispheric-wide, climate changes. Subsequent works have confirmed the causal role of orbital cycles in ocean and climate, together with the timing of ice cycles (Hays et al., 1976; Lüthi et al., 2008). Nonetheless, it has been argued that orbital control alone does not explain the causes of the glacier changes worldwide over the LGM and the LGT (Mercer, 1984; Broecker and Denton, 1990; Raymo, 1997; Denton et al., 1999a, 2005, 2010, 2021, 2022; Huybers and Denton, 2008; Doughty et al., 2015; García et al., 2018). Although the low summer insolation in the Northern Hemisphere is out of phase with the high summer insolation intensity in the Southern Hemisphere, several works have suggested that glacier growth occurred almost synchronously during the LGM in both hemispheres (Mercer, 1984; Lowell et al., 1995; Denton et al., 1999a, 1999b, 2021; Schaefer et al., 2009; Putnam et al., 2013). Similar paradox is observed in the LGT, as despite the opposite interhemispheric insolation signal, it has been propossed that the decay of the glaciers was a global phenomenon (Denton et al., 2021; Soteres et al., 2022). Some works suggested the existence of interhemispheric teleconnections that implied atmospherical and oceanic readjustments to explain the near synchronous responses of the glaciers at the end of the last glacial period (Mercer, 1984; Broecker, 1998; Broecker and Denton, 1990; Ruddiman, 2006; Toggweiler et al., 2006; Anderson et al., 2009; Denton et al., 2021b). The near-simultaneous climate change in both hemispheres posed a problem that Mercer (1984) dubbed early as the “fly in the ointment of the Milankovitch theory”.

Mid-latitude glaciers are suitable for reconstructing the evolution of the global atmospheric and oceanic systems during the end of the last glacial (Harrison, 2004; Zech et al., 2006, 2007). The Andes of central Chile (29°—35° S; Figure 16a) are a key region in the Southern Hemisphere to reconstructing the late-Quaternary climate because they are located between the tropical and the

Antarctic influence. The few reconstructions of glacial changes over the last glacial period in this area suggest certain synchrony with the LGM (Zech et al., 2006, 2007; Charrier et al., 2019; Aguilar et al., 2022). Although there are no works particularly dedicated to understanding the evolution of glaciers in central Chile during the LGT, it was proposed a possible influence of the Trade winds during the transition glacial-non glacial climate (Zech et al., 2007).

Unveiling the timing, magnitude, and structure of the Andes of central Chile responses during the end of the last glacial period is required to understand the interhemispheric teleconnections and the atmospheric-oceanic forcings that control the ice ages and their terminations. In this work, we aim to establish the late-Quaternary glacier fluctuations in the Andes of central Chile, and, in addition, we discuss the possible causal mechanisms that triggered those ice changes. We reconstruct the extent changes of the Universidad Glacier (34° 42' S, 70° 20' W) over the LGM and the LGT using geomorphological mapping and $^{10}$Be exposure dating of moraines to help answer the following questions: When did late-Quaternary glacial advances occur in the Andes of central Chile? These glacier advances were synchronous or not with glacier events global or hemispheric? Which atmospheric system triggered those glacier expansions? The Universidad Glacier valley, together with other sites in central Chile, includes preserved late-Quaternary glacial landforms, such as moraines, that allow establishing the extent and timing of former glacier fluctuations (e.g., Santana, 1967; Caviedes and Paskoff, 1975; Abele, 1982; Zech et al., 2006, 2007, 2008; Charrier et al., 2019; Fernández-Navarro et al., 2023).

## 4.2. **Study area**

The Andes of central Chile (Figure 16a) are a tectonic and volcanically active mountain range. Their highest peaks are above ~6000 m a.s.l. and are usually covered by ice (e.g., Tupungato volcano). The successive Quaternary glaciations sculpted deep and long u-shape valleys and many of them have been reworked with sediments associated with paraglacial (Riquelme et al., 2011), volcanic (Abele, 1982), or tectonic (Antinao and Gosse, 2009) processes . The high rate of debris supply from the Andes slopes has covered Quaternary moraines making challenge their identification and mapping (Abele, 1984; Deckart et al., 2014).

The present-day regional climate is characterized by a Mediterranean climate with dry summers and wet winters. During the austral summer, a south-shifted Subtropical Southeast Pacific Anticyclone (SPA) blocks the influence of the Southern Westerly Winds (SWW) in central Chile (Garreaud, 2009). In the winter, the SWW reach the Andes of central Chile, bringing precipitations and colder temperatures due to a weaker SPA (Figure. 16b; Rutllant and Fuenzalida, 1991; Escobar and Aceituno, 1998; Flores-Aqueveque et al., 2020). The high altitude that reaches the Andes makes this mountain range very sensitive to climate variations due to the orographic effect (Garreaud, 2009).

The mean annual precipitation above 2500 m a.s.l. varies approximately from 500 mm at ~30° S to 1500 mm at ~34° S (Carrasco et al., 2005). The glaciers' equilibrium line altitude (ELA) at 4300-4400 m a.s.l. occurs at 32° S, falling to 3700-3800 m a.s.l. at 34° S (Azócar and Brenning, 2010). The regional mean annual air temperature at ~2400 m a.s.l. is 8.3 °C, according to the data recovered from the Embalse El Yeso station (33° S; Barcaza et al., 2017).

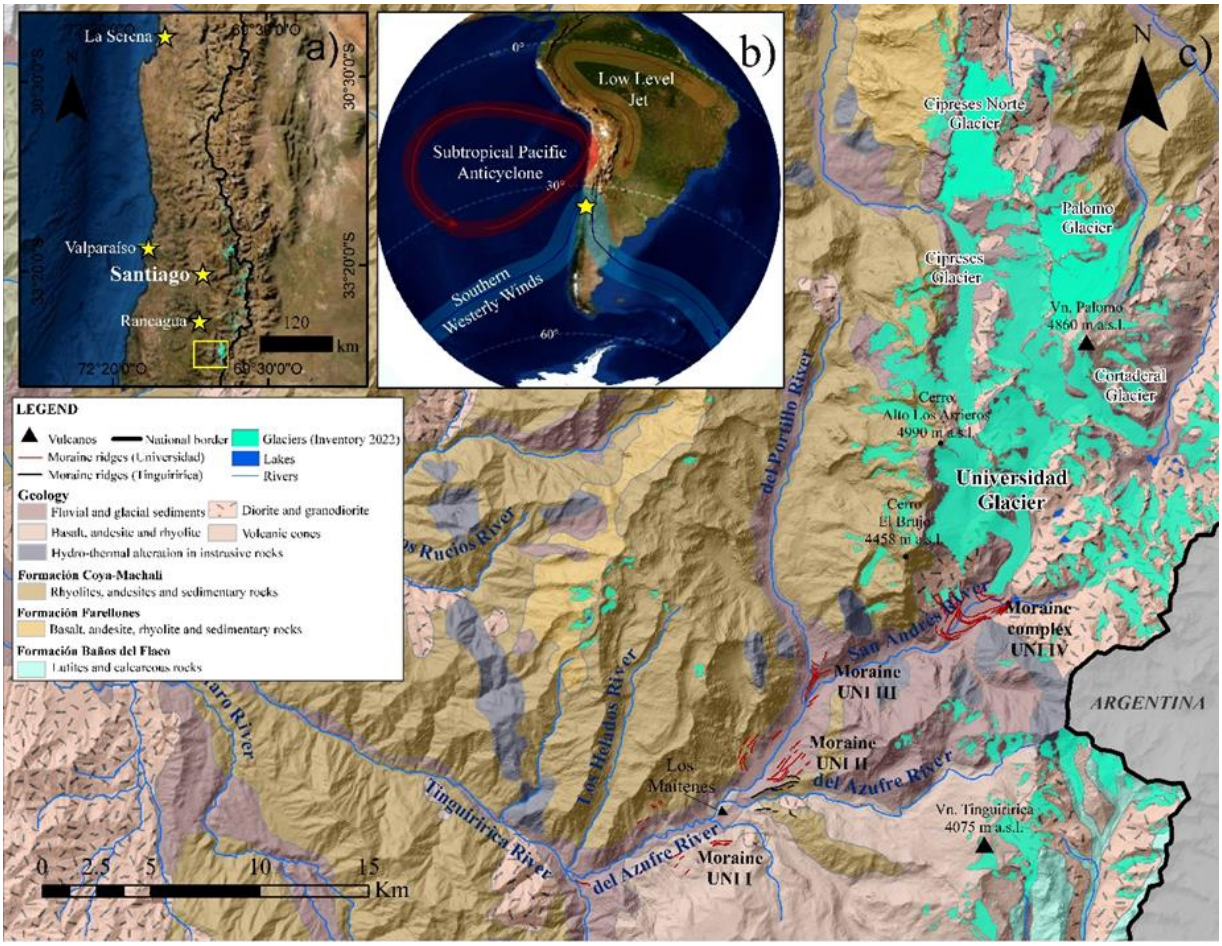


**Figure 16. Study area in the hemispherical and regional context. (a)** Universidad Glacier is the largest ice mass in the Andes of central Chile. The study area is framed by the yellow box; **(b)** Main atmospheric systems in South America. The yellow star indicates the study area; **(c)** Universidad Glacier and nearby ice bodies framed in the geological context. The four moraines (UNI I-IV) mapped along the Universidad Glacier valley are shown in red color.

The glaciers in the Andes of central Chile respond to moisture supply and temperature changes related to the SWW circulation patterns. The recent interannual variability in the latitudinal position of the SWW has been linked with the El Niño Southern Oscillation (ENSO) cycle (Rutllant and Fuenzalida, 1991; Escobar and Aceituno, 1998; Montecinos and Aceituno, 2003; Garreaud, 2009) and the Southern Annular Mode (Garreaud et al., 2020). In a millennial scale, it was suggested that the SWW changed their intensity and latitudinal position through the last ice age in the Southern Hemisphere, becoming the paleoclimate conditions from central Chile to Patagonia wetter and colder (Heusser, 1989, 1990; Lamy et al., 1998, 1999, 2000, 2015; Valero-Garcés et al., 2005; Rojas et al., 2009; García et al., 2012, 2019; Sagredo et al., 2014; Masiokas et al., 2016; Mendelova et al., 2017).

The Universidad Glacier is located in the southern position of the Andes of central Chile (Figure 16c). Its altitudinal range is from ~2500 to 4540 m a.s.l. and the glaciated area covers 26 $km^2$ (Dirección General de Aguas, 2022b), making it the largest glacier in the Andes of central Chile. The Universidad Glacier and the Cipreses, Cipreses Norte, Cortaderal, and Palomo glaciers add up to ~70 $km^2$ of ice surface (Dirección General de Aguas, 2022b). These glaciers are part of the "La Sierra del Brujo", a mountain chain composed of granodiorites, rhyolites, and andesites (Charrier and Lillo, 1973) that includes the Cerro El Brujo (4458 m a.s.l.), the Cerro Alto Arrieros (4990 m a.s.l.), and the volcano El Palomo (4860 m a.s.l.). The Universidad Glacier valley has ~20 km from the present-day glacier front to the junction of the Tinguiririca and del Azufre rivers (Figure 16c). Recently, Fernández et al. (2022, 2023) identified four moraine belts between ~1100 and 2500 m a.s.l. and labeled them as UNI I to UNI IV, from the distal to the proximal position. The UNI IV moraine is a moraine complex produced in the last millennium (Fernández et al., 2022, 2023). In this work, we present and discuss the geomorphic and geochronologic data of the UNI I-III moraines and their paleoclimatic implications.

## 4.3. **Material and methods**

### 4.3.1. Geomorphological mapping

The geomorphological mapping of glacial landforms (e.g., moraines) was conducting using the interpretation of the GEOTEC stereoscopic aerial photographs (1:50,000) produced by the Servicio Aerofotogramétrico de Chile (SAF), in addition to GeoEye (2015) and DigitalGlobe (2018) satellite imagery provided by Google Earth Pro and Maxar (2020) available in ESRI ArcGIS (version 10.8.1). The remote mapping was complemented with a Digital Elevation Model (DEM) with a 12.5 m resolution obtained from the ALOS-PALSAR data mission from 2006 to 2011 (https://asf.alaska.edu/). We conducted fieldwork in 2018, 2019, and 2020 to corroborate our mapping of moraines along the ~20 km of the Universidad Glacier valley. We composited a regional geological map (1:500,000) using as references the data published by (Charrier and Lillo, 1973; SERNAGEOMIN, 2004). The geological setting was corroborated in the field. The names and altitudes of the mountains and glaciers are based on the official cartography of the Instituto Geográfico Militar (IGM; 1:50,000) and the latest public national glacier inventory (Dirección General de Aguas, 2022b).

### 4.3.2. Geochronology

We collected twenty-seven granodioritic boulders samples for $^{10}Be$ surface exposure dating from the top of moraines UNI I, UNI II and UNI III moraines. We sought the largest available boulders in each moraine (>50 to 198 cm) with evidence of glacial erosion. The sampled boulders had no evidence of post-depositional movement or exhumation. The samples were extracted from the upper <4.3 cm of the boulder surface using drilling and blasting. We used a handheld GPS with ± 3 m horizontal accuracy to document each $^{10}Be$ sample location. The clean quartz was extracted at the Cosmogenic Isotope and Quaternary Paleoclimate Laboratory at the Pontificia Universidad Católica de Chile. The Beryllium-10 was isolated at the Surface Exposure Lab at the University of Zurich following standard procedures (Kohl and Nishiizumi, 1992). All $^{10}Be/^{9}Be$ ratios were measured at the ETH Zurich on the TANDY (in 2019) and MILEA (in 2021) AMS systems (Christl et al., 2013; Maxeiner et al., 2019) and normalized to the ETH in-house AMS standards S2007N and S2010N ($^{10}Be/^{9}Be = 28.1 \cdot 10^{-12}$ and $3.3 \cdot 10^{-12}$, respectively), which were calibrated to the ICN 01-5-1 standard (Nishiizumi et al., 2007). All AMS standards are linked with a $^{10}Be$ half-life of 1.387±0.012 Myr (Chmeleff et al., 2010; Korschinek et al., 2010). The samples were prepared and measured in separate batches in 2019 and 2021. Each batch's $^{10}Be/^{9}Be$ sample ratios were corrected with their blanks (Table 4). The $^{10}Be$ exposure ages were calculated using the CRONUS-Earth calculator version 3 (http://hess.ess.washington.edu/math/; Table 5). The exposure ages were calculated with the local $^{10}Be$ production rate for southern South America by Kaplan et al. (2011). We use a sample rock density of 2.65 g/cm$^3$ and apply no erosion correction and the time-dependent scaling scheme (Lm) after Lal (1991) and Stone (2000). The exposure ages recovered from the top of the UNI I to UNI III moraines are interpreted as the culmination of former advances of the Universidad Glacier. We obtained the summed probability to calculate the age culmination of glacial events for each moraine. As well, we use one-sigma error and the

mean exposure ages to establish the timing of the moraine abandonement. Plots were made using the online calculator *iceTEA* (ice-tea.org/en/; Jones et al., 2019).

## 4.4. **Results**

### 4.4.1. Glacial geomorphology

The following geomorphological description refers to the UNI I-III moraines, which represent three different margin positions of the Universidad Glacier (Figure 17). The moraine UNI I is the most distal moraine in the valley. It extends for ~15 km from the mid to the lowest section of the valley interrupted by mountain talwegs (Figure 18a). In the mid-section of the valley, from the confluence of the del Portillo and San Andrés River until the junction of the del Portillo and del Azufre rivers, the moraine UNI I take the form of kame terraces in both flanks of the valley at ~1940 m a.s.l. (Figure 18a). These features reach ~80 m wide, and their surface are covered with sand, gravel, and grass. Scattered volcanic and highly weathered granodioritic boulders occur on it (Figure 18b). The angle of the ice-contact slope of the moraine UNI I varies from 30° to 35°. A left (eastern) latero-frontal UNI I ridge occurs in the junction of the Azufre and Tinguiririca Rivers at ~1100 m a.s. l. (Figure 19a). This latero-frontal moraine is c. 1 km length 5-10 m height, and its surface is entirely covered by native forest. A road crosses the latero-frontal moraine UNI I and exposes two diamictic sedimentary units, a massive lower one, and a stratified upper one (Figure 19c).

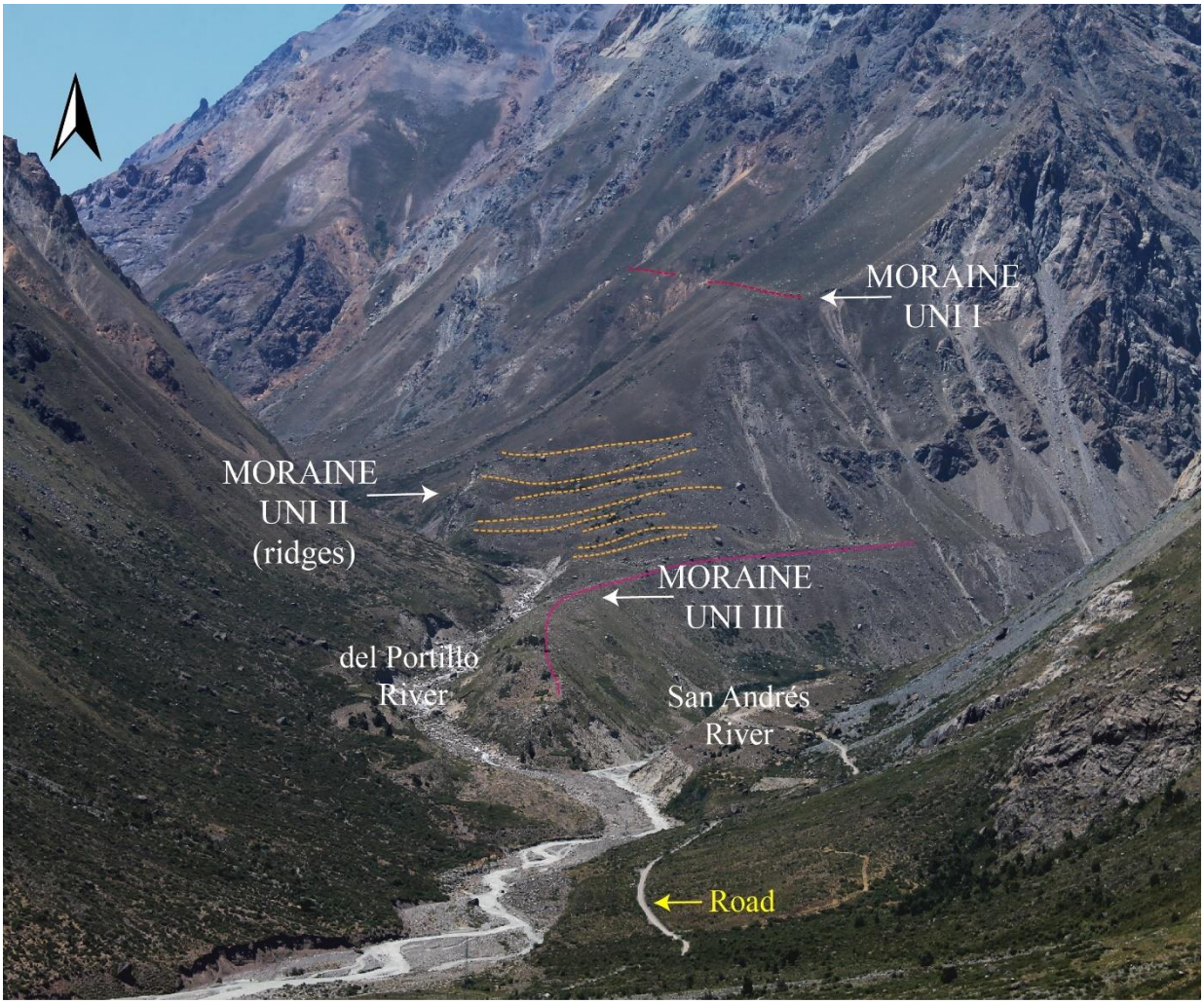


**Figure 17. Moraines UNI I, UNI II, and UNI III on the right side of the valley.** View is to the north from the left lateral moraine UNI I. The upstream section of the moraine UNI II is expressed as a sequence of eight ridges oriented E-W to N-W, from the highest to the lowest. These moraine ridges are above the right latero frontal moraine UNI III, a prominent glacial landform with an N-S orientation adjacent to the del Portillo and San Andrés rivers junction. Samples of UNI II and UNI III come from this location. Yellow arrow indicates the road.

**Figure 18. Surface of the left lateral moraine UNI I. (a)** View of the top of the left lateral moraine at 1950 m a.s.l. close to the confluence of the del Portillo and del Azufre rivers. Subrounded granodioritic boulders are sprinkled on the moraine surface. In the background, the right lateral moraines of UNI I with a terraced shape; **(b)** High weathered granodioritic boulder (not sampled) on the moraine surface UNI I suggest a long period of exposition. Near the center of the photo, downhill from the weathered boulder, the del Portillo River and a moraine ridge of the UNI II with a boulder on top can be seen.

The moraine UNI II extends about 5 km in the middle section of the valley as a sequence of multiple morainic ridges below the moraine UNI I (Figure 17). The del Portillo River crosscut the moraine UNI II and splits it into upstream and downstream sections. The upstream section is composed of eight morainic ridges of 5 to 7 m height that show a notorious shift in their orientation. The highest morainic ridges are oriented E-W while the lower ones are oriented N-S, suggesting a change in the glacier geometry as it thinned. The downstream section of the moraine UNI II is attached to the valley flanks and is better preserved on the left side (Figure 20). There, the moraine UNI II comprises at least six lateral morainic ridges with distinct degrees of preservation arranged in a stepped sequence. The two highest lateral morainic ridges are the better preserved and they end in latero-frontal moraines by the del Azufre River at ~1750 m a.s.l. (Figure 16c). The lower lateral morainic ridges occur at ~1550 m a.s.l., have less preserved morphology and they do not show latero-frontal crests. The surface of the highest ridges of the moraine UNI II is colonized by grass and shrubs, whereas the lower ones is covered by native trees. The ice contact slopes of the moraine UNI II ridges grade from highest to lowest from 35° to 25°, indicating again a thinning ice after UNI II maximum.

Lastly, the moraine UNI III is an outstanding and well-preserved latero-frontal arc composed of a single and large ridge in both sides of the valley at the confluence of the del Portillo and San Andrés rivers at ~1650 m a.s.l. (Figure 17). Its right (western) ridge crosscuts the UNI I and UNI II moraines and can be followed uninterruptedly for 1.7 km. The proximal and distal flanks of this crest have been fluvially eroded, exhibiting slopes that ranges from 30° to 35°. The left moraine is attached to the valley flank and is partially covered by debris cones, so it can be followed continuously for only 0.5 km. The surface of the moraine UNI III is vegetated by grass and shrubs. Subangular to subrounded granodioritic boulders are distributed along the moraine

ridges. The moraine UNI III was eroded up-valley by mountain debris production such as rock falls, debris cones, and alluvial fans.

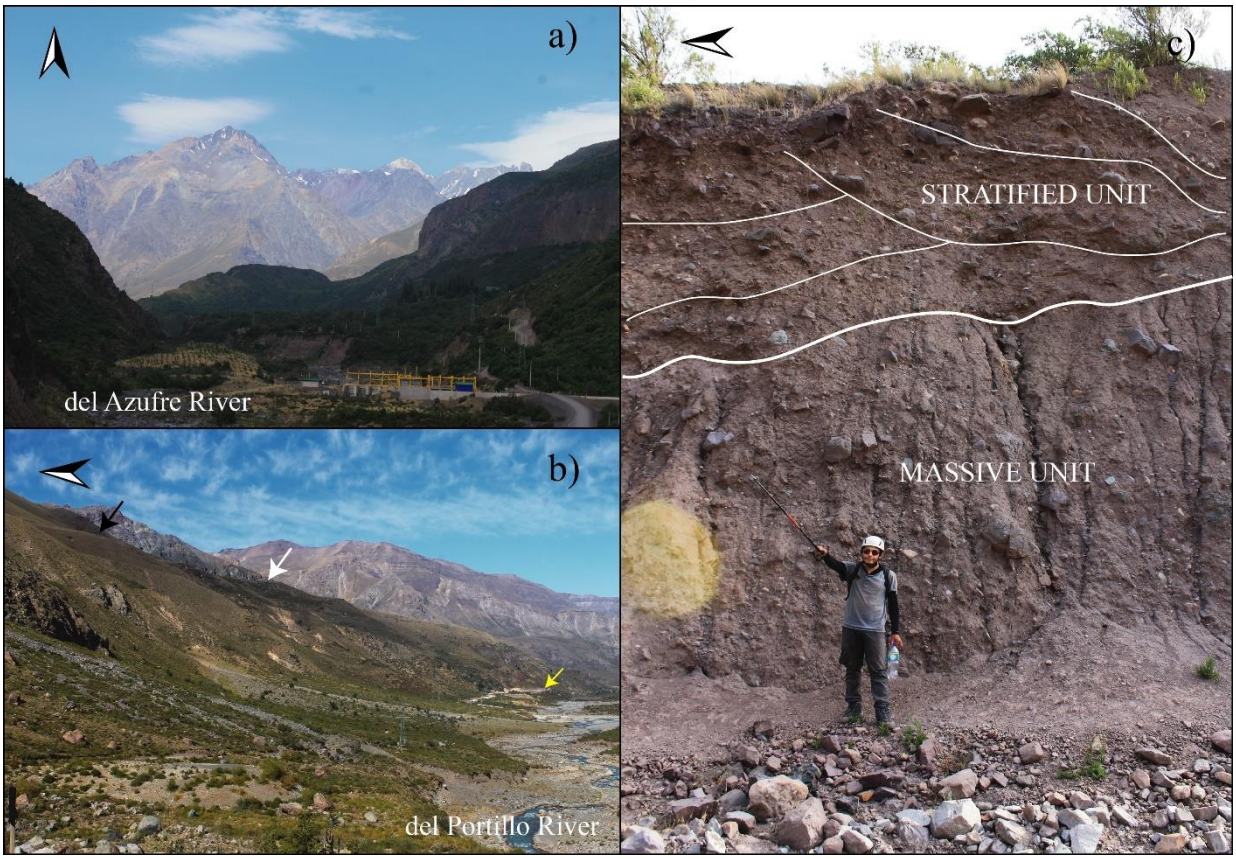


**Figure 19. The left latero-frontal moraine UNI I (a)** View up the valley from the top of the moraine UNI I at ~1100 m a.s.l. A distinct u-shape valley is observed until this elevation where the del Azufre and Tinguiririca rivers merge; **(b)** Moraine UNI I in the midsection of the Universidad Glacier valley at ~1950 to 1930 m. a.s.l. Yellow arrow indicates the road. The black arrow points out to the left lateral moraine UNI I, while the white arrow indicates the highest ridge of the moraine UNI II; **(c)** Sedimentary profile of the left-latero frontal moraine of moraine UNI I.

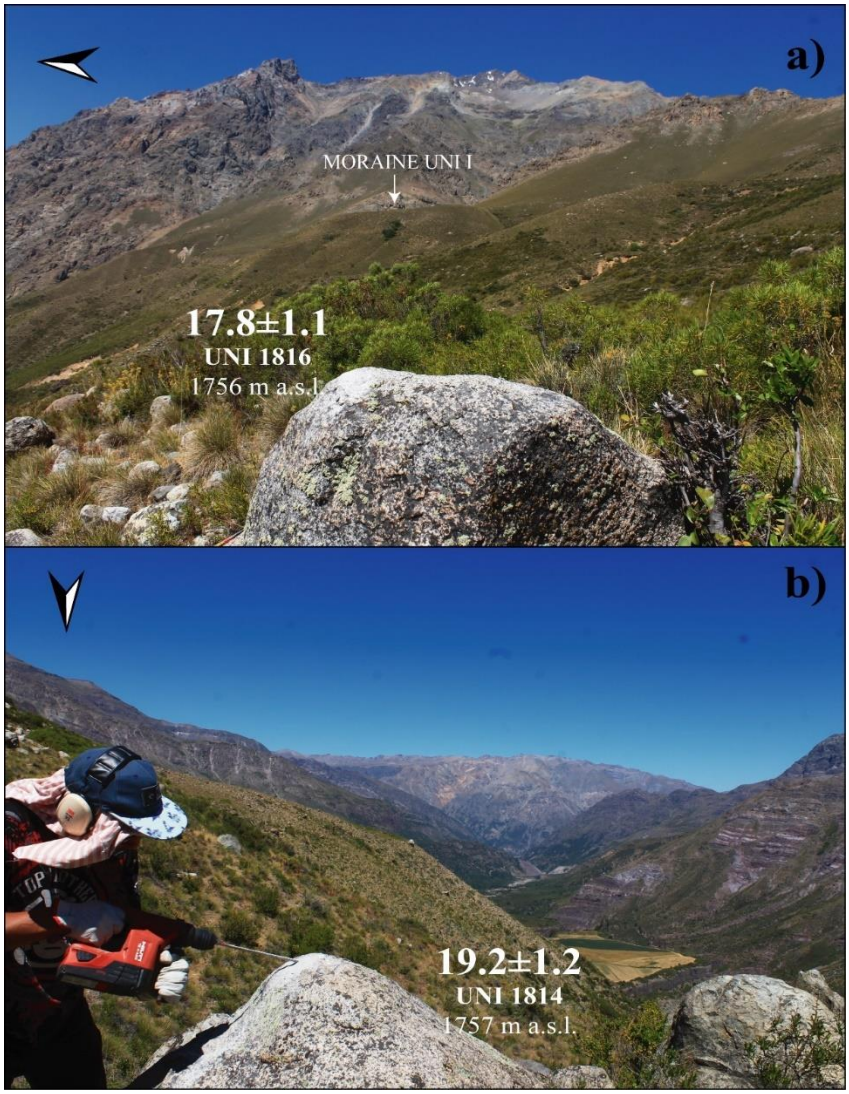


**Figure 20. Boulders on the downstream section of the moraine UNI II (LGM). (a)** Close-up to the sample UNI 1816 on UNI II surface near the confluence of the del Portillo and del Azufre rivers; **(b)** View downvalley from the left lateral moraine UNI II. Granodioritic boulders are at the top of the moraine.

### 4.4.2. Geochronology

The following description is organized from the outer (UNI I) to the proximal moraine (UNI III). Geographical details of $^{10}$Be samples are shown in Table 4 and Figure 21. Three $^{10}$Be samples (UNI 1818, UNI 1820, and UNI 1821) retrieved from erratic boulders resting on the moraine UNI I yielded exposure ages of 51.4±2.7, 100.8±5.8 and 135.9±7.1 ka. The dispersion of ages does not make it possible to produce a meaningful mean age.

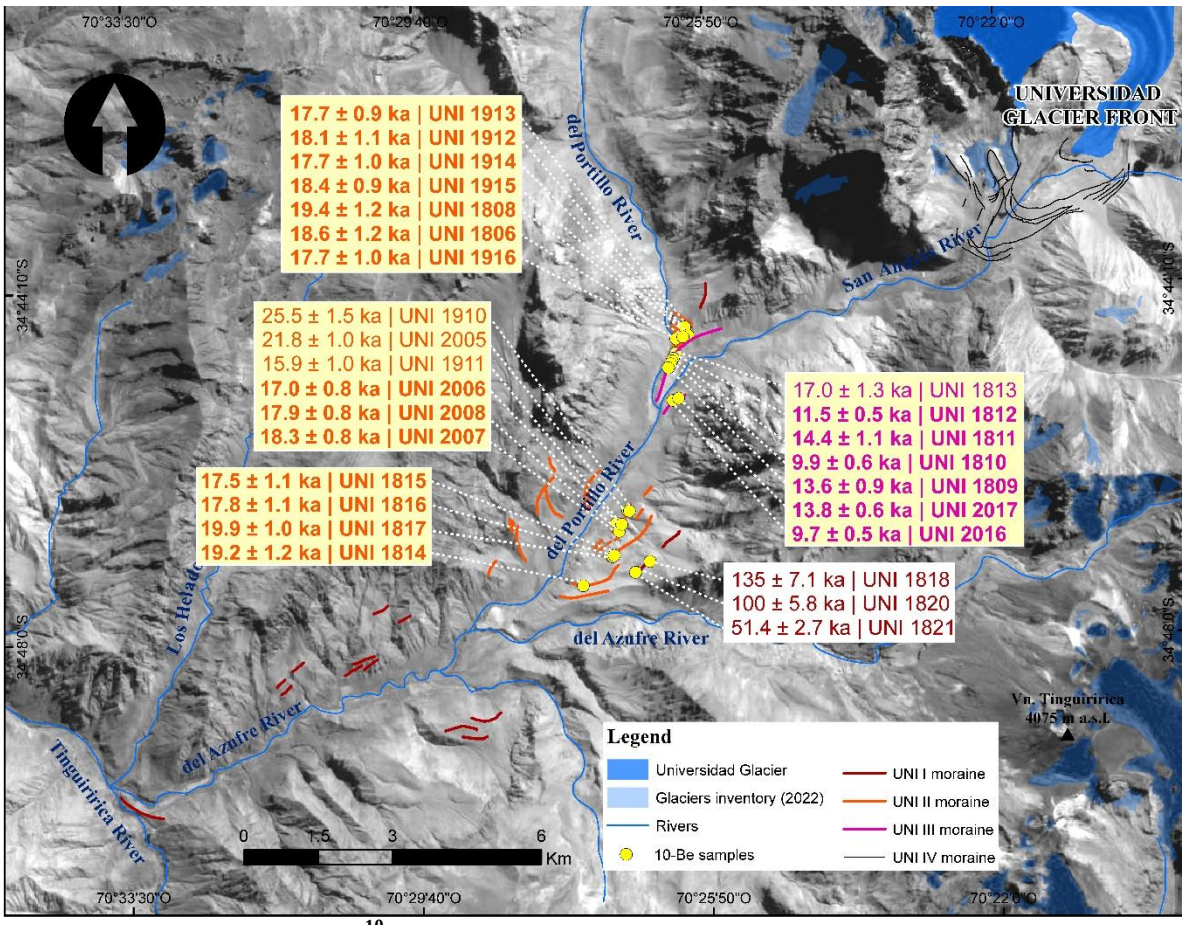


**Figure 21. Last glacial period $^{10}$Be chronology of the Universidad Glacier.** Moraines UNI I-IV are distributed along the 20 km of the Universidad Glacier valley. The samples are represented as yellow dots. $^{10}$Be exposure ages were calculated for moraines UNI I-III and are presented in kilo annum (1 ka=1000 years) with their error (±1σ). The not bolded ages are considered outliers.

Seventeen $^{10}$Be samples were obtained from boulders resting on different ridges of the UNI II moraine (Figure 23). Seven samples were recovered from the upstream section and ten samples were obtained from the downstream section. The distribution of exposure ages showed no differences associated with the sections that compose the UNI II moraine. The seventeen samples yielded exposure ages ranging from 15.9±1.0 to 25.5±1.5 ka; two of these samples (UNI 1910 and UNI 2005) were considered outlier. Thus, the remaining fifteen samples ranged between 15.9±1.0 - 19.9±1.0 ka, providing a UNI II moraine mean exposure age of 18.0±0.9 ka (Figure 24a).

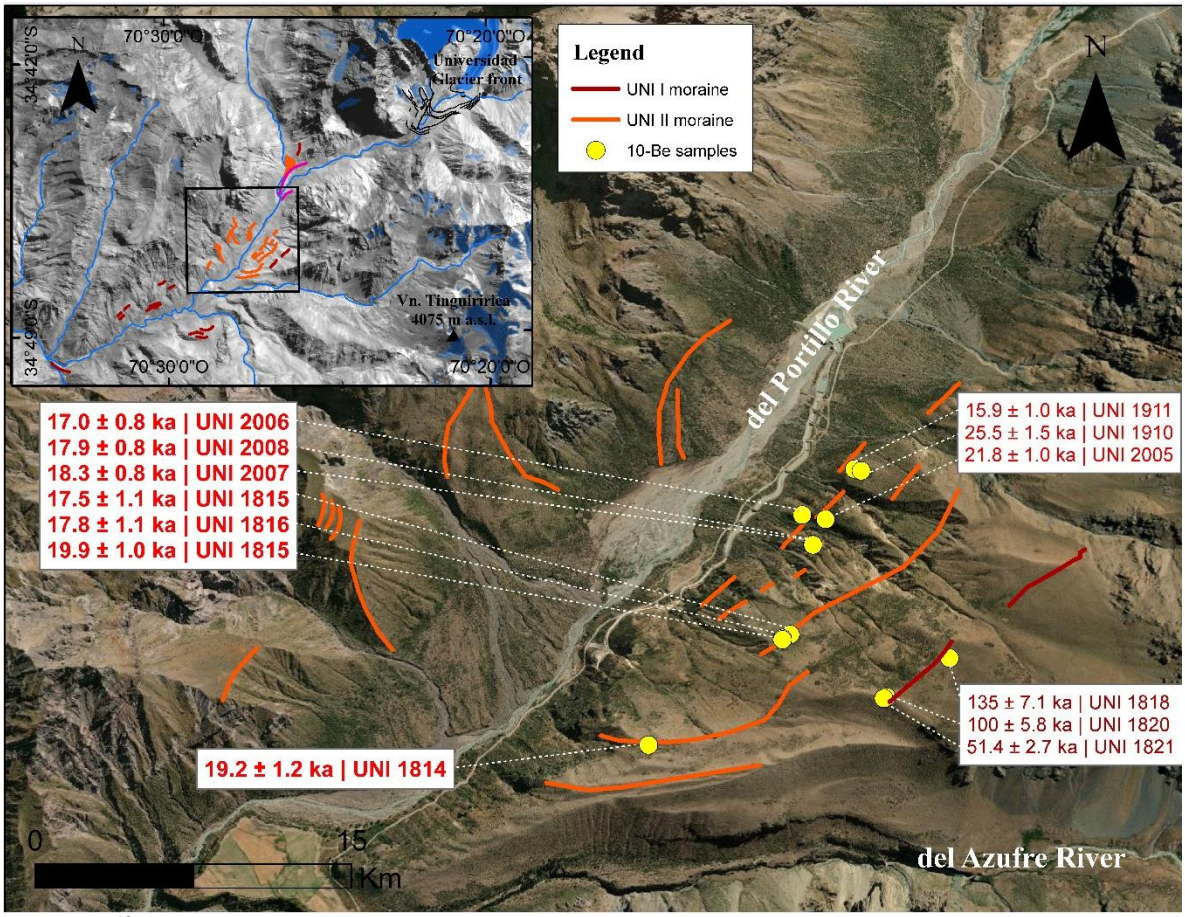


**Figure 22. $^{10}$Be exposure ages of the moraines UNI I and UNI II in the Universidad Glacier valley.** The moraine UNI I (in red) yielded the oldest exposure ages of this study. The downstream section of moraine UNI II (in orange) shows the margin of the ice in the LGM near the confluence of the del Portillo and del Azufre rivers. The sequence of moraine ridges in UNI II suggests a thinning process of the ice after the maximum extent. The sample sites are presented as yellow dots, and the exposure ages are presented in kilo annum (1 ka=1000 years) with their error (±1σ). The not bolded ages are considered outliers.

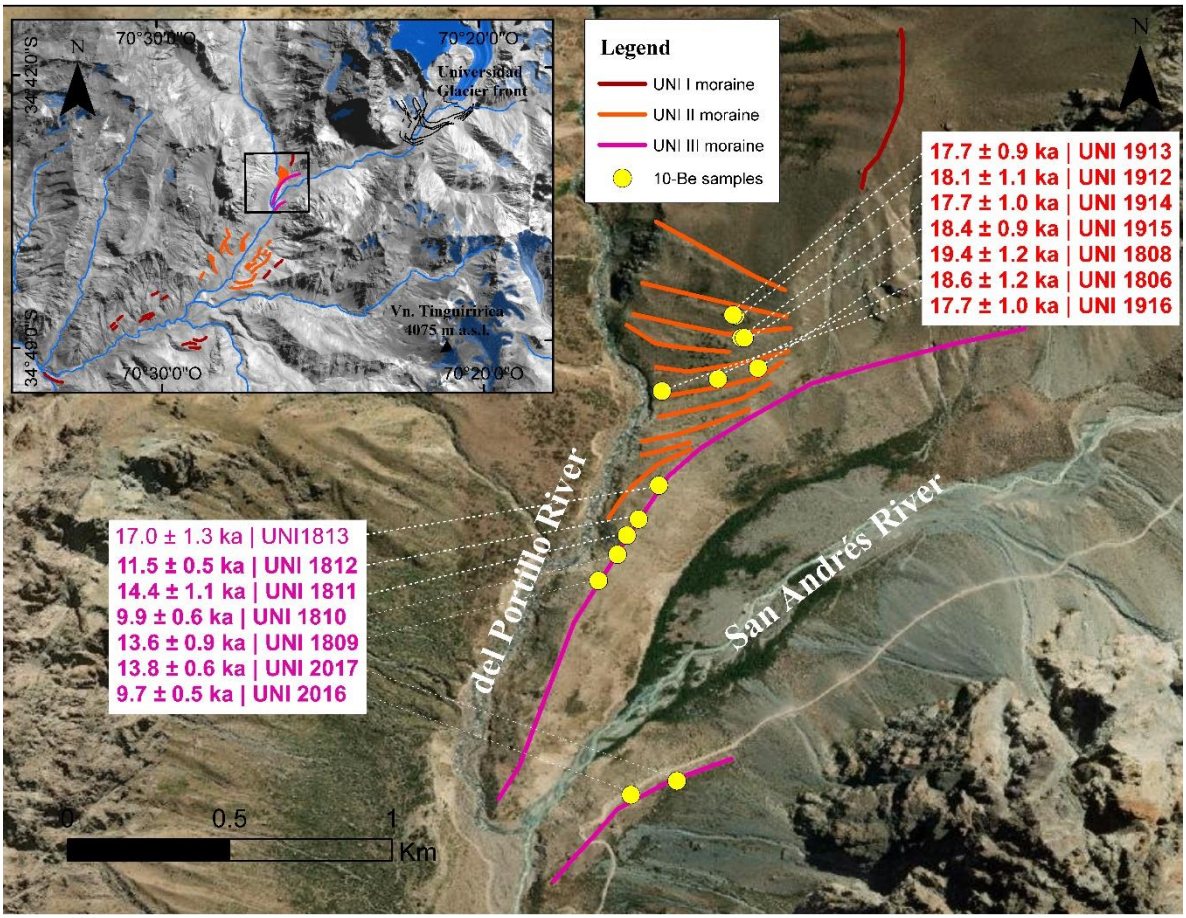


**Figure 23. $^{10}$Be exposure ages of the moraines UNI II and UNI III in the Universidad Glacier valley.** The upstream section of the moraine UNI II (in orange) is near the junction of the del Portillo and San Andrés rivers. It is composed of a sequence of well-defined ridges that change their orientation (E-W to N-S) from the highest to the lowest altitude, suggesting a geometry change of the ice after its maximum extension in the LGM. The moraine UNI II is above the moraine UNI III. UNI III is well-preserved latero-frontal moraines that were built during the LGT. The sample locations are presented as yellow dots, and the exposure ages are presented in kilo annum (1 ka=1000 years) with their error (±1σ). The not bolded ages are considered outliers.

Seven $^{10}$Be samples were retrieved from the moraine UNI III. Five of them were obtained from the right crest and two from the left ridge. Six exposure ages ranged from 9.7±0.5 to 14.4±1.1 ka. One sample (UNI 1813) yielded an exposure age of 17.0±1.3 ka, we rejected as an outlier when one-sigma error is considered. Thus, the mean exposure age of the moraine UNI III is 11.8±1.8 ka (Figure 24b).

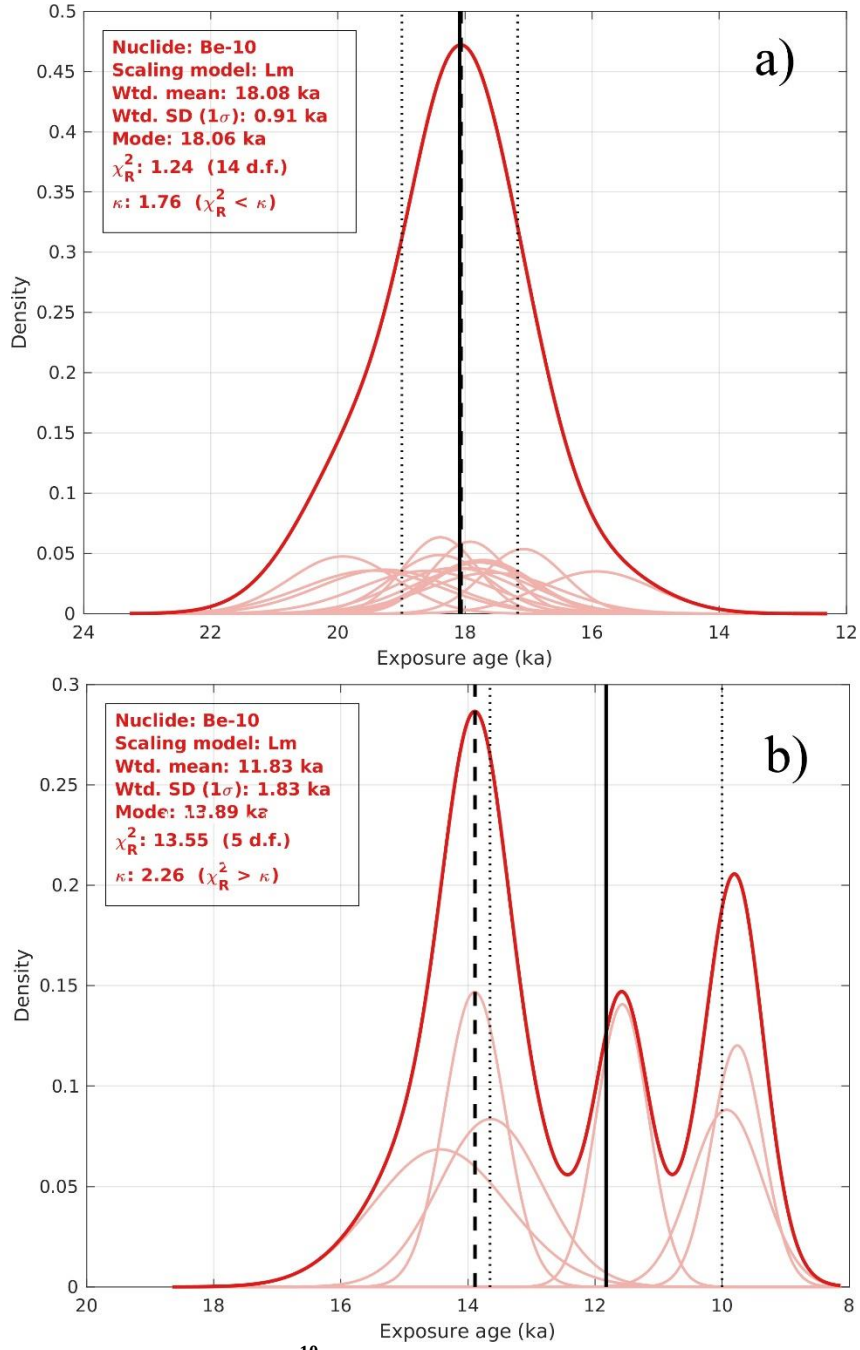


**Figure 24. Probability density plot of $^{10}$Be exposure ages. (a)** UNI II moraine; **(b)** UNI III moraine. The exposure ages are based on the Lm scheme (Lal, 1991; Stone, 2000). The mode (dashed black line), weighted mean (solid black line), and weighted standard deviation (dotted black line) are presented. The calculations do not include outliers.

**Table 4.** Geographical and analytical data of $^{10}$Be samples of the moraines UNI I, UNI II, and UNI III.

| Sample name | Latitude (DD) | Longitude (DD) | Elevation (m a.s.l.) | Shielding factor | Sample thickness (cm) | Quartz dissolved (g) | $^{9}$Be carrier (mg) | $^{10}$Be/$^{9}$Be ($10^{-12}$)* | $^{10}$Be conc. ($x10^{4}$) (at/g) | Error (%)* |
|---|---|---|---|---|---|---|---|---|---|---|
| UNI 1913 | -34.743694 | -70.435000 | 1784 | 0.971 | 2.5 | 27.28 | 0.3032 | 0.308 | 22.260 | 4.5 |
| UNI 1914 | -34.744306 | -70.434750 | 1772 | 0.973 | 1.6 | 27.67 | 0.3021 | 0.315 | 22.373 | 4.5 |
| UNI 1915 | -34.744306 | -70.434833 | 1771 | 0.972 | 2.7 | 28.09 | 0.3010 | 0.330 | 23.024 | 4.1 |
| UNI 1916 | -34.745778 | -70.437028 | 1687 | 0.965 | 1.9 | 25.99 | 0.3018 | 0.277 | 20.882 | 4.7 |
| UNI 1811 | -34.749782 | -70.438000 | 1665 | 0.971 | 1.8 | 35.80 | 0.1989 | 0.454 | 16.487 | 7.3 |
| UNI 1810 | -34.750311 | -70.438261 | 1656 | 0.967 | 2.9 | 35.69 | 0.1982 | 0.291 | 10.506 | 5.7 |
| UNI 1813 | -34.748395 | -70.437113 | 1671 | 0.968 | 1.5 | 23.76 | 0.2000 | 0.361 | 19.844 | 6.9 |
| UNI 1818 | -34.786172 | -70.443452 | 1950 | 0.983 | 3.0 | 22.85 | 0.3070 | 2.317 | 206.913 | 3.8 |
| UNI 1820 | -34.788083 | -70.446534 | 1935 | 0.990 | 4.3 | 26.31 | 0.3028 | 1.953 | 149.292 | 4.6 |
| UNI 1821 | -34.788145 | -70.446677 | 1930 | 0.987 | 2.2 | 24.31 | 0.3020 | 0.930 | 76.235 | 4.0 |
| UNI 1814 | -34.790424 | -70.458204 | 1757 | 0.991 | 1.4 | 21.24 | 0.3033 | 0.271 | 24.734 | 5.4 |
| UNI 1815 | -34.785006 | -70.451256 | 1749 | 0.986 | 1.6 | 25.68 | 0.3032 | 0.293 | 22.140 | 5.8 |
| UNI 1816 | -34.785200 | -70.451642 | 1756 | 0.984 | 2.0 | 30.36 | 0.3055 | 0.346 | 22.473 | 5.3 |
| UNI 1817 | -34.785254 | -70.451643 | 1755 | 0.984 | 1.2 | 18.74 | 0.3035 | 0.248 | 25.507 | 4.2 |
| UNI 1809 | -34.751035 | -70.438787 | 1654 | 0.966 | 4.0 | 25.10 | 0.3054 | 0.196 | 14.964 | 6.0 |
| UNI 1808 | -34.745145 | -70.43437 | 1738 | 0.964 | 2.3 | 21.10 | 0.3041 | 0.259 | 23.755 | 5.6 |
| UNI 1806 | -34.745448 | -70.435478 | 1729 | 0.964 | 1.8 | 25.29 | 0.3030 | 0.290 | 22.587 | 5.6 |
| UNI 1910 | -34.776972 | -70.447778 | 1572 | 0.976 | 3.6 | 36.36 | 0.3034 | 0.524 | 28.767 | 4.9 |
| UNI 1911 | -34.776889 | -70.448111 | 1566 | 0.971 | 1.7 | 26.78 | 0.3032 | 0.235 | 17.152 | 5.7 |
| UNI 1912 | -34.743667 | -70.435056 | 1783 | 0.973 | 2.6 | 25.42 | 0.2930 | 0.305 | 22.861 | 5.3 |
| Preparation blank BI 11 | | | | | | | 0.1997 | 0.010** | | 11.6** |
| Preparation blank BI 12 | | | | | | | 0.1982 | 0.008** | | 18.3** |
| Preparation blank BI 13 | | | | | | | 0.2959 | 0.012** | | 11.5** |
| Preparation blank BI 14 | | | | | | | 0.3006 | 0.008** | | 18.3** |
| UNI 2005 | -34.779361 | -70.449528 | 1557 | 0.971 | 3.5 | 30.32 | 0.3085 | 0.365 | 23.868 | 3.1 |
| UNI 2006 | -34.779139 | -70.450667 | 1536 | 0.969 | 3.1 | 31.24 | 0.3091 | 0.285 | 17.940 | 3.7 |
| UNI 2007 | -34.780611 | -70.450139 | 1564 | 0.969 | 2.4 | 32.70 | 0.3080 | 0.331 | 19.938 | 3.1 |
| UNI 2008 | -34.780583 | -70.450167 | 1562 | 0.970 | 2.0 | 25.80 | 0.3081 | 0.256 | 19.359 | 3.3 |
| UNI 1812 | -34.749335 | -70.437676 | 1666 | 0.971 | 1.5 | 28.11 | 0.3083 | 0.190 | 12.892 | 3.5 |
| UNI 2016 | -34.756972 | -70.437889 | 1607 | 0.956 | 1.9 | 30.51 | 0.3090 | 0.161 | 9.927 | 4.2 |
| UNI 2017 | -34.756583 | -70.436611 | 1614 | 0.950 | 2.1 | 30.06 | 0.3086 | 0.232 | 14.940 | 3.4 |
| Preparation blank BI 25 | | | | | | | 0.3093 | 0.014** | | 3.2** |

* The ratios are corrected to the background of the blank samples. The errors include the error of the blanks and AMS standards.
** Blank ratios and errors are presented without background correction.
The samples UNI 1812, UNI 2005 – 2008, UNI 2016 and UNI 2017 were corrected to the background of the blank BI 25. The rest of the samples were corrected to a weighted average of blanks BI 11 – 14.

## 4.5. **Discussion**

### 4.5.1. Glacial geomorphology

The Universidad Glacier valley includes four moraine belts (UNI I-IV), evidencing distinct ice-marginal positions. The moraine UNI I extends discontinuously from the mid to the lowest section of the valley, constituting the highest and most distal glacial-derived landform preserved in our study area. (Abele, 1984) reported glaciofluvial terraces near the confluence of the del Portillo and del Azufre rivers (Figure 16; Figure 22). We interpret that the glaciofluvial terraces reported by Abele are referred to as the UNI I moraine, as they coincide in shape and location. The kame terraces result from the meltwater sediment accumulation between the ice margin and the slope against which the ice buttressed on (Gray, 1995; Bitinas et al., 2004). The elevation of the kame terraces depends on the glacier's thickness and, consequently, on the amount of meltwater stream running by the valley flanks (Bennett and Glasser, 2009). The lateral moraines of UNI I are the highest preserved glacial landforms in the mid-section of the valley, indicating the maximum magnitude of the glacier during the late-Quaternary. The scale of the glacier extension that built the moraine UNI I is also evidenced by the left latero-frontal moraine, which occurs at ~1100 m a.s.l. and 20 km from the present-day glacier. Opposing to our interpretations, Abele (1982) this distal latero-frontal moraine as a fluvial deposit. Nevertheless, we did not observe typical fluvial sediment arrangement nor the shape of a fluvial landform such as a terrace or fluvial bar (Figure 19c). In fact, the sediments that compose the left latero-frontal moraine of UNI I include two depositional units. The lower unit resembles a till, while the upper one could be interpreted as postglacial alluvial deposit. We suggest that the latero-frontal moraine of UNI I is the most distal expression of the maximum glacier stage, and it has been reworked for wasting

mountain processes along the valley flanks. Our interpretation rules out that this deposit results from fluvial deposition as described by Abele (1982).

The moraine UNI I is not the only moraine mapped in the Andes of central Chile which suggest a maximum glacier stage. Santana (1967) mapped the El Manzanar moraine in the Cachapoal valley (34° S) as a Quaternary glaciofluvial terrace at 1100 m a.s.l, a similar altitude where the latero-frontal ridge UNI I occurs. Other works interpreted Quaternary moraines in similar altitudes in central Chile, as the Maipo (33° S) and Aconcagua (32° S) valleys (Caviedes and Paskoff, 1975). Nonetheless recent studies dismissed part of such observations arguing that those deposits were originated or were reworked by mountain gravity processes (Abele, 1984; Antinao and Gosse, 2009; Deckart et al., 2014). The distinction of Quaternary moraines is challenging in Andes of central Chile due to the high sediment supply from the mountain environment. Despite this, the well-preserved condition of the moraine UNI I along the Universidad Glacier valley and the former descriptions by Santana (1967) support the hypothesis of a maximum regional glacier extent during the late-Quaternary that still maintains some intact records poorly studied.

The moraine UNI II occurs in the mid-section of the Universidad Glacier valley as the second most distal glacial-derived landform. We interpret that, in the upstream section of this moraine, the higher morainic ridges (E-W) indicate an overflow of the Universidad Glacier into the Portillo River valley (Figure 17). Subsequently, once the glacier became thinner, the local glacier flow changed and occupied only the main axis of the valley (N-S). The process of the Universidad Glacier thinning and subsequent glacier fluctuations might explain the stepped lateral moraines arrangement in the downstream section. Abele (1982, 1984) described several marginal moraines near the junction of the del Portillo and del Azufre rivers as the expression of different size of a

former glacier. We have associated the Abele's mapping with the geomorphic composition of the moraine UNI II. Charrier et al. (2019) described a sequence of lateral moraines in the Cachapoal River and associated these ridges with an ice decay after a glacier advance. The reports of Abele and Charrier et al. are coherent with our interpretation of a second distal extension of the Universidad Glacier and its subsequent thinning that built the moraine UNI II.

The moraine UNI III is composed of two latero-frontal crests (left and right) that span in the mid-section of the valley marking the third distal glacier margin along the valley. The glacial advance that built the UNI III moraine did not flow beyond the current confluence of the del Portillo and San Andrés rivers (Figure 17). The next moraine up valley is the UNI VI moraine, which was described as a massive dead-ice moraine punctuated for minor ridges and other glacial features such as flutes (Fernández et al., 2022).

### 4.5.2. Geochronology

#### 4.5.2.1. Pre-Last Glacial Maximum

Three boulders sampled on the moraine UNI I yielded exposure ages dating to the pre-LGM, but the dispersion of exposure ages between 51.4±2.0 to 135.9±5.3 ka does not allow to us establishing a specific age for the culmination of the moraine construction (Figure 22; Table 5). The sampled boulders were in a stable position and have a size >70 cm in height, so they complied with sampling requirements. The distribution of the exposure ages in the moraine UNI I could be related both to high weathering of the boulder surfaces, a long-term period of boulders deposition (e.g., composite moraine) or inheritance. Despite the dispersion of ages, it is worth noting that the geochronology of the moraine UNI I covers between the Marine Isotope Stage (MIS) 3 to 6, a period with scarce precedents of glacial events in the Andes of central Chile. Zech et al. (2017) presented exposure ages of moraines obtained from the Cerro Fredes (31° S) that fluctuated between MIS 5 and 8. Our data and the exposure ages presented by Zech et al. suggest a glacial stage predating the LGM.

#### 4.5.2.2. Last Glacial Maximum

##### 4.5.2.2.1. Southern glacier advances

Our fourteen ages indicate that the moraine UNI II represents the culmination of a main Universidad Glacier advance occurred ~18 ka during the LGM (MIS 2). Our glacial chronology is one of the most robust pieces of evidence for a glacier expansion during the LGM in the Andes of central Chile. In addition, it is consistent with other regional studies that used Terrestrial Cosmogenic Nuclides $^{10}$Be (TCN) dating on moraines and that found glacier expansions between ~18 to 22 ka (Zech et al., 2006, 2007, 2017; Charrier et al., 2019; Aguilar et al., 2022). The LGM in the Andes of central Chile seems there have occurred in-phase with other southern glaciers. In Patagonia, several studies using $^{10}$Be TCN on moraines have recorded glacier expansions between ~18 to 24 ka (Douglass et al., 2006; Kaplan et al., 2008; Hein et al., 2010; Sagredo et al., 2011; García et al., 2018, 2019; Peltier et al., 2021; Lira et al., 2022). Altogether, available data indicate a synchronous glacier expansion along the extratropical Andes during the LGM.

The glacier fluctuations in the New Zealand Alps (44°—45° S) are suitable for obtaining a hemispheric perspective of glacial fluctuations during the LGM in the light of our new records in the Andes of central Chile. Several studies using $^{10}$Be TCN on moraines recorded glacier advances between ~16 to 23 ka (Putnam et al., 2013; Kelley et al., 2014; Doughty et al., 2015; Strand et al., 2019; Moore et al., 2022). Recently, Denton et al. (2021, 2022) synthesized the glacial chronologies in New Zealand and concluded glacier expansions at ~22-23 ka and then at 18 ka. The available glacial chronology data in the New Zealand Alps and the Andes of central Chile and Patagonia suggests that the LGM stage was in-phase from mid to subantarctic latitudes.

#### 4.5.2.2.2. Interhemispheric glacier advances during the LGM

Geochronology established from moraines throughout the Northern Hemisphere confirms that the LGM occurred a few millennia apart from place to place. Schaefer et al (2006) summarized $^{10}$Be exposure ages obtained from moraines in United States and Switzerland and demonstrated that the last LGM glacier advance occurred between 16 and 21 ka. In a similar manner, Clark et al. (2009) integrated TCN ages to constrain the LGM in North America, Europe and Tibet and found maximum glacier positions between 19/20 ka and 26 ka. Previously, Rinterknecht et al. (2006) dated the LGM moraines of the Fennoscandinavian Ice Sheet at 19 ka. Whilst, the recalculation of those exposure ages might involve that the Fennoscandinavian moraines have 21 ka (Hughes & Gibbard, 2015). To provide an integrated perspective on glacier fluctuations, Recent studies that used $^{10}$Be dating in the European Alps found that the outermost position of the Swiss and Italian glaciers during the LGM occurred at ~23 to 24 ka (Scapozza et al., 2014; Ivy-Ochs, 2015; Kamleitner et al., 2022). In a similar manner, Monegato et al. (2017) suggested that the culmination of the maximum expansion of the Rhine and Tagliamento glaciers occurred between 17 and 23 ka. Using TCN along the Himalayas has given new ideas about quaternary glaciations in central Asia. Li et al. (2014) found glacier advances within the LGM between 22 and 33 ka. This data is added to earlier studies that dated the LGM between 18 and 24 ka (Koppes et al., 2008; Zech, 2012). The studies carried out in the along Northern Hemisphere confirm that the glacier expansions during the LGM occurred at different times in a millennia scale. Such difference is also found along the Southern Hemisphere (section 4.5.2.2.1).

#### 4.5.2.2.3. Late-glacial advances in southern latitudes

The exposure ages obtained from the moraine UNI III evidence a return of glacial conditions during the LGT between 9.7±0.5 to 14.4±1.1 ka (mean age=11.8±1.8 ka), a glacier advance that until now had no record in the Andes of central Chile. The distribution of the exposure ages might be associated with a glacier advance that remained in the same marginal position for relative long-time. Alternatively, UNI III may be a composite moraine that was built during at least two glacial advances to the same position first by 14 ka and then by 10 ka. For now, and in the light of the available chronological constrain, we discuss the implication of this late glacial advance culminating by 11.8±1.8 ka.

Although late-glacial advances were ruled out for the northern margin (30° S) of the Andes of central Chile (Aguilar et al., 2022), evidence for a return to glacial condition during the LGT is numerous in Patagonia. In Lago Argentino, Ackert et al. (2008) dated the Puerto Banderas moraine between 9.8±1.4 to 12.2±2.2 ka, whereas Strelin et al. (2011) and Kaplan et al. (2011) established glacier advances ~13 ka. Sagredo et al. (2011) recorded a late-glacial pulse between 12.8 to 14.8 ka in Última Esperanza (52° S) and García et al. (2012) established exposure ages of 14.2±05 ka for a late-glacial ice extent in the Torres del Paine moraines (51° S). In Monte San Lorenzo (47° S), Sagredo et al. (2018) constrained a glacial expansion occurred between 12.7±0.4 to 14.9±0.4 ka, as well Mendelova et al. (2020) found both a glacier advance/stillstand at 12.4±0.3 ka and an extensive glacier advance at 13.1±0.6 ka. Recently, Soteres et al. (2022) found glacier readvances between 12.5 ± 0.4 and 13.5±0.4 ka in the Lago Palena/General Vintter (44° S).

Late-glacial advances not only were recorded from mid to subantarctic latitudes of South America, but also in New Zealand glaciers (44° S). Kaplan et al. (2010) $^{10}$Be dated moraines

between 11.7 to 12.9 ka in the Ben Ohau range and Putnam et al. (2010) established a range of $^{10}$Be exposure ages from 12.7 to 14.5 ka in the inner moraines of Lake Pukaku. Likewise, Kaplan et al. (2013) use $^{10}$Be on moraines of the Whale Stream area and found exposure ages of 11.5 to 15.0 ka for a glacial advance during the late-glacial. Similarly, in the Rakaia catchment, late-glacial moraines were dated between 11.4 to 13.4 ka (Koffman et al., 2017). Thus, the chronology of moraines in the southern mid-latitudes evidence a near in-phase return to glacial conditions that interrupted the LGT, which could be related to the same atmospheric and oceanic mechanism throughout the south of the southern hemisphere.

### 4.5.3. Paleoclimate forcings of the LGM and LGT

Here we discuss the atmospheric and oceanic teleconnections that frame the glacial events that built the moraines UNI II-III. The moraine UNI I will not be a matter of discussion because it is not possible to tie it to a specific paleoclimatic event. Then, the focus of this section will be the LGM and the LGT.

#### 4.5.3.1. Hemispheric and interhemispheric teleconnections during the LGM

Our data suggest that the maximum expansion of the Universidad Glacier during the LGM was at the end of this event. Although some southern and northern glaciers also had their last expansion at 18 ka, there are other glacial records in both hemispheres that this advance occurred a few millennia earlier (~23 ka). The LGM implied a global cooling with no obvious link with the summer insolation intensity dominated by precession in that period (Figure 25a). One explanation for this near-synchronous apparent climate cooling might be related to the seasonality (Huybers and Denton, 2008; Putnam et al., 2013). The larger southern winter duration, synchronic with the declining northern summer insolation, could explain extended colder conditions around Antarctica (Huybers and Denton, 2008) and the affectation to the atmospheric system worldwide (Broecker and Denton, 1990; Denton et al., 2021). As follows, the low temperatures around Antarctica promoted the formation and growth of sea ice (Wolff et al., 2006), and, in turn, reduced-deep water ventilation of the Southern Ocean due its stratification (Gordon, 1991; Stephens and Keeling, 2000; Bouttes et al., 2010). A direct result of the above was the reduction of the atmospheric $CO_2$ which provoked overall lower temperatures (Stephens and Keeling, 2000; Toggweiler et al., 2006). Distinct proxies evidenced the reduction of atmospheric $CO_2$ and consequent decreasing of temperature in the Southern Hemisphere. For

instance, ice core records obtained from the West Antarctic Ice Sheet (WAIS) evidenced a minimum of $CO_2$ of ~190 ppm in the LGM which contrasts with ~270 ppm observed in the early Holocene (Figure 25b; Bauska et al., 2021). The minimum temperatures also were inferred from the Antarctic ice cores (Figure. 25c; Jouzel et al., 2007; Bauska et al., 2021) and sea surface temperature reconstruction in the southwest Pacific Ocean (Figure. 25d; Kaiser et al., 2005) and offshore of the North-central Chile (Kaiser et al., 2008). The temperature depletion during the LGM was estimated at 6 to 7 °C in southern South America (Porter, 1981; Heusser et al., 1999; Moreno et al., 2015) and New Zealand (Putnam et al., 2013).

The global cooling of the LGM was mostly related to variations in atmospheric $CO_2$ triggered by the latitudinal migration of the SWW, thus the ocean-atmosphere reorganization in the southern latitudes modulated the switch of the global climate (Broccoli and Manabe, 1987; Broecker and Denton, 1990; Denton et al., 2021; Toggweiler et al., 2006). The higher albedo effect of extended northern hemisphere ice sheets exerted a significant influence on climate (Broccoli and Manabe, 1987; Deblonde et al., 1992) and ocean heat transport (Lynch-Stieglitz et al., 2007), but other factors are needed to account for the LGM (Broecker and Denton, 1990). Thus, the Universidad Glacier advance that occurred in the LGM was contextualized in a worldwide cooling event that was prompted by the migration of the SWW.

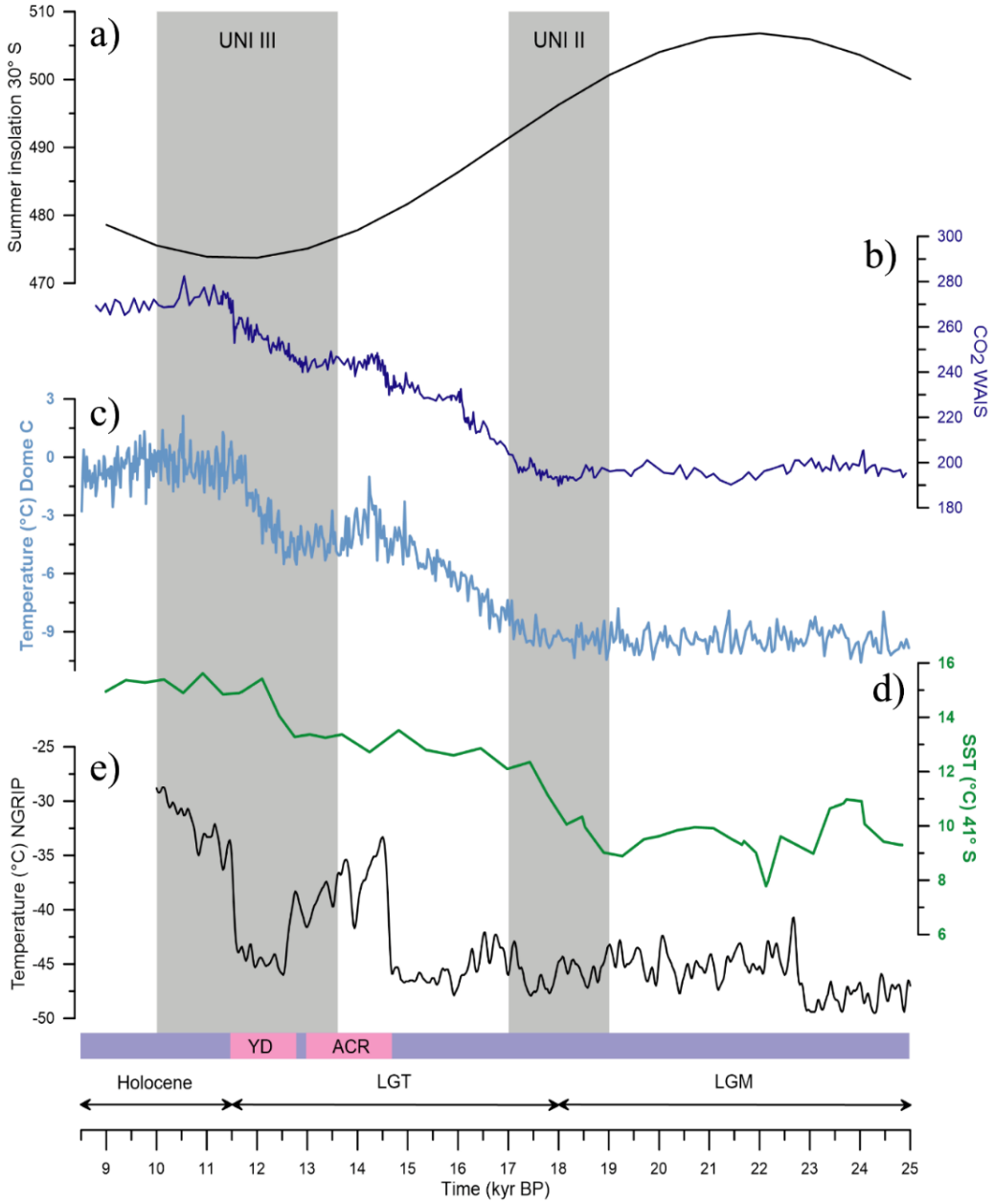


**Figure 25. Paleoclimate context in which late-Quaternary fluctuations of the Universidad Glacier occurred. (a)** summer (December) insolation calculated for the 30° S (Berger and Loutre, 1991); **(b)** changes in the atmospheric $CO_2$ derived from ice core records obtained in the West Antarctic Ice Sheet (WAIS) (Marcott et al., 2014; Bauska et al., 2021); **(c)** Air temperature (°C) estimated for DOME C in Antarctica (Jouzel et al., 2007); **(d)** Sea Surface Temperature (SST) obtained from alkenone in the southwest Pacific Ocean (Kaiser et al., 2005); **(e)** Air temperature (°C) reconstructed from ice core records retrieved in the North Greenland Ice Core Project (NGRIP) site (Kindler et al., 2014); Grey bars indicate the age and weighted standard deviation of the Universidad Glacier advances.

#### 4.5.3.2. How was the climate in the Andes of central Chile during the LGM?

During the LGM, the enhanced pole-to-equator temperature gradient attendant with the growth of the Antarctic Ice Sheet and pack ice caused the northward migration of the SWW (Heusser, 1989; Hulton et al., 2002; Toggweiler et al., 2006) causing colder and wetter conditions in most of southern South America. The magnitude and timing of this SWW equatorward shift is still not entirely clear, but colder and wetter conditions seem to be generalized from, at least, the south of the Atacama throughout Patagonia. Some studies inferred the latitudinal displacement of the SWW over the LGM at 7° to 10° north of their present position at 50° S (Moreno et al., 1999; Toggweiler et al., 2006). There are geological and ecological proxies recovered from central Chile that suggest such a displacement of the SWW until to subtropical latitudes. Lamy et al. (1999) analyzed terrigenous material in offshore central Chile marine sediments (33° S) and found a precipitation peak between 18 and 22 cal ka BP. Sedimentological and pollen analysis in the Laguna de Tagua Tagua (34° S, 200 m a.s.l.) revealed that the most humid interval was between 17.0 to 19.5 cal ka BP (Valero-Garcés et al., 2005). Recently, García et al. (2019) dated buried coastal paleodune-paleosols sequences (32° S), and inferred that the latest wetter period was at 22 ka for central Chile. In the Atacama Desert (25° S), based on pollen analysis and radiocarbon dating, Maldonado et al. (2005) recorded increased winter precipitations between 17 to 24 cal ka BP. While Lamy et al. (2000) examined and dated terrigenous sediments from the continental slope off at 27.5° S and determined a domain of wetter climate between ~18 and 22 ka. To the south, in the Chilean Lake District (40°—42° S), pollen stratigraphy and radiocarbon chronology afford evidence for colder and wetter conditions between 17.8 and 24 cal ka BP (Moreno et al., 2015, 1999).

**Table 5.** $^{10}$Be exposure ages of the samples from moraines UNI I, UNI II and UNI III in the Universidad Glacier valley.

| Sample name | Sample height (cm) | Exposure age (St) (year) | External error (St) (year) | Exposure age (Lm) (year) | External error (Lm) (year) | Exposure age (LSDn) (year) | External error (LSDn) (year) |
|---|---|---|---|---|---|---|---|
| **MORAINE UNI I** | | | | | | | |
| UNI 1818 | 120 | 151930 | 8070 | **135900** | 7140 | 136790 | 7110 |
| UNI 1820 | 97 | 109670 | 6460 | **100860** | 5890 | 102610 | 5950 |
| UNI 1821 | 71 | 54740 | 2890 | **51420** | 2700 | 53030 | 2760 |
| **MORAINE UNI II** | | | | | | | |
| UNI 1806 | 198 | 18860 | 1240 | **18610** | 1220 | 19440 | 1270 |
| UNI 1808 | 169 | 19820 | 1300 | **19460** | 1270 | 20280 | 1310 |
| UNI 1814 | 107 | 19590 | 1260 | **19260** | 1240 | 20050 | 1280 |
| UNI 1815 | 55 | 17730 | 1200 | **17580** | 1190 | 18390 | 1240 |
| UNI 1816 | 83 | 18070 | 1140 | **17890** | 1120 | 18690 | 1170 |
| UNI 1817 | 60 | 20350 | 1100 | **19920** | 1070 | 20710 | 1100 |
| UNI 1910 | 147 | 26890 | 1610 | **25540** | 1520 | 26480 | 1570 |
| UNI 1911 | 118 | 15930 | 1060 | **15940** | 1050 | 16840 | 1110 |
| UNI 1912 | 111 | 18360 | 1150 | **18160** | 1130 | 18950 | 1170 |
| UNI 1913 | 86 | 17880 | 1010 | **17710** | 990 | 18510 | 1030 |
| UNI 1914 | 69 | 17950 | 1020 | **17780** | 1000 | 18580 | 1040 |
| UNI 1915 | 126 | 18630 | 990 | **18400** | 980 | 19200 | 1010 |
| UNI 1916 | 140 | 17940 | 1040 | **17780** | 1030 | 18640 | 1070 |
| UNI 2005 | 174 | 22630 | 1040 | **21860** | 1000 | 22770 | 1030 |
| UNI 2006 | 50 | 17160 | 870 | **17080** | 860 | 18030 | 890 |
| UNI 2007 | 126 | 18600 | 860 | **18390** | 850 | 19340 | 880 |
| UNI 2008 | 96 | 18090 | 860 | **17920** | 850 | 18880 | 880 |
| **MORAINE UNI III** | | | | | | | |
| UNI 1809 | 109 | 13370 | 920 | **13640** | 940 | 14330 | 980 |
| UNI 1810 | 52 | 9250 | 610 | **9930** | 650 | 10560 | 690 |
| UNI 1811 | 67 | 14280 | 1150 | **14440** | 1160 | 15150 | 1210 |
| UNI 1812 | 67 | 11120 | 550 | **11570** | 560 | 12290 | 590 |
| UNI 2016 | 94 | 9080 | 490 | **9760** | 520 | 10370 | 550 |
| UNI 2017 | 234 | 13680 | 660 | **13890** | 660 | 14660 | 690 |
| UNI 1813 | 107 | 17080 | 1330 | **17000** | 1320 | 17840 | 1380 |

The exposure ages are calculated using CRONUS-Earth calculator (http://hess.ess.washington.edu/math/) version 3 for three different scaling schemes (St, Lm, LSD; Lal, 1991; Stone, 2000; Balco et al., 2008; Lifton et al., 2014). The exposure ages calculated with "Lm" time-dependent scaling scheme and standard atmospheric pressure are used for discussion and result presentation (Lal, 1991; Stone, 2000). All ages are calculated with the local $^{10}$Be production rate for southern South America of 3.71±0.11 atoms/g/yr (Kaplan et al., 2011). We use a sample rock density of 2.65 g/cm$^3$ and apply no erosion correction. Reported $^{10}$Be/$^{9}$Be for 07KNSTD is $2.85 \cdot 10^{-12}$ (Nishiizumi et al., 2007).

#### 4.5.3.3. Hemisphere return to glacial conditions during the LGT

Our moraine-based $^{10}$Be data show that a return to wetter and colder conditions in the Andes of central Chile occurred at near the same time of other glaciers in the Southern Hemisphere during the LGT. The LGT frame one of the largest reorganizations of the climate between both hemispheres over the late-Quaternary (Denton et al., 2010), which is commonly referred as an oceanic and atmospheric "bipolar seesaw" (Broecker, 1998). The bipolar seesaw is based on the apparent opposite glacial-to-interglacial conditions between the northern and southern hemispheres during the LGT. The winter cooling of the Northern Hemisphere produced extended sea ice that prompted a southward shift of the global atmospheric system, including the SWW. The southward displacement of the SWW would have caused the ventilation of $CO_2$ from the Southern Ocean (Anderson et al., 2009; Toggweiler et al., 2006). Thus, the poleward shift of the SWW during the early LGT (17.5 -14.5 ka) increased the temperatures in Antarctica and worldwide, producing seasonal extremes in the North Atlantic during the Heinrich Stadial (Denton et al., 2005) (Figure 25e). At that time central Chile and the Chilean Lake District recorded a warmer and drier early LGT compared to the LGM (Lamy et al., 1999; Valero-Garcés et al., 2005; Pesce and Moreno, 2014; Henríquez et al., 2021; Moreno et al., 2022).

The warming trend of the early LGT in the Southern Hemisphere was interrupted by a millennial-scale cooling stadial known as Antarctic Cold Reversal (Blunier et al., 1997; Pedro et al., 2011, 2016). During the ACR, the return to glacial conditions produced, one more time, a northward shift of the SWW that triggered glacier advances in the southern mid-latitudes (Fletcher et al., 2021). The equatorward shift of the SWW during the ACR reduced the ventilation of the $CO_2$

from the deep Southern Ocean (Toggweiler et al., 2006) thus lowering the air temperature. From a global perspective, the return to cooling conditions in the Southern Hemisphere coincided partly with the warm phase in the Northern Hemisphere called Bølling-Allerød (Figure. 25e; Liu et al., 2009; Portilho-Ramos et al., 2017).

Sedimentological and ecological records of the central Chile paleoclimate expose wetter and colder conditions between 11.5 to 13.5 ka (Villagrán and Varela, 1990; Lamy et al., 1999; Valero-Garcés et al., 2005), as well as the Chilean Lake District, according to palynological studies (Moreno et al., 1999, 2022; Moreno and Videla, 2016; Henríquez et al., 2021). Radiocarbon and TCN dating as well confirmed the return to wetter and colder conditions during late-glacial times in southern Patagonia (Douglass et al., 2006; Moreno et al., 2009; Strelin et al., 2011; García et al., 2012; Sagredo et al., 2018; Mendelová et al., 2020; Soteres et al., 2022) and New Zealand (Newnham and Lowe, 2000; Vandergoes et al., 2008; Doughty et al., 2013; Kaplan et al., 2013), evidencing again a symmetric paleoclimate trend at both sides of the Pacific. The records that evidence a return to wetter and colder conditions from mid to southernmost latitudes remarks the origin of this late-glacial advance in the equatorward shift of the SWW linked to cooling in the Antarctic region , (Kaiser et al., 2005, 2008; Lamy et al., 1999, 2000).

The paleoclimate proxies recovered from central Chile and Northern Patagonia, afford evidence for wetter and colder conditions not only in the ACR, but also during the Younger Dryas timeframe. The YD is the latest Stadial period that occurred in the Northern Hemisphere between 11.5 to 12.8 ka (Figure. 25; Muscheler et al., 2008). A glacial advance at this time in the southern mid-latitudes is concurrent by warming in Antarctic (Figure 25b, c). The late-glacial expansion of the Universidad could be explained by lingered low temperatures in response to Antarctic deglacial discharge of freshwater into the Southern Ocean which would lead to surface ocean

stratification and limited outgassing of $CO_2$ (Marcott et al., 2014). This could explain a stabilization of temperatures which, in turn, could have been favored by a standstill or minor readvance phase of glaciers within the YD and beginning of the Holocene in Andes of central Chile (e.g., this work), Patagonia , (Strelin et al., 2011, Mendelová et al., 2017, 2020; Soteres et al., 2022) and New Zealand (Kaplan et al., 2013, Denton and Hendy, 1994). This interpretation suggests a decoupling of the bipolar seesaw mechanism and favours a global paleoclimate signal at the end of the LGT and the early Holocene.

## 4.6. Conclusions

Here we present the most detailed reconstruction of the late-Quaternary glaciations for the Andes of central Chile, as based on the geomorphology and geochronology of the Universidad Glacier (34° S). Main conclusions of this chapter are:

- Moraine UNI I reaches ~1100 m. a.s.l. and is 20 km from the present-day glacier front. This moraine yielded exposure ages dating to the pre-LGM, representing the most extensive and oldest documented glacier stage in the valley. The available data does not allow for establishing a clear link with a specific climate event.
- Moraine UNI II occurs between 1550 to 1750 m a.s.l., at 15 km further down-valley from the present-day glacier and it was built during the LGM (culminating at 18.2±1.0 ka). The equatorward migration of the SWW, which brought humid and cold conditions to low latitudes, is considered the primary atmospheric forcing for this glacier expansion. The LGM, which was expressed as a glacier expansion worldwide, was triggered by orbital forcings and, particularly, by the marked winter seasonality in the Southern Hemisphere that allowed the cooling in and around Antarctica.
- Moraine UNI III is a well-preserved glacial landform that occurs at 1650 m a.s.l. and ~10 km away from the present-day glacier. The moraine UNI III evidences a return of glacial conditions during the LGT between 9.7±0.5 to 14.4±1.1 (mean of 11.8±1.8 ka). The analysis of different proxies along the extratropical Andes suggests that the origin this late-glacial readvance is tied mainly to the northward shift of the SWW and, possibly, stabilization of decreased temperatures during the end of LGT and beginning of the Holocene.

- After moraine UNI III there is no clear evidence of glacier readvances until, at least, the last millennium in the Universidad Glacier valley (Fernández et al., 2022).

# 5. CONCLUSIONES GENERALES

El Glaciar Universidad (34° 42' S, 70° 20' S; ~2500 a 4990 m s.n.m.) y sus registros geológicos han sido la base para una de las reconstrucciones glaciales y paleoclimáticas más completas de los Andes subtropicales.

El Glaciar Universidad tuvo condiciones frías y húmedas que lo llevaron a su máxima extensión en periodos Pre-Último Máximo Glacial, en algún momento entre los 51.4±2.7 a 135.9±7.1 ka. En aquel estadio, el Glaciar Universidad se extendió hasta los ~1100 m s.n.m. y su posición de frente del hielo estuvo a ~20 km de su frente actual. En esta tesis no se ha podido brindar una geocronología ni contexto paleoclimático detallado para los cambios glaciares Pre-Último Máximo, por lo que se sugiere mejorar el mapeo de la geomorfología glacial y la geocronología en estudios futuros. Esto permitiría comprender mejor la magnitud y el momento de una de las mayores glaciaciones que aún mantiene registros geológicos bien preservados en los Andes de Chile central.

Los datos generados en esta tesis indican que el Glaciar Universidad alcanzó una segunda extensión máxima durante la culminación del Último Máximo Glacial (~18 ka). En aquel periodo el Glaciar Universidad se extendió hasta los ~1540 m.s.n.m. y su límite inferior estuvo a ~15 km de distancia del frente glaciar actual. Nuestros datos son consistentes con otros trabajos llevados a cabo en Chile central, a lo largo de Patagonia y en los Alpes Neozelandeses. A pesar de los avances asociados a la reconstrucción del Último Máximo Glacial en los Andes de Chile central, se observa como necesario lograr mayor claridad respecto a los límites de la extensión de hielo cordillerano y las condiciones atmosféricas de aquel momento, tales como la cantidad de precipitaciones y/o la temperatura.

Tras la culminación del Último Máximo Glacial comenzó la Última Terminación Glacial, fase que marcó la transición desde condiciones generales glaciales (frías y húmedas) a interglaciales (cálidas y secas). Los datos obtenidos en esta investigación indican que la Última Terminación Glacial en los Andes de Chile central no fue lineal. Hubo un retorno de condiciones frías y húmedas que provocaron la expansión del Glaciar Universidad hasta los 1650 m.s.n.m y a ~10 km del frente glaciar en los últimos ~11.8±1.8 ka. La reversión a condiciones más frías y húmedas durante la Última Terminación Glacial coincide, una vez más, con datos obtenidos en Chile central, Patagonia y los Alpes neozelandeses. Por lo cual sugerimos que esta reversión climática tuvo un alcance hemisférico, al menos, desde las latitudes medias hasta las regiones subantárticas.

Los datos geomorfológicos y geocronológicos presentados aquí permiten indicar que el Holoceno se ha caracterizado como un periodo de alto reajuste sedimentario en la parte alta del valle del Glaciar Universidad. Procesos gravitatorios de alta montaña (ej. derrumbes, deslizamientos de laderas, y flujos y conos de escombros) han cubierto los flancos y el fondo del valle, lo que ha limitado la identificación de cualquier geoforma de origen glaciar. A pesar de lo anterior, se han podido mapear y fechar registros glaciales generados principalmente al último milenio.

El complejo morrénico UNI IV, que ocupa toda el área proglacial actual, evidencia al menos dos extensiones máximas del Glaciar Universidad, los que a su vez reflejan condiciones más frías y húmedas que las actuales. Estos reavances, que alcanzaron el límite distal del complejo morrénico UNI IV (a ~3 km del frente glaciar actual), ocurrieron primero entre el siglo 13 y finales del siglo 16, y luego entre principios y mediados del siglo 19. Un reavance glacial ocurrido

a mediados del siglo 20 cubrió la mitad del complejo morrénico UNI IV. Tras aquel evento, el glaciar solo ha tendido a decaer y a tener pulsos discretos.

La evolución geomorfológica del Glaciar Universidad durante los periodos cálidos y secos del último milenio, se ha caracterizado el desarrollo de una cobertura sedimentaria en los márgenes del hielo. Esto se explica por el intenso reajuste paraglacial que promueve tanto el colapso de las paredes del valle como de las morrenas laterales sobre el glaciar. Se ha catastrado en este trabajo que el proceso de balance de masa negativo actual y subactual del Glaciar Universidad se distingue por proceso glaciológicos y geomorfológicos que parecen ser propios del Holoceno tardío. Es decir, la degradación del Glaciar Universidad durante los últimos milenios ocurre mientras que el hielo activo (glaciar superior) fluye valle abajo sobre un hielo estancado o de flujo lento que se encuentra cubierto de escombros (glaciar inferior), y que ya se ha separado o que ha comenzado a separarse del resto del glaciar. La diferencia en la dinámica de flujo entre el glaciar superior e inferior provoca fracturas de origen glaciotectónicos. La diferencia de presión en la zona del fallamiento glaciotectónico facilita el afloramiento de material sedimentario de origen subglacial el que, a su vez, aporta material al desarrollo de una cobertura sedimentaria en el frente glaciar. De esta manera, la mejor forma de entender la evolución holocénica del glaciar Universidad es desde un glaciar sin cobertura de escombros (o limpio), a un glaciar con sus márgenes cubiertos por sedimentos, a morrenas con núcleo de hielo a, finalmente, un topografía irregular y masiva de morrena de hielo muerto. Concluimos que la degradación y evolución del hielo glaciar bajo una cobertura sedimentaria será una de las improntas del paisaje alto andino en el contexto de calentamiento y desecación atmosférica del siglo 21.

Los principales forzantes atmosféricos que controlan el balance de masa positivo y negativo del Glaciar Universidad en el mediano y largo plazo son los Vientos del Oeste y el Anticiclón del Pacífico Subtropical. La migración de los Vientos del Oeste hacia latitudes medias transporta humedad y condiciones frías que favorecen la caída de precipitación nival en las secciones altas de la cordillera. Sugerimos que este movimiento latitudinal de los Vientos del Oeste ha sido el principal factor de la expansión del Glaciar Universidad durante el Último Máximo Glacial, la reversión fría de la Última Terminación Glacial y los dos máximos del hielo del último milenio. Lo anterior implica que los Vientos del Oeste migraron hacia Chile central y se mantuvieron en la misma posición latitudinal por un periodo más largo que en la actualidad. La migración hacia el norte del cinturón de los Vientos del Oeste se provoca por un enfriamiento de la Antártica y sus regiones adyacentes. Por lo cual asumimos que la expansión del Glaciar Universidad tiene un control atmosférico de origen subantártico.

Condiciones cálidas y secas en Chile central se asocian al fortalecimiento del Anticiclón del Pacífico Subtropical, que es el principal generador de condiciones cálidas y secas durante el verano austral. Inferimos que los periodos de retroceso glaciar ocurridos a comienzos de la Última Terminación Glacial y, al parecer, durante buena parte del Holoceno, se debieron a la intensificación del Anticiclón del Pacífico Subtropical y, por tanto, al debilitamiento de los Vientos del Oeste.

## 6. REFERENCIAS


Abele, G., 1984. Derrumbes de montaña y morrenas en los Andes chilenos. Revista de Geografia Norte Grande 11, 17–30.

Abele, G., 1982. El Lahar Tinguiririca: su significado entre los Lahares chilenos. Investigaciones Geográficas 29, 21–34. https://doi.org/10.5354/0719-5370.1982.27670

Abraham, E.M., Rodríguez, M.D., Rubio, M.C., Guida-Johnson, B., Gomez, L., Rubio, C., 2020. Disentangling the concept of "South American Arid Diagonal." Journal of Arid Environments 175, 104089. https://doi.org/10.1016/j.jaridenv.2019.104089

Abram, N.J., Mulvaney, R., Vimeux, F., Phipps, S.J., Turner, J., England, M.H., 2014. Evolution of the Southern Annular Mode during the past millennium. Nature Climate Change 4, 564–569. https://doi.org/10.1038/nclimate2235

Ackert, R.P., Becker, R.A., Singer, B.S., Kurz, M.D., Caffee, M.W., Mickelson, D.M., 2008. Patagonian glacier response during the Late Glacial–Holocene transition. Science 321, 392–395. https://doi.org/10.1126/science.1157215

Aguilar, G., Riquelme, R., Lohse, P., Cabré, A., García, J.-L., 2022. Chronology of glacial advances and deglaciation in the Encierro River Valley (29° Lat. S), Southern Atacama Desert, based on geomorphological mapping and cosmogenic 10Be exposure ages. Frontiers in Earth Science 10, 1–8. https://doi.org/10.3389/feart.2022.878318

Anderson, R.F., Ali, S., Bradtmiller, L.I., Nielsen, S.H.H., Fleisher, M.Q., Anderson, B.E., Burckle, L.H., 2009. Wind-driven upwelling in the Southern Ocean and the deglacial rise in atmospheric CO 2. Science 323, 1443–1448. https://doi.org/10.1126/science.1167441

Antinao, J.L., Gosse, J., 2009. Large rockslides in the Southern Central Andes of Chile (32–34.5°S): Tectonic control and significance for Quaternary landscape evolution. Geomorphology 104, 117–133. https://doi.org/10.1016/j.geomorph.2008.08.008

Araneda, A., Torrejón, F., Aguayo, M., Mendoza, C., Urrutia, R., 2009. Historical records of Cipreses glacier (34°S): combining documentary-inferred 'Little Ice Age' evidence from Southern and Central Chile. The Holocene 19, 1173–1183. https://doi.org/10.1177/0959683609345079

Ayala, A., Pellicciotti, F., MacDonell, S., McPhee, J., Vivero, S., Campos, C., Egli, P., 2016. Modelling the hydrological response of debris-free and debris-covered glaciers to present climatic conditions in the semiarid Andes of central Chile. Hydrological Processes. https://doi.org/10.1002/hyp.10971

Azócar, G.F., Brenning, A., 2010. Hydrological and geomorphological significance of rock glaciers in the dry Andes, Chile (27°-33°S). Permafrost and Periglacial Processes 21, 42–53. https://doi.org/10.1002/ppp.669

Azócar, G.F., Brenning, A., Bodin, X., 2017. Permafrost distribution modelling in the semi-arid Chilean Andes. Cryosphere 11, 877–890. https://doi.org/10.5194/tc-11-877-2017

Balco, G., Stone, J.O., Lifton, N.A., Dunai, T.J., 2008. A complete and easily accessible means

of calculating surface exposure ages or erosion rates from 10Be and 26Al measurements. Quaternary Geochronology 3, 174–195. https://doi.org/10.1016/j.quageo.2007.12.001

Ballantyne, C.K., 2008. After the ice: Holocene geomorphic activity in the Scottish Highlands, Scottish Geographical Journal. https://doi.org/10.1080/14702540802300167

Ballantyne, C.K., 2002. Paraglacial geomorphology. Quaternary Science Reviews 21, 1935–2017. https://doi.org/10.1016/S0277-3791(02)00005-7

Ballantyne, C.K., 1995. Paraglacial debris-cone formation on recently deglaciated terrain, western Norway. Holocene 5, 25–33. https://doi.org/10.1177/095968369500500104

Barcaza, G., Nussbaumer, S.U., Tapia, G., Valdés, J., García, J.-L., Videla, Y., Albornoz, A., Arias, V., 2017. Glacier inventory and recent glacier variations in the Andes of Chile, South America. Annals of Glaciology 58, 166–180. https://doi.org/10.1017/aog.2017.28

Barker, S., Diz, P., Vautravers, M.J., Pike, J., Knorr, G., Hall, I.R., Broecker, W.S., 2009. Interhemispheric Atlantic seesaw response during the last deglaciation. Nature 457, 1097–1102. https://doi.org/10.1038/nature07770

Barria, I., Carrasco, J., Casassa, G., Barria, P., 2019. Simulation of long-term changes of the equilibrium line altitude in the central Chilean Andes mountains derived from atmospheric variables during the 1958–2018 Period. Frontiers in Environmental Science 7. https://doi.org/10.3389/fenvs.2019.00161

Barsch, D., Liedtke, H., 1980. Principles, scientific value and practical applicability of the geomorphological map of the Federal Republic of Germany at the scale 1:50000 (GMK 25) and 1:100000 (GMK 100). Zeitschrift für Geomorphologie, Supplementary Issues 296–313.

Bauska, T.K., Marcott, S.A., Brook, E.J., 2021. Abrupt changes in the global carbon cycle during the last glacial period. Nature Geoscience 14, 91–96. https://doi.org/10.1038/s41561-020-00680-2

Bellisario, A., Ferrando, F., Janke, J., 2013. Water resources in Chile: The critical relation between glaciers and mining for sustainable water management. Investigación Geográfica de Chile 46, 3–24.

Benn, D., I., Evans, D.J.A., 2014. Glaciers and glaciation, Second. ed. Routledge, London. https://doi.org/10.4324/9780203785010

Benn, D.I., 2021. Surging glaciers in Scotland. Scottish Geographical Journal 0, 1–40. https://doi.org/10.1080/14702541.2021.1922738

Benn, D.I., 1992. The genesis and significance of “hummocky moraine”: Evidence from the Isle of Skye, Scotland. Quaternary Science Reviews 11, 781–799. https://doi.org/10.1016/0277-3791(92)90083-K

Benn, D.I., Owen, L., 2002. Himalayan glacial sedimentary environments: A framework for reconstructing and dating the former extent of glaciers in high mountains. Quaternary International 97–98, 3–25. https://doi.org/10.1016/S1040-6182(02)00048-4

Benn, D.I., Thompson, S., Gulley, J., Mertes, J., Luckman, A., Nicholson, L., 2017. Structure

and evolution of the drainage system of a Himalayan debris-covered glacier, and its relationship with patterns of mass loss. The Cryosphere 11, 2247–2264. https://doi.org/10.5194/tc-11-2247-2017

Bennett, M.R., Glasser, N.F., 2009. Glacial Geology: Ice sheets and landforms, Second edi. ed. Wiley-Blackwell, Sussex, UK.

Bennett, M.R., Huddart, D., Glasser, N.F., Hambrey, M.J., 2000. Resedimentation of debris on an ice-cored lateral moraine in the high-Arctic (Kongsvegen, Svalbard). Geomorphology 35, 21–40. https://doi.org/10.1016/S0169-555X(00)00017-9

Berger, A., Loutre, M.F., 1991. Insolation values for the climate of the last 10 million years. Quaternary Science Reviews 10, 297–317. https://doi.org/10.1016/0277-3791(91)90033-Q

Bhambri, R., Hewitt, K., Kawishwar, P., Pratap, B., 2017. Surge-type and surge-modified glaciers in the Karakoram. Scientific Reports 7, 1–14. https://doi.org/10.1038/s41598-017-15473-8

Bitinas, A., Karmaziene, D., Jusiene, A., 2004. Glaciolacustrine kame terraces as an indicator of conditions of deglaciation in Lithuania during the Last Glaciation. Sedimentary Geology 165, 285–294. https://doi.org/10.1016/j.sedgeo.2003.11.012

Blunier, T., Schwander, J., Stauffer, B., Stocker, T., Dällenbach, A., Indermühle, A., Tschumi, J., Chappellaz, J., Raynaud, D., Barnola, J.M., 1997. Timing of the Antarctic Cold Reversal and the atmospheric CO2 increase with respect to the Younger Dryas event. Geophysical Research Letters 24, 2683–2686. https://doi.org/10.1029/97GL02658

Bodin, X., Rojas, F., Brenning, A., 2010. Status and evolution of the cryosphere in the Andes of Santiago (Chile, 33.5°S.). Geomorphology 118, 453–464. https://doi.org/10.1016/j.geomorph.2010.02.016

Boisier, J.P., Alvarez-Garreton, C., Cordero, R.R., Damiani, A., Gallardo, L., Garreaud, R.D., Lambert, F., Ramallo, C., Rojas, M., Rondanelli, R., 2018. Anthropogenic drying in central-southern Chile evidenced by long-term observations and climate model simulations. Elementa 6. https://doi.org/10.1525/elementa.328

Boulton, G.S., 1976. The origin of glacially fluted surfaces-observations and theory. Journal of Glaciology 17, 287–309. https://doi.org/10.3189/S0022143000013605

Bouttes, N., Paillard, D., Roche, D.M., 2010. Impact of brine-induced stratification on the glacial carbon cycle. Climate of the Past 6, 575–589. https://doi.org/10.5194/cp-6-575-2010

Bown, F., Rivera, A., Acuña, C., 2008. Recent glacier variations at the Aconcagua basin, central Chilean Andes. Annals of Glaciology 48, 43–48. https://doi.org/10.3189/172756408784700572

Bradley, R.S., Briffa, K.R., Cole, J., Hughes, M.K., Osborn, T.J., 2003. The Climate of the Last Millennium, in: Alverson K.D., Pedersen T.F., Bradley R.S. (Eds.), Paleoclimate, Global Change and the Future. Global Change. Springer, Berlin, Heidelberg, pp. 105–141. https://doi.org/10.1007/978-3-642-55828-3_6

Bravo, C., Loriaux, T., Rivera, A., Brock, B.W., 2017. Assessing glacier melt contribution to

streamflow at Universidad Glacier, central Andes of Chile. Hydrology and Earth System Sciences 21, 3249–3266. https://doi.org/10.5194/hess-21-3249-2017

Brenning, A., 2005. Geomorphological, hydrological and climatic significance of rock glaciers in the Andes of Central Chile (33-35°S). Permafrost and Periglacial Processes 16, 231–240. https://doi.org/10.1002/ppp.528

Broccoli, A.J., Manabe, S., 1987. The influence of continental ice, atmospheric CO2, and land albedo on the climate of the last glacial maximum. Climate Dynamics 1, 87–99. https://doi.org/10.1007/BF01054478

Broecker, W.S., 1998. Paleocean circulation during the Last Deglaciation: A bipolar seesaw? Paleoceanography 13, 119–121. https://doi.org/10.1029/97PA03707

Broecker, W.S., Denton, G.H., 1990. The role of ocean-atmosphere reorganizations in glacial cycles. Quaternary Science Reviews 9, 305–341. https://doi.org/10.1016/0277-3791(90)90026-7

Buri, P., Miles, E.S., Steiner, J.F., Ragettli, S., Pellicciotti, F., 2021. Supraglacial ice cliffs can substantially increase the mass loss of debris-covered glaciers. Geophysical Research Letters 48. https://doi.org/10.1029/2020GL092150

Carrasco, J.F., Casassa, G., Quintana, J., 2005. Changes of the 0°C isotherm and the equilibrium line altitude in central Chile during the last quarter of the 20th century. Hydrological Sciences Journal 50, 933–948. https://doi.org/10.1623/hysj.2005.50.6.933

Caviedes, C., Paskoff, R., 1975. Quaternary glaciations in the Andes of north-central Chile. Journal of Glaciology 14, 155–170. https://doi.org/10.1002/jqs.1050

Charrier, R., Iturrizaga, L., Carretier, S., Regard, V., 2019. Geomorphologic and Glacial Evolution of the Cachapoal and southern Maipo catchments in the Andean Principal Cordillera, Central Chile (34°-35º S). Andean Geology 46, 240. https://doi.org/10.5027/andgeoV46n2-3108

Charrier, R., Lillo, F., 1973. Geología regional y geoquímica del drenaje de las provincias de O'Higgins y Colchagua. Instituto de Investigaciones de Recursos Naturales, Santiago.

Chavaillaz, Y., Codron, F., Kageyama, M., 2013. Southern westerlies in LGM and future (RCP4.5) climates. Climate of the Past 9, 517–524. https://doi.org/10.5194/cp-9-517-2013

Chmeleff, J., von Blanckenburg, F., Kossert, K., Jakob, D., 2010. Determination of the 10 Be half-life by multicollector ICP-MS and liquid scintillation counting. Nuclear Instruments and Methods in Physics Research, Section B: Beam Interactions with Materials and Atoms 268, 192–199. https://doi.org/10.1016/j.nimb.2009.09.012

Christie, D.A., Boninsegna, J.A., Cleaveland, M.K., Lara, A., Le Quesne, C., Morales, M.S., Mudelsee, M., Stahle, D.W., Villalba, R., 2011. Aridity changes in the Temperate-Mediterranean transition of the Andes since AD 1346 reconstructed from tree-rings. Climate Dynamics 36, 1505–1521. https://doi.org/10.1007/s00382-009-0723-4

Christl, M., Vockenhuber, C., Kubik, P.W., Wacker, L., Lachner, J., Alfimov, V., Synal, H.A., 2013. The ETH Zurich AMS facilities: Performance parameters and reference materials. Nuclear Instruments and Methods in Physics Research, Section B: Beam Interactions with

Materials and Atoms 294, 29–38. https://doi.org/10.1016/j.nimb.2012.03.004

Clark, P.U., Dyke, A.S., Shakun, J.D., Carlson, A.E., Clark, J., Wohlfarth, B., Mitrovica, J.X., Hostetler, S.W., McCabe, A.M., 2009. The Last Glacial Maximum. Science 325, 710–714. https://doi.org/10.1126/science.1172873

Clark, P.U., Mix, A.C., 2002. Ice sheets and sea level of the Last Glacial Maximum. Quaternary Science Reviews 21, 1–7. https://doi.org/10.1016/S0277-3791(01)00118-4

Clayton, L., 1964. Karst topography on stagnant glaciers. Journal of Glaciology 5, 107–112. https://doi.org/10.3189/S0022143000028628

Crump, S.E., Anderson, L.S., Miller, G.H., Anderson, R.S., 2017. Interpreting exposure ages from ice-cored moraines: a Neoglacial case study on Baffin Island, Arctic Canada. Journal of Quaternary Science 32, 1049–1062. https://doi.org/10.1002/jqs.2979

Curry, A.M., Cleasby, V., Zukowskyj, P., 2006. Paraglacial response of steep, sediment-mantled slopes to post-'Little Ice Age' glacier recession in the central Swiss Alps. Journal of Quaternary Science 21, 211–225. https://doi.org/10.1002/jqs.954

Dätwyler, C., Grosjean, M., Steiger, N.J., Neukom, R., 2020. Teleconnections and relationship between the El Niño–Southern Oscillation (ENSO) and the Southern Annular Mode (SAM) in reconstructions and models over the past millennium. Climate of the Past 16, 743–756. https://doi.org/10.5194/cp-16-743-2020

Dätwyler, C., Neukom, R., Abram, N.J., Gallant, A.J.E., Grosjean, M., Jacques-Coper, M., Karoly, D.J., Villalba, R., 2018. Teleconnection stationarity, variability and trends of the Southern Annular Mode (SAM) during the last millennium. Climate Dynamics 51, 2321–2339. https://doi.org/10.1007/s00382-017-4015-0

De Jong, R., Von Gunten, L., Maldonado, A., Grosjean, M., 2013. Late Holocene summer temperatures in the central Andes reconstructed from the sediments of high-elevation Laguna Chepical, Chile (32 S). Climate of the Past 9, 1921–1932. https://doi.org/10.5194/cp-9-1921-2013

Deblonde, G., Peltier, W.R., Hyde, W.T., 1992. Simulations of continental ice sheet growth over the last glacial-interglacial cycle: experiments with a one level seasonal energy balance model including seasonal ice albedo feedback. Global and Planetary Change 6, 37–55. https://doi.org/10.1016/0921-8181(92)90021-2

Deckart, K., Pinochet, K., Sepúlveda, S., Pinto, L., Moreiras, S.M., 2014. New insights on the origin of the Mesón Alto deposit , Yeso Valley , Central Chile: A composite deposit of glacial and landslide processes? Andean Geology 41, 248–258. https://doi.org/10.5027/andgeoV41n1-a10

Denton, G., Alley, R., Comer, G., Broecker, W., 2005. The role of seasonality in abrupt climate change. Quaternary Science Reviews 24, 1159–1182. https://doi.org/10.1016/j.quascirev.2004.12.002

Denton, G.H., Anderson, R.F., Toggweiler, J.R., Edwards, R.L., Schaefer, J.M., Putnam, A.E., 2010b. The Last Glacial Termination. Science 328, 1652–1656. https://doi.org/10.1126/science.1184119

Denton, G.H., Hendy, C.H., 1994. Younger Dryas age advance of Franz Josef Glacier in the Southern Alps of New Zealand. Science 264, 1434–1437. https://doi.org/10.1126/science.264.5164.1434

Denton, G.H., Heusser, C.J., Lowel, T.V., Moreno, P.I., Andersen, B.G., Heusser, L.E., Schluhter, C., Marchant, D.R., 1999a. Interhemispheric Linkage of Paleoclimate During the Last Glaciation. Geografiska Annaler, Series A: Physical Geography 81, 107–153. https://doi.org/10.1111/1468-0459.00055

Denton, G.H., Lowell, T.V., Heusser, C.J., Schluchter, C., Andersen, B.G., Heusser, L.E., Moreno, P.I., Marchant, D.R., 1999b. Geomorphology, Stratigraphy, and Radiocarbon Chronology of LlanquihueDrift in the Area of the Southern Lake District, Seno Reloncavi, and Isla Grande de Chiloe, Chile. Geografiska Annaler, Series A: Physical Geography 81, 167–229. https://doi.org/10.1111/j.0435-3676.1999.00057.x

Denton, G.H., Putnam, A.E., Russell, J.L., Barrell, D.J.A., Schaefer, J.M., Kaplan, M.R., Strand, P.D., 2021. The Zealandia Switch: Ice age climate shifts viewed from Southern Hemisphere moraines. Quaternary Science Reviews 257, 106771. https://doi.org/10.1016/j.quascirev.2020.106771

Denton, G.H., Toucanne, S., Putnam, A.E., Barrell, D.J.A., Russell, J.L., 2022. Heinrich summers. Quaternary Science Reviews 295, 107750. https://doi.org/10.1016/j.quascirev.2022.107750

Dirección General de Aguas, 2014. Catastro nacional de glaciares. Unidad de Glaciología y Nieves, Dirección General de Aguas. Ministerio de Obras Públicas.

Dirección General de Aguas (DGA), 2022a. Monitoreo de detalle del Glaciar Juncal Norte, Región de Valparaíso, Macrozona Centro, 2020-2021.

Dirección General de Aguas (DGA), 2022b. Inventario Público de Glaciares. Santiago, Chile.

Dobreva, I., Bishop, M., Bush, A., 2017. Climate–glacier dynamics and topographic forcing in the Karakoram Himalaya: concepts, issues and research directions. Water 9, 405. https://doi.org/10.3390/w9060405

Dong, B., Dai, A., 2015. The influence of the Interdecadal Pacific Oscillation on Temperature and Precipitation over the Globe. Climate Dynamics 2667–2681. https://doi.org/10.1007/s00382-015-2500-x

Doughty, A.M., Anderson, B.M., Mackintosh, A.N., Kaplan, M.R., Vandergoes, M.J., Barrell, D.J.A., Denton, G.H., Schaefer, J.M., Chinn, T.J.H., Putnam, A.E., 2013. Evaluation of Lateglacial temperatures in the Southern Alps of New Zealand based on glacier modelling at Irishman Stream, Ben Ohau Range. Quaternary Science Reviews 74, 160–169. https://doi.org/10.1016/j.quascirev.2012.09.013

Doughty, A.M., Schaefer, J.M., Putnam, A.E., Denton, G.H., Kaplan, M.R., Barrell, D.J.A., Andersen, B.G., Kelley, S.E., Finkel, R.C., Schwartz, R., 2015. Mismatch of glacier extent and summer insolation in Southern Hemisphere mid-latitudes. Geology 43, 407–410. https://doi.org/10.1130/G36477.1

Douglass, D., Singer, B.S., Kaplan, M.R., Mickelson, D., Caffee, M.W., 2006. Cosmogenic

nuclide surface exposure dating of boulders on last-glacial and late-glacial moraines, Lago Buenos Aires, Argentina: Interpretive strategies and paleoclimate implications. Quaternary Geochronology 1, 43–58. https://doi.org/10.1016/j.quageo.2006.06.001

Dunai, T.J., 2010. Cosmogenic nuclides: principles, concepts and applications in the earth surface sciences. Cambridge University Press, Cambridge.

Dussaillant, I., Berthier, E., Brun, F., Masiokas, M., Hugonnet, R., Favier, V., Rabatel, A., Pitte, P., Ruiz, L., 2019. Two decades of glacier mass loss along the Andes. Nature Geoscience 12, 802–808. https://doi.org/10.1038/s41561-019-0432-5

Eaves, S.R., Winckler, G., Mackintosh, A.N., Schaefer, J.M., Townsend, D.B., Doughty, A.M., Jones, R.S., Leonard, G.S., 2019. Late-glacial and Holocene glacier fluctuations in North Island, New Zealand. Quaternary Science Reviews 223, 105914. https://doi.org/10.1016/j.quascirev.2019.105914

Eichel, J., Draebing, D., Meyer, N., 2018. From active to stable: Paraglacial transition of Alpine lateral moraine slopes. Land Degradation & Development 29, 4158–4172. https://doi.org/10.1002/ldr.3140

Escobar, F., Aceituno, P., 1998. Influencia del fenómeno ENSO sobre la precipitación nival en el sector andino de Chile central durante el invierno. Bulletin de l'Institut français d'études andines 27.

Espizua, L.E., 2005. Holocene glacier chronology of Valenzuela Valley, Mendoza Andes, Argentina. The Holocene 15, 1079–1085. https://doi.org/10.1191/0959683605hl866rr

Espizua, L.E., 2004. Pleistocene glaciations in the Mendoza Andes, Argentina, in: Ehlers, J., Gibbard, P. (Eds.), Quaternary Glaciations:Extent and Chronology. Elsevier B.V, Cambridge, pp. 69–73. https://doi.org/10.1016/S1571-0866(04)80112-X

Espizua, L.E., 1993. Quaternary Glaciations in the Río Mendoza Valley, Argentine Andes. Quaternary Research 40, 150–162. https://doi.org/10.1006/qres.1993.1067

Espizua, L.E., Pitte, P., 2009. The Little Ice Age glacier advance in the Central Andes (35°S), Argentina. Palaeogeography, Palaeoclimatology, Palaeoecology 281, 345–350. https://doi.org/10.1016/j.palaeo.2008.10.032

Evans, D.J.A., 2014. Glacial landsystems, 1st ed. Routledge. https://doi.org/10.4324/9780203784976

Evans, D.J.A., 2013. Glacial Landsystems, in: Evans, David J.A. (Ed.), Glacial Landsystems. Arnold, New York, p. 532.

Evans, D.J.A., 2011. Glacial landsystems of Satujökull, Iceland: A modern analogue for glacial landsystem overprinting by mountain icecaps. Geomorphology 129, 225–237. https://doi.org/10.1016/j.geomorph.2011.01.025

Evans, D.J.A., 2009. Controlled moraines: origins, characteristics and palaeoglaciological implications. Quaternary Science Reviews 28, 183–208. https://doi.org/10.1016/j.quascirev.2008.10.024

Evans, D.J.A., Rea, B.R., 1999. Geomorphology and sedimentology of surging glaciers : a

land-systems approach. Annals of Glaciology 28, 75–82.

Evans, D.J.A., Twigg, D.R., 2002. The active temperate glacial landsystem: a model based on Breiðamerkurjökull and Fjallsjökull, Iceland. Quaternary Science Reviews 21, 2143–2177. https://doi.org/10.1016/S0277-3791(02)00019-7

Evans, D.J.A., Twigg, D.R., Rea, B.R., Orton, C., 2009. Surging glacier landsystem of tungnaárjökull, iceland. Journal of Maps 5, 134–151. https://doi.org/10.4113/jom.2009.1064

Ewertowski, M.W., Tomczyk, A.M., 2015. Quantification of the ice-cored moraines' short-term dynamics in the high-Arctic glaciers Ebbabreen and Ragnarbreen, Petuniabukta, Svalbard. Geomorphology 234, 211–227. https://doi.org/10.1016/j.geomorph.2015.01.023

Eyles, N., 1979. Facies of supraglacial sedimentation on Icelandic and Alpine temperate glaciers. Canadian Journal of Earth Sciences 16, 1341–1361. https://doi.org/10.1139/e79-121

Eyles, N., Rogerson, R.J., 1978. A framework for the investigation of medial moraine formation: Austerdalsbreen, Norway, and Berendon Glacier, British Columbia, Canada. Journal of Glaciology 20, 99–113. https://doi.org/10.3189/s0022143000021249

Falaschi, D., Bolch, T., Lenzano, M.G., Tadono, T., Lo Vecchio, A., Lenzano, L., 2018. New evidence of glacier surges in the Central Andes of Argentina and Chile. Progress in Physical Geography: Earth and Environment 42, 792–825. https://doi.org/10.1177/0309133318803014

Falvey, M., Garreaud, D., 2009. Regional cooling in a warming world : Recent temperature trends in the southeast Pacific and along the west coast of subtropical South America ( 1979 – 2006 ) 114, 1–16. https://doi.org/10.1029/2008JD010519

Farías-Barahona, D., Vivero, S., Casassa, G., Schaefer, M., Burger, F., Seehaus, T., Iribarren-Anacona, P., Escobar, F., Braun, M.H., 2019. Geodetic mass balances and area changes of Echaurren Norte Glacier (Central Andes, Chile) between 1955 and 2015. Remote Sensing 11. https://doi.org/10.3390/rs11030260

Fernández-Navarro, H., García, J.L., Nussbaumer, S.U., Tikhomirov, D., Pérez, F., Gärtner-Roer, I., Christl, M., Egli, M., 2023. Fluctuations of the Universidad Glacier in the Andes of central Chile (34° S) during the latest Holocene derived from a 10Be moraine chronology. Quaternary Science Reviews 300. https://doi.org/10.1016/j.quascirev.2022.107884

Fernández, H., Ferrando, F., 2018. Glaciares rocosos en la zona semiárida de Chile: relevancia de un recurso hídrico sin protección normativa. Cuadernos de Geografia: Revista Colombiana de Geografia 27, 338–355. https://doi.org/10.15446/rcdg.v27n2.63370

Fernández, H., García, J.-L., Nussbaumer, S.U., Geiger, A.J., Gärtner-Roer, I., Pérez, F., Tikhomirov, D., Christl, M., Egli, M., 2022a. De-icing landsystem model for the Universidad Glacier (34° S) in the Central Andes of Chile during the past ~660 years. Geomorphology 400, 108096. https://doi.org/10.1016/j.geomorph.2021.108096

Fletcher, M.-S., Pedro, J., Hall, T., Mariani, M., Alexander, J.A., Beck, K., Blaauw, M.,

Hodgson, D.A., Heijnis, H., Gadd, P.S., Lise-Pronovost, A., 2021. Northward shift of the southern westerlies during the Antarctic Cold Reversal. Quaternary Science Reviews 271, 107189. https://doi.org/10.1016/j.quascirev.2021.107189

Flores-Aqueveque, V., Rojas, M., Aguirre, C., Arias, P.A., González, C., 2020. South Pacific Subtropical High from the late Holocene to the end of the 21st century: insights from climate proxies and general circulation models. Climate of the Past 16, 79–99. https://doi.org/10.5194/cp-16-79-2020

Fogt, R.L., Marshall, G.J., 2020. The Southern Annular Mode: Variability, trends, and climate impacts across the Southern Hemisphere. Wiley Interdisciplinary Reviews: Climate Change 11, 1–24. https://doi.org/10.1002/wcc.652

Folland, C.K., Renwick, J.A., Salinger, M.J., Mullan, A.B., Nin, E., 2002. Relative influences of the Interdecadal Pacific Oscillation and ENSO on the South Pacific Convergence Zone 29, 2–5.

García, J.-L., Hein, A.S., Binnie, S.A., Gómez, G.A., González, M.A., Dunai, T.J., 2018. The MIS 3 maximum of the Torres del Paine and Última Esperanza ice lobes in Patagonia and the pacing of southern mountain glaciation. Quaternary Science Reviews 185, 9–26. https://doi.org/10.1016/j.quascirev.2018.01.013

García, J.-L., Pizarro, F., Calcagni, V., 2014. Fluctuaciones glaciales holocénicas en el Cajón del Maipo, Andes centrales de Chile: observaciones morfoestratigráficas de los glaciares Loma Larga y Nieves Negras, in: GEOlibros (Ed.), Los Riesgos Traen Oportunidades. Transformaciones Globales En Los Andes Sudamericanos. Instituto de Geografía de la Pontificia Universidad Católica de Chile, Santiago, pp. 35–52.

García, J., Andrade, B., Calderón, M., Lüthgens, C., 2019. Multi-millennial scale climate variability during MIS 3 and MIS 2 inferred from luminescence dating of coastal sand dunes and buried paleosol sequences in central Chile, 32°S. Journal of Quaternary Science 34, 203–214. https://doi.org/10.1002/jqs.3092

García, J.L., Hall, B.L., Kaplan, M.R., Gómez, G.A., De Pol-Holz, R., García, V.J., Schaefer, J.M., Schwartz, R., 2020. 14C and 10Be dated Late Holocene fluctuations of Patagonian glaciers in Torres del Paine (Chile, 51°S) and connections to Antarctic climate change. Quaternary Science Reviews 246. https://doi.org/10.1016/j.quascirev.2020.106541

García, J.L., Kaplan, M.R., Hall, B.L., Schaefer, J.M., Vega, R.M., Schwartz, R., Finkel, R., 2012. Glacier expansion in southern Patagonia throughout the Antarctic cold reversal. Geology 40, 859–862. https://doi.org/10.1130/G33164.1

García, J.L., Maldonado, A., De Porras, M.E., Delaunay, A.N., Reyes, O., Ebensperger, C.A., Binnie, S.A., Lüthgens, C., Méndez, C., 2019. Early deglaciation and paleolake history of Río Cisnes Glacier, Patagonian Ice Sheet (44°S). Quaternary Research (United States) 91, 194–217. https://doi.org/10.1017/qua.2018.93

Garreaud, R. D., 2009. The Andes climate and weather. Advances in Geosciences 22, 3–11. https://doi.org/10.5194/adgeo-22-3-2009

Garreaud, R D, 2009. The Andes climate and weather. Advances in Geosciences 7, 1–9.

Garreaud, R.D., Boisier, J.P., Rondanelli, R., Montecinos, A., Sepúlveda, H.H., Veloso-Aguila, D., 2020. The Central Chile Mega Drought (2010–2018): A climate dynamics perspective. International Journal of Climatology 40, 421–439. https://doi.org/10.1002/joc.6219

Garreaud, R.D., Vuille, M., Compagnucci, R., Marengo, J., 2009. Present-day South American climate. Palaeogeography, Palaeoclimatology, Palaeoecology 281, 180–195. https://doi.org/10.1016/j.palaeo.2007.10.032

Glasser, N.F., Hambrey, M.J., 2002. Sedimentary facies and landform genesis at a temperate outlet glacier: Soler glacier, North Patagonian Icefield. Sedimentology 49, 43–64. https://doi.org/10.1046/j.1365-3091.2002.00431.x

Gordon, A.L., 1991. Two Stable Modes of Southern Ocean Winter Stratification. pp. 17–35. https://doi.org/10.1016/S0422-9894(08)70058-8

Gordon, J.E., Brian Whalley, W., Gellatly, A.F., Vere, D.M., 1992. The formation of glacial flutes: Assessment of models with evidence from Lyngsdalen, North Norway. Quaternary Science Reviews 11, 709–731. https://doi.org/10.1016/0277-3791(92)90079-N

Gosse, J.C., Phillips, F.M., 2001. Terrestrial in situ cosmogenic nuclides: theory and application. Quaternary Science Reviews 20, 1475–1560. https://doi.org/10.1016/S0277-3791(00)00171-2

Gray, M., 1995. The kame terraces of lower Loch Etive. Scottish Geographical Magazine 111, 113–118. https://doi.org/10.1080/00369229518736949

Hambrey, M.J., Quincey, D.J., Glasser, N.F., Reynolds, J.M., Richardson, S.J., Clemmens, S., 2008. Sedimentological, geomorphological and dynamic context of debris-mantled glaciers, Mount Everest (Sagarmatha) region, Nepal. Quaternary Science Reviews 27, 2361–2389. https://doi.org/10.1016/j.quascirev.2008.08.010

Harrison, S., 2004. The Pleistocene glaciations of Chile, in: Developments in Quaternary Science. pp. 89–103. https://doi.org/10.1016/S1571-0866(04)80115-5

Hays, J.D., Imbrie, J., Shackleton, N.J., 1976. Variations in the Earth's Orbit: Pacemaker of the Ice Ages. Science 194, 1121–1132. https://doi.org/10.1126/science.194.4270.1121

Hein, A.S., Hulton, N.R.J., Dunai, T.J., Sugden, D.E., Kaplan, M.R., Xu, S., 2010. The chronology of the Last Glacial Maximum and deglacial events in central Argentine Patagonia. Quaternary Science Reviews 29, 1212–1227. https://doi.org/10.1016/j.quascirev.2010.01.020

Henríquez, C.A., Moreno, P.I., Dunbar, R.B., Mucciarone, D.A., 2021. The last glacial termination in northwestern Patagonia viewed from the Lago Fonk (∼40°S) record. Quaternary Science Reviews 271, 107197. https://doi.org/10.1016/j.quascirev.2021.107197

Hermanns, R.L., Fauqué, L., Wilson, C.G.J., 2015. $^{36}$Cl terrestrial cosmogenic nuclide dating suggests Late Pleistocene to Early Holocene mass movements on the south face of Aconcagua mountain and in the Las Cuevas–Horcones valleys, Central Andes, Argentina. Geological Society, London, Special Publications 399, 345–368. https://doi.org/10.1144/SP399.19

Heusser, C.J., 1990. Ice age vegetation and climate of subtropical Chile. Palaeogeography, Palaeoclimatology, Palaeoecology 80, 107–127. https://doi.org/10.1016/0031-0182(90)90124-P

Heusser, C.J., 1989. Southern Westerlies during the Last Glacial Maximum. Quaternary Research 31, 423–425. https://doi.org/10.1016/0033-5894(89)90049-5

Heusser, C.J., Heusser, L.E., Lowell, T. V., 1999. Paleoecology of The Southern Chilean Lake District-Isla Grande de Chiloe During Middle-late Llanquihue Glaciation and Deglaciation. Geografiska Annaler, Series A: Physical Geography 81, 231–284. https://doi.org/10.1111/1468-0459.00058

Hughes, P.D., Gibbard, P.L., 2015. A stratigraphical basis for the Last Glacial Maximum (LGM). Quaternary International 383, 174–185. https://doi.org/10.1016/j.quaint.2014.06.006

Hugonnet, R., McNabb, R., Berthier, E., Menounos, B., Nuth, C., Girod, L., Farinotti, D., Huss, M., Dussaillant, I., Brun, F., Kääb, A., 2021. Accelerated global glacier mass loss in the early twenty-first century. Nature 592, 726–731. https://doi.org/10.1038/s41586-021-03436-z

Hulton, N.R.J., Purves, R.S., McCulloch, R.D., Sugden, D.E., Bentley, M.J., 2002. The Last Glacial Maximum and deglaciation in southern South America. Quaternary Science Reviews 21, 233–241. https://doi.org/10.1016/S0277-3791(01)00103-2

Huston, A., Siler, N., Roe, G.H., Pettit, E., Steiger, N.J., 2021. Understanding drivers of glacier-length variability over the last millennium. Cryosphere 15, 1645–1662. https://doi.org/10.5194/tc-15-1645-2021

Huybers, P., Denton, G., 2008. Antarctic temperature at orbital timescales controlled by local summer duration. Nature Geoscience 1, 787–792. https://doi.org/10.1038/ngeo311

Huybers, P., Wunsch, C., 2005. Obliquity pacing of the late Pleistocene glacial terminations. Nature 434, 491–494. https://doi.org/10.1038/nature03401

Ingólfsson, Ó., Benediktsson, Í.Ö., Schomacker, A., Kjær, K.H., Brynjólfsson, S., Jónsson, S.A., Korsgaard, N.J., Johnson, M.D., 2016. Glacial geological studies of surge-type glaciers in Iceland - Research status and future challenges. Earth-Science Reviews 152, 37–69. https://doi.org/10.1016/j.earscirev.2015.11.008

Iturrizaga, L., Charrier, R., 2021. Sudden glacier advances in the Cachapoal Valley, Southern Central Andes of Chile (34°S). Journal of South American Earth Sciences 105, 102787. https://doi.org/10.1016/j.jsames.2020.102787

Ivy-Ochs, S., 2015. Glacier variations in the European Alps at the end of the last glaciation. Cuadernos de Investigación Geográfica 41, 295–315. https://doi.org/10.18172/cig.2750

Janke, J. R., Bellisario, A.C., Ferrando, F.A., 2015. Classification of debris-covered glaciers and rock glaciers in the Andes of central Chile. Geomorphology 241, 98–121. https://doi.org/10.1016/j.geomorph.2015.03.034

Jenny, B., Valero-Garcés, B.L., Urrutia, R., Kelts, K., Veit, H., Appleby, P.G., Geyh, M., 2002. Moisture changes and fluctuations of the Westerlies in Mediterranean Central Chile during

the last 2000 years: The Laguna Aculeo record (33°50′S). Quaternary International 87, 3–18. https://doi.org/10.1016/S1040-6182(01)00058-1

Johnson, Z.F., Chikamoto, Y., Wang, S.Y.S., Mcphaden, M.J., Mochizuki, T., 2020. Pacific decadal oscillation remotely forced by the equatorial Pacific and the Atlantic Oceans. Climate Dynamics 55, 789–811. https://doi.org/10.1007/s00382-020-05295-2

Jomelli, V., Favier, V., Rabatel, A., Brunstein, D., Hoffmann, G., Francou, B., 2009. Fluctuations of glaciers in the tropical Andes over the last millennium and palaeoclimatic implications: A review. Palaeogeography, Palaeoclimatology, Palaeoecology 281, 269–282. https://doi.org/10.1016/j.palaeo.2008.10.033

Jones, D.B., Harrison, S., Anderson, K., 2019. Mountain glacier-to-rock glacier transition. Global and Planetary Change 181, 102999. https://doi.org/10.1016/j.gloplacha.2019.102999

Jones, R.S., Small, D., Cahill, N., Bentley, M.J., Whitehouse, P.L., 2019. iceTEA: Tools for plotting and analysing cosmogenic-nuclide surface-exposure data from former ice margins. Quaternary Geochronology 51, 72–86. https://doi.org/10.1016/j.quageo.2019.01.001

Jouzel, J., Masson-Delmotte, V., Cattani, O., Dreyfus, G., Falourd, S., Hoffmann, G., Minster, B., Nouet, J., Barnola, J.M., Chappellaz, J., Fischer, H., Gallet, J.C., Johnsen, S., Leuenberger, M., Loulergue, L., Luethi, D., Oerter, H., Parrenin, F., Raisbeck, G., Raynaud, D., Schilt, A., Schwander, J., Selmo, E., Souchez, R., Spahni, R., Stauffer, B., Steffensen, J.P., Stenni, B., Stocker, T.F., Tison, J.L., Werner, M., Wolff, E.W., 2007. Orbital and Millennial Antarctic Climate Variability over the Past 800,000 Years. Science 317, 793–796. https://doi.org/10.1126/science.1141038

Kaiser, J., Lamy, F., Hebbeln, D., 2005. A 70-kyr sea surface temperature record off southern Chile (Ocean Drilling Program Site 1233). Paleoceanography 20, n/a-n/a. https://doi.org/10.1029/2005PA001146

Kaiser, J., Schefuß, E., Lamy, F., Mohtadi, M., Hebbeln, D., 2008. Glacial to Holocene changes in sea surface temperature and coastal vegetation in north central Chile: high versus low latitude forcing. Quaternary Science Reviews 27, 2064–2075. https://doi.org/10.1016/j.quascirev.2008.08.025

Kamleitner, S., Ivy-Ochs, S., Manatschal, L., Akçar, N., Christl, M., Vockenhuber, C., Hajdas, I., Synal, H.-A., 2022. Last Glacial Maximum glacier fluctuations on the northern Alpine foreland: Geomorphological and chronological reconstructions from the Rhine and Reuss glacier systems. Geomorphology 108548. https://doi.org/10.1016/j.geomorph.2022.108548

Kaplan, M.R., Fogwill, C.J., Sugden, D.E., Hulton, N.R.J., Kubik, P.W., Freeman, S.P.H.T., 2008. Southern Patagonian glacial chronology for the Last Glacial period and implications for Southern Ocean climate. Quaternary Science Reviews 27, 284–294. https://doi.org/10.1016/j.quascirev.2007.09.013

Kaplan, M. R., Schaefer, J.M., Denton, G.H., Doughty, A.M., Barrell, D.J.A., Chinn, T.J.H., Putnam, A.E., Andersen, B.G., Mackintosh, A., Finkel, R.C., Schwartz, R., Anderson, B.,

2013. The anatomy of long-term warming since 15 ka in New Zealand based on net glacier snowline rise. Geology 41, 887–890. https://doi.org/10.1130/G34288.1

Kaplan, Michael R., Schaefer, J.M., Denton, G.H., Doughty, A.M., Barrell, D.J.A., Chinn, T.J.H., Putnam, A.E., Andersen, B.G., Mackintosh, A., Finkel, R.C., Schwartz, R., Anderson, B., 2013. The anatomy of long-term warming since 15 ka in New Zealand based on net glacier snowline rise. Geology 41, 887–890. https://doi.org/10.1130/G34288.1

Kaplan, M.R., Schaefer, J.M., Strelin, J.A., Denton, G.H., Anderson, R.F., Vandergoes, M.J., Finkel, R.C., Schwartz, R., Travis, S.G., Garcia, J.L., Martini, M.A., Nielsen, S.H.H., 2016. Patagonian and southern South Atlantic view of Holocene climate. Quaternary Science Reviews 141, 112–125. https://doi.org/10.1016/j.quascirev.2016.03.014

Kaplan, M.R., Strelin, J.A., Schaefer, J.M., Denton, G.H., Finkel, R.C., Schwartz, R., Putnam, A.E., Vandergoes, M.J., Goehring, B.M., Travis, S.G., 2011. In-situ cosmogenic 10Be production rate at Lago Argentino, Patagonia: Implications for late-glacial climate chronology. Earth and Planetary Science Letters 309, 21–32. https://doi.org/10.1016/j.epsl.2011.06.018

Kelley, S.E., Kaplan, M.R., Schaefer, J.M., Andersen, B.G., Barrell, D.J.A., Putnam, A.E., Denton, G.H., Schwartz, R., Finkel, R.C., Doughty, A.M., 2014. High-precision 10 Be chronology of moraines in the Southern Alps indicates synchronous cooling in Antarctica and New Zealand 42,000 years ago. Earth and Planetary Science Letters 405, 194–206. https://doi.org/10.1016/j.epsl.2014.07.031

Kindler, P., Guillevic, M., Baumgartner, M., Schwander, J., Landais, A., Leuenberger, M., 2014. Temperature reconstruction from 10 to 120 kyr b2k from the NGRIP ice core. Climate of the Past 10, 887–902. https://doi.org/10.5194/cp-10-887-2014

King, O., Turner, A.G.D., Quincey, D.J., Carrivick, J.L., 2020. Morphometric evolution of Everest region debris-covered glaciers. Geomorphology 371, 107422. https://doi.org/10.1016/j.geomorph.2020.107422

Kirkbride, M.P., Winkler, S., 2012. Correlation of Late Quaternary moraines: Impact of climate variability, glacier response, and chronological resolution. Quaternary Science Reviews 46, 1–29. https://doi.org/10.1016/j.quascirev.2012.04.002

Kjær, K.H., Krüger, J., 2001. The final phase of dead-ice moraine development: processes and sediment architecture, Kötlujökull, Iceland. Sedimentology 48, 935–952.

Kneisel, C., 1988. Legende für geomorphologische Kartierungen in Hochgebirgen (GMK Hochgebirge). - Trierer Geographische Studien, 18.

Knight, J., Harrison, S., 2014. Mountain glacial and paraglacial environments under global climate change: Lessons from the past, future directions and policy implications. Geografiska Annaler, Series A: Physical Geography 96, 245–264. https://doi.org/10.1111/geoa.12051

Koffman, T.N.B., Schaefer, J.M., Putnam, A.E., Denton, G.H., Barrell, D.J.A., Rowan, A. V., Finkel, R.C., Rood, D.H., Schwartz, R., Plummer, M.A., Brocklehurst, S.H., 2017. A beryllium-10 chronology of late-glacial moraines in the upper Rakaia valley, Southern

Alps, New Zealand supports Southern-Hemisphere warming during the Younger Dryas. Quaternary Science Reviews 170, 14–25. https://doi.org/10.1016/j.quascirev.2017.06.012

Kohl, C.P., Nishiizumi, K., 1992. Chemical isolation of quartz for measurement of in-situ-produced cosmogenic nuclides. Geochimica et Cosmochimica Acta 56, 3583–3587.

Koppes, M., Gillespie, A. R., Burke, R. M., Thompson, S. C., & Stone, J. (2008). Late Quaternary glaciation in the Kyrgyz Tien Shan. *Quaternary Science Reviews*, *27*(7–8), 846–866. https://doi.org/10.1016/j.quascirev.2008.01.009

Korschinek, G., Bergmaier, A., Faestermann, T., Gerstmann, U.C., Knie, K., Rugel, G., Wallner, A., Dillmann, I., Dollinger, G., von Gostomski, C.L., Kossert, K., Maiti, M., Poutivtsev, M., Remmert, A., 2010. A new value for the half-life of 10Be by Heavy-Ion Elastic Recoil Detection and liquid scintillation counting. Nuclear Instruments and Methods in Physics Research, Section B: Beam Interactions with Materials and Atoms 268, 187–191. https://doi.org/10.1016/j.nimb.2009.09.020

Krüger, J., Aber, J., 1998. Formation ofsupraglacial sediment accumulations on Kötlujökull, Iceland. Journal of Glaciology 42, 400–402.

Krüger, J., Kjær, K.H., 2000. De-icing progression of ice-cored moraines in a humid, subpolar climate, Kötlujökull, Iceland. The Holocene 10, 737–747. https://doi.org/10.1191/09596830094980

Krüger, J., Kjær, K.H., 1999. A data chart for field description and genetic interpretation of glacial diamicts and associated sediments - with examples from Greenland, Iceland, and Denmark. Boreas 28, 386–402. https://doi.org/10.1111/j.1502-3885.1999.tb00228.x

Krüger, J., Kjær, K.H., Schomacker, A., 2010. Dead-ice environments: a landsystems model for a debris-charged, stagnant lowland glacier margin, Kötlujökull, in: Developments in Quaternary Science. pp. 105–126. https://doi.org/10.1016/S1571-0866(09)01307-4

Kuhn, P.P., 1930. Zwei Touren im Tinguiririca-Gebiet. Andina. Zeitschrift für Naturfreunde und Wanderer 5, 115–121.

Lal, D., 1991. Cosmic ray labeling of erosion surfaces: in situ nuclide production rates and erosion models. Earth and Planetary Science Letters 104, 424–439. https://doi.org/10.1016/0012-821X(91)90220-C

Lamy, F., Arz, H.W., Kilian, R., Lange, C.B., Lembke-Jene, L., Wengler, M., Kaiser, J., Baeza-Urrea, O., Hall, I.R., Harada, N., Tiedemann, R., 2015. Glacial reduction and millennial-scale variations in Drake Passage throughflow. Proceedings of the National Academy of Sciences 112, 13496–13501. https://doi.org/10.1073/pnas.1509203112

Lamy, F., Hebbeln, D., Wefer, G., 1999a. High-resolution marine record of climatic change in mid-latitude Chile during the last 28,000 years based on terrigenous sediment parameters. Quaternary Research 51, 83–93. https://doi.org/10.1006/qres.1998.2010

Lamy, F., Hebbeln, D., Wefer, G., 1999b. High-Resolution Marine Record of Climatic Change in Mid-latitude Chile during the Last 28,000 Years Based on Terrigenous Sediment Parameters. Quaternary Research 51, 83–93. https://doi.org/10.1006/qres.1998.2010

Lamy, F., Hebbeln, D., Wefer, G., 1998. Late Quaternary precessional cycles of terrigenous sediment input off the Norte Chico, Chile (27.5°S) and paleoclimatic implications. Palaeogeography, Palaeoclimatology, Palaeoecology 141, 233–251.

Lamy, F., Klump, J., Hebbeln, D., Wefer, G., 2000. Late Quaternary rapid climate change in northern Chile. Terra Nova 12, 8–13. https://doi.org/10.1046/j.1365-3121.2000.00265.x

Le Quesne, C., Acuña, C., Boninsegna, J.A., Rivera, A., Barichivich, J., 2009. Long-term glacier variations in the Central Andes of Argentina and Chile, inferred from historical records and tree-ring reconstructed precipitation. Palaeogeography, Palaeoclimatology, Palaeoecology 281, 334–344. https://doi.org/10.1016/j.palaeo.2008.01.039

Le Quesne, C., Stahle, D.W., Cleaveland, M.K., Therrell, M.D., Aravena, J.C., Barichivich, J., 2006. Ancient Austrocedrus tree-ring chronologies used to reconstruct central Chile precipitation variability from A.D. 1200 to 2000. Journal of Climate 19, 5731–5744. https://doi.org/10.1175/JCLI3935.1

Li, Y., Liu, G., Chen, Y., Li, Y., Harbor, J., Stroeven, A. P., Caffee, M., Zhang, M., Li, C., & Cui, Z. (2014). Timing and extent of Quaternary glaciations in the Tianger Range, eastern Tian Shan, China, investigated using 10Be surface exposure dating. *Quaternary Science Reviews*, *98*, 7–23. https://doi.org/10.1016/j.quascirev.2014.05.009

Licdardi, J.M., Schaefer, J.M., Taggart, J.R., Lund, D.C., 2009. Holocene glacier fluctuations in the peruvian andes indicate northern climate linkaqes. Science 325, 1677–1679. https://doi.org/10.1126/science.1175010

Lifton, N., Sato, T., Dunai, T.J., 2014. Scaling in situ cosmogenic nuclide production rates using analytical approximations to atmospheric cosmic-ray fluxes. Earth and Planetary Science Letters 386, 149–160. https://doi.org/10.1016/j.epsl.2013.10.052

Lira, M., García, J., Bentley, M.J., Jamieson, S.S.R., Darvill, C.M., Hein, A.S., Fernández, H., Rodés, Á., Fabel, D., Smedley, R.K., Binnie, S.A., 2022. The Last Glacial Maximum and Deglacial History of the Seno Skyring Ice Lobe (52°S), Southern Patagonia. Frontiers in Earth Science 10, 1–27. https://doi.org/10.3389/feart.2022.892316

Liu, Z., Otto-Bliesner, B.L., He, F., Brady, E.C., Tomas, R., Clark, P.U., Carlson, A.E., Lynch-Stieglitz, J., Curry, W., Brook, E., Erickson, D., Jacob, R., Kutzbach, J., Cheng, J., 2009. Transient Simulation of Last Deglaciation with a New Mechanism for Bølling-Allerød Warming. Science 325, 310–314. https://doi.org/10.1126/science.1171041

Lliboutry, L., 1998. Glaciers of Chile and Argentina, in: Richards, W., Ferrigno, J. (Eds.), Satellite Image Atlas of Glaciers of the World - South America. U.S. Geological Survey, Washington D.C., p. 229.

Lliboutry, L., 1958. Studies of the Shrinkage After a Sudden Advance, Blue Bands and Wave Ogives on Glaciar Universidad (Central Chilean Andes). Journal of Glaciology 3, 261–270. https://doi.org/10.3189/S002214300002390X

Lliboutry, L., 1956. Nieves y glaciares de Chile: Fundamentos de glaciología. Ediciones de la Universidad, Santiago de Chile. https://doi.org/10.2307/211691

Lowell, T. V., Heusser, C.J., Andersen, B.G., Moreno, P.I., Hauser, A., Heusser, L.E.,

Schlüchter, C., Marchant, D.R., Denton, G.H., 1995. Interhemispheric Correlation of Late Pleistocene Glacial Events. Science 269, 1541–1549. https://doi.org/10.1126/science.269.5230.1541

Lukas, S., Nicholson, L.I., Humlum, O., 2007. Comment on Lønne and Lyså (2005): "Deglaciation dynamics following the Little Ice Age on Svalbard: Implications for shaping of landscapes at high latitudes", Geomorphology 72, 300-319. Geomorphology 84, 145–149. https://doi.org/10.1016/j.geomorph.2006.07.003

Lukas, S., Nicholson, L.I., Ross, F.H., Humlum, O., 2005. Formation, meltout processes and landscape alteration of high-arctic ice-cored moraines - Examples from Nordenskiöld land, central Spitsbergen. Polar Geography 29, 157–187. https://doi.org/10.1080/789610198

Lüthi, D., Le Floch, M., Bereiter, B., Blunier, T., Barnola, J.-M., Siegenthaler, U., Raynaud, D., Jouzel, J., Fischer, H., Kawamura, K., Stocker, T.F., 2008. High-resolution carbon dioxide concentration record 650,000–800,000 years before present. Nature 453, 379–382. https://doi.org/10.1038/nature06949

Lynch-Stieglitz, J., Adkins, J.F., Curry, W.B., Dokken, T., Hall, I.R., Herguera, J.C., Hirschi, J.J.M., Ivanova, E. V., Kissel, C., Marchal, O., Marchitto, T.M., McCave, I.N., McManus, J.F., Mulitza, S., Ninnemann, U., Peeters, F., Yu, E.-F., Zahn, R., 2007. Atlantic Meridional Overturning Circulation During the Last Glacial Maximum. Science 316, 66–69. https://doi.org/10.1126/science.1137127

Mackintosh, A.N., Anderson, B.M., Pierrehumbert, R.T., 2017. Reconstructing climate from glaciers. Annual Review of Earth and Planetary Sciences 45, 649–680. https://doi.org/10.1146/annurev-earth-063016-020643

Magrin, G.O., Marengo, J.A., Boulanger, J.-P., Buckeridge, M.S., Castellanos, E., Poveda, G., Scarano, F.R., Vicuña, S., 2014. Central and South America, in: Barros, V.R., Field, C.B., Dokken, D.J., Mastrandrea, M.D., Mach, K.J. (Eds.), Climate Change 2014: Impacts, Adaptation and Vulnerability. Cambridge University Press, Cambridge, pp. 1499–1566. https://doi.org/10.1017/CBO9781107415386.007

Maldonado, A., Betancourt, J.L., Latorre, C., Villagran, C., 2005. Pollen analyses from a 50 000-yr rodent midden series in the southern Atacama Desert (25° 30′ S). Journal of Quaternary Science 20, 493–507. https://doi.org/10.1002/jqs.936

Maldonado, A., Villagrán, C., 2002. Paleoenvironmental Changes in the Semiarid Coast of Chile (~32°S) during the Last 6200 cal Years Inferred from a Swamp–Forest Pollen Record. Quaternary Research 58, 130–138. https://doi.org/10.1006/qres.2002.2353

Malmros, J.K., Mernild, S.H., Wilson, R., Yde, J.C., Fensholt, R., 2016. Glacier area changes in the central Chilean and Argentinean Andes 1955-2013/14. Journal of Glaciology 62, 391–401. https://doi.org/10.1017/jog.2016.43

Mantua, N.J., 2002. Pacific – Decadal Oscillation ( PDO ), in: McCracken, M.C., Perry, J.S. (Eds.), The Encyclopedia of Global Environmental Change, The Earth System—Physical and Chemical Dimensions of Global Environmental Change. Whiley, pp. 592–594.

Mantua, N.J., Hare, S.R., Zhang, Y., Wallace, J.M., Francis, R.C., 1997. A Pacific Interdecadal

Climate Oscillation with Impacts on Salmon Production. Bulletin of the American Meteorological Society 78, 1069–1079. https://doi.org/10.1175/1520-0477(1997)078<1069:APICOW>2.0.CO;2

Marcott, S.A., Bauska, T.K., Buizert, C., Steig, E.J., Rosen, J.L., Cuffey, K.M., Fudge, T.J., Severinghaus, J.P., Ahn, J., Kalk, M.L., McConnell, J.R., Sowers, T., Taylor, K.C., White, J.W.C., Brook, E.J., 2014. Centennial-scale changes in the global carbon cycle during the last deglaciation. Nature 514, 616–619. https://doi.org/10.1038/nature13799

Marshall, G.J., 2003. Trends in the Southern Annular Mode from observations and reanalyses. Journal of Climate 16, 4134–4143. https://doi.org/10.1175/1520-0442(2003)016<4134:TITSAM>2.0.CO;2

Martel-Cea, A., Maldonado, A., Grosjean, M., Alvial, I., de Jong, R., Fritz, S.C., von Gunten, L., 2016. Late Holocene environmental changes as recorded in the sediments of high Andean Laguna Chepical, Central Chile (32°S; 3050 m a.s.l.). Palaeogeography, Palaeoclimatology, Palaeoecology 461, 44–54. https://doi.org/10.1016/j.palaeo.2016.08.003

Masiokas, M.H., Christie, D.A., Le Quesne, C., Pitte, P., Ruiz, L., Villalba, R., Luckman, B.H., Berthier, E., Nussbaumer, S.U., González-Reyes, Á., McPhee, J., Barcaza, G., 2016. Reconstructing the annual mass balance of the Echaurren Norte glacier (Central Andes, 33.5° S) using local and regional hydroclimatic data. Cryosphere 10, 927–940. https://doi.org/10.5194/tc-10-927-2016

Masiokas, M.H., Rivera, A., Espizua, L.E., Villalba, R., Delgado, S., Aravena, J.C., 2009. Glacier fluctuations in extratropical South America during the past 1000years. Palaeogeography, Palaeoclimatology, Palaeoecology 281, 242–268. https://doi.org/10.1016/j.palaeo.2009.08.006

Masiokas, M.H., Villalba, R., Christie, D.A., Betman, E., Luckman, B.H., Le Quesne, C., Prieto, M.R., Mauget, S., 2012. Snowpack variations since AD 1150 in the Andes of Chile and Argentina (30°-37°S) inferred from rainfall, tree-ring and documentary records. Journal of Geophysical Research Atmospheres 117, 1–11. https://doi.org/10.1029/2011JD016748

Masiokas, M.H., Villalba, R., Luckman, B.H., Mauget, S., 2010. Intra-to multidecadal variations of snowpack and streamflow records in the andes of Chile and Argentina between 30° and 37°S. Journal of Hydrometeorology 11, 822–831. https://doi.org/10.1175/2010JHM1191.1

Maxeiner, S., Synal, H.-A., Christl, M., Suter, M., Müller, A., Vockenhuber, C., 2019. Proof-of-principle of a compact 300 kV multi-isotope AMS facility. Nuclear Instruments and Methods in Physics Research Section B: Beam Interactions with Materials and Atoms 439, 84–89. https://doi.org/10.1016/j.nimb.2018.11.028

McCulloch, R.D., Bentley, M.J., Purves, R.S., Hulton, N.R.J., Sugden, D.E., Clapperton, C.M., 2000. Climatic inferences from glacial and palaeoecological evidence at the last glacial termination, southern South America. Journal of Quaternary Science 15, 409–417. https://doi.org/10.1002/1099-1417(200005)15:43.0.CO;2-#

Meier, M.F., Post, A., 1969. What are glacier surges? Canadian Journal of Earth Sciences 6, 807–817. https://doi.org/10.1139/e69-081

Mendelova, M., Hein, A.S., McCulloch, R., Davies, B., 2017. The Last Glacial Maximum and deglaciation in central Patagonia, 44°S–49°S. Cuadernos de Investigación Geográfica 43, 719. https://doi.org/10.18172/cig.3263

Mendelová, M., Hein, A.S., Rodés, Á., Smedley, R.K., Xu, S., 2020. Glacier expansion in central Patagonia during the Antarctic Cold Reversal followed by retreat and stabilisation during the Younger Dryas. Quaternary Science Reviews 227, 106047. https://doi.org/10.1016/j.quascirev.2019.106047

Menviel, L., Timmermann, A., Timm, O.E., Mouchet, A., 2011. Deconstructing the Last Glacial termination: the role of millennial and orbital-scale forcings. Quaternary Science Reviews 30, 1155–1172. https://doi.org/10.1016/j.quascirev.2011.02.005

Mercer, J.H., 1984. Simultaneous climatic change in both hemispheres and similar bipolar interglacial warming: Evidence and implications. pp. 307–313. https://doi.org/10.1029/GM029p0307

Milankovitch, M., 1941. Kanon der Erdbestrahlung und seine Anwendung auf das Eiszeitenproblem. Royal Serbian Academy Special Publication 33, 633.

Mix, A.C., Bard, E., Schneider, R., 2001. Environmental processes of the ice age: Land, oceans, glaciers (EPILOG). Quaternary Science Reviews 20, 627–657. https://doi.org/10.1016/S0277-3791(00)00145-1

Mölg, N., Ferguson, J., Bolch, T., Vieli, A., 2020. On the influence of debris cover on glacier morphology: How high-relief structures evolve from smooth surfaces. Geomorphology 357, 107092. https://doi.org/10.1016/j.geomorph.2020.107092

Monegato, G., Scardia, G., Hajdas, I., Rizzini, F., Piccin, A., 2017. The Alpine LGM in the boreal ice-sheets game. Scientific Reports 7, 1–8. https://doi.org/10.1038/s41598-017-02148-7

Monnier, S., Kinnard, C., 2017. Pluri-decadal (1955–2014) evolution of glacier–rock glacier transitional landforms in the central Andes of Chile (30–33° S). Earth Surface Dynamics 5, 493–509. https://doi.org/10.5194/esurf-5-493-2017

Monnier, S., Kinnard, C., 2015. Reconsidering the glacier to rock glacier transformation problem: new insights from the central Andes of Chile. Geomorphology 238, 47–55. https://doi.org/10.1016/j.geomorph.2015.02.025

Monnin, E., Indermühle, A., Dällenbach, A., Flückiger, J., Stauffer, B., Stocker, T.F., Raynaud, D., Barnola, J.-M., 2001. Atmospheric CO 2 Concentrations over the Last Glacial Termination. Science 291, 112–114. https://doi.org/10.1126/science.291.5501.112

Montecinos, A., Aceituno, P., 2003. Seasonality of the ENSO-Related Rainfall Variability in Central Chile and Associated Circulation Anomalies. Journal of Climate 16, 281–296. https://doi.org/10.1175/1520-0442(2003)016<0281:SOTERR>2.0.CO;2

Moore, E.M.M., Eaves, S.R., Norton, K.P., Mackintosh, A.N., Anderson, B.M., Dowling, L.H., Hidy, A.J., 2022. Climate reconstructions for the Last Glacial Maximum from a simple

cirque glacier in Fiordland, New Zealand. Quaternary Science Reviews 275, 107281. https://doi.org/10.1016/j.quascirev.2021.107281

Morales, M.S., Cook, E.R., Barichivich, J., Christie, D.A., Villalba, R., LeQuesne, C., Srur, A.M., Eugenia Ferrero, M., González-Reyes, Á., Couvreux, F., Matskovsky, V., Aravena, J.C., Lara, A., Mundo, I.A., Rojas, F., Prieto, M.R., Smerdon, J.E., Bianchi, L.O., Masiokas, M.H., Urrutia-Jalabert, R., Rodriguez-Catón, M., Muñoz, A.A., Rojas-Badilla, M., Alvarez, C., Lopez, L., Luckman, B.H., Lister, D., Harris, I., Jones, P.D., Park Williams, A., Velazquez, G., Aliste, D., Aguilera-Betti, I., Marcotti, E., Flores, F., Muñoz, T., Cuq, E., Boninsegna, J.A., 2020. Six hundred years of South American tree rings reveal an increase in severe hydroclimatic events since mid-20th century. Proceedings of the National Academy of Sciences of the United States of America 117, 16816–16823. https://doi.org/10.1073/pnas.2002411117

Moreiras, S.M., Páez, M.S., Lauro, C., Jeanneret, P., 2017a. First cosmogenic ages for glacial deposits from the Plata range (33° S): New inferences for Quaternary landscape evolution in the Central Andes. Quaternary International 438, 50–64. https://doi.org/10.1016/j.quaint.2016.08.041

Moreiras, S.M., Páez, M.S., Lauro, C., Jeanneret, P., 2017b. First cosmogenic ages for glacial deposits from the Plata range (33° S): New inferences for Quaternary landscape evolution in the Central Andes. Quaternary International 438, 50–64. https://doi.org/10.1016/j.quaint.2016.08.041

Moreno, P.I., Denton, G.H., Moreno, H., Lowell, T. V., Putnam, A.E., Kaplan, M.R., 2015a. Radiocarbon chronology of the last glacial maximum and its termination in northwestern Patagonia. Quaternary Science Reviews 122, 233–249. https://doi.org/10.1016/j.quascirev.2015.05.027

Moreno, P.I., Denton, G.H., Moreno, H., Lowell, T. V, Putnam, A.E., Kaplan, M.R., 2015b. Radiocarbon chronology of the last glacial maximum and its termination in northwestern Patagonia. Quaternary Science Reviews 122, 233–249. https://doi.org/10.1016/j.quascirev.2015.05.027

Moreno, P.I., Fercovic, E.I., Soteres, R.L., Ugalde, P.I., Sagredo, E.A., Villa-Martínez, R.P., 2022. Glacier and terrestrial ecosystem evolution in the Chilotan archipelago sector of northwestern Patagonia since the Last Glacial Termination. Earth-Science Reviews 235, 104240. https://doi.org/10.1016/j.earscirev.2022.104240

Moreno, P.I., Kaplan, M.R., François, J.P., Villa-Martínez, R., Moy, C.M., Stern, C.R., Kubik, P.W., 2009. Renewed glacial activity during the Antarctic cold reversal and persistence of cold conditions until 11.5 ka in southwestern Patagonia. Geology 37, 375–378. https://doi.org/10.1130/G25399A.1

Moreno, P.I., Lowell, T.V., Jacobson Jr, G.L., Denton, G.H., 1999. Abrupt Vegetation and Climate Changes During the Last Glacial Maximumand Last Termination in The Chilean Lake District: A Case Study from Canal De La Puntilla (41oS). Geografiska Annaler, Series A: Physical Geography 81, 285–311. https://doi.org/10.1111/1468-0459.00059

Moreno, P.I., Videla, J., 2016. Centennial and millennial-scale hydroclimate changes in northwestern Patagonia since 16,000 yr BP. Quaternary Science Reviews 149, 326–337.

https://doi.org/10.1016/j.quascirev.2016.08.008

Moreno, P.I., Vilanova, I., Villa-Martínez, R., Dunbar, R.B., Mucciarone, D.A., Kaplan, M.R., Garreaud, R.D., Rojas, M., Moy, C.M., De Pol-Holz, R., Lambert, F., 2018. Onset and Evolution of Southern Annular Mode-Like Changes at Centennial Timescale. Scientific Reports 8, 1–9. https://doi.org/10.1038/s41598-018-21836-6

Muscheler, R., Kromer, B., Björck, S., Svensson, A., Friedrich, M., Kaiser, K.F., Southon, J., 2008. Tree rings and ice cores reveal 14C calibration uncertainties during the Younger Dryas. Nature Geoscience 1, 263–267. https://doi.org/10.1038/ngeo128

Newnham, R.M., Lowe, D.J., 2000. Fine-resolution pollen record of late-glacial climate reversal from New Zealand. Geology 28, 759. https://doi.org/10.1130/0091-7613(2000)28<759:FPROLC>2.0.CO;2

Nishiizumi, K., Imamura, M., Caffee, M.W., Southon, J.R., Finkel, R.C., McAninch, J., 2007. Absolute calibration of 10 Be AMS standards. Nuclear Instruments and Methods in Physics Research, Section B: Beam Interactions with Materials and Atoms 258, 403–413. https://doi.org/10.1016/j.nimb.2007.01.297

Oerlemans, J., 1994. Quantifying Global Warming from the Retreat of Glaciers. Science 264, 243–245. https://doi.org/10.1126/science.264.5156.243

Oliva, M., Ruiz-Fernández, J., 2015. Coupling patterns between para-glacial and permafrost degradation responses in Antarctica. Earth Surface Processes and Landforms 40, 1227–1238. https://doi.org/10.1002/esp.3716

Osman, M.B., Tierney, J.E., Zhu, J., Tardif, R., Hakim, G.J., King, J., Poulsen, C.J., 2021. Globally resolved surface temperatures since the Last Glacial Maximum. Nature 599, 239–244. https://doi.org/10.1038/s41586-021-03984-4

Otto-Bliesner, B.L., Brady, E.C., Clauzet, G., Tomas, R., Levis, S., Kothavala, Z., 2006. Last Glacial Maximum and Holocene Climate in CCSM3. Journal of Climate 19, 2526–2544. https://doi.org/10.1175/JCLI3748.1

Owen, L.A., 1991. Mass movement deposits in the Karakoram Mountains: their sedimentary characteristics, recognition and role in Karakoram landform evolution. Z. Geomorph, N. F.

Patterson, C.J., 1998. Laurentide glacial landscapes: The role of ice streams. Geology 26, 643. https://doi.org/10.1130/0091-7613(1998)026<0643:LGLTRO>2.3.CO;2

Pedro, J.B., Bostock, H.C., Bitz, C.M., He, F., Vandergoes, M.J., Steig, E.J., Chase, B.M., Krause, C.E., Rasmussen, S.O., Markle, B.R., Cortese, G., 2016. The spatial extent and dynamics of the Antarctic Cold Reversal. Nature Geoscience 9, 51–55. https://doi.org/10.1038/ngeo2580

Pedro, J.B., van Ommen, T.D., Rasmussen, S.O., Morgan, V.I., Chappellaz, J., Moy, A.D., Masson-Delmotte, V., Delmotte, M., 2011. The last deglaciation: timing the bipolar seesaw. Climate of the Past 7, 671–683. https://doi.org/10.5194/cp-7-671-2011

Peltier, C., Kaplan, M.R., Birkel, S.D., Soteres, R.L., Sagredo, E.A., Aravena, J.C., Araos, J., Moreno, P.I., Schwartz, R., Schaefer, J.M., 2021. The large MIS 4 and long MIS 2 glacier

maxima on the southern tip of South America. Quaternary Science Reviews 262, 106858. https://doi.org/10.1016/j.quascirev.2021.106858

Pesce, O.H., Moreno, P.I., 2014. Vegetation, fire and climate change in central-east Isla Grande de Chiloé (43°S) since the Last Glacial Maximum, northwestern Patagonia. Quaternary Science Reviews 90, 143–157. https://doi.org/10.1016/j.quascirev.2014.02.021

Phillips, E., Everest, J., Evans, D.J.A., Finlayson, A., Ewertowski, M., Guild, A., Jones, L., 2017. Concentrated, 'pulsed' axial glacier flow: structural glaciological evidence from Kvíárjökull in SE Iceland. Earth Surface Processes and Landforms 42, 1901–1922. https://doi.org/10.1002/esp.4145

Pizarro, A.O., Hormazabal F. S., González C, A., Yáñez R. E., 1994. Variabilidad del viento, nivel del mar y temperatura en la costa norte de Chile. Investigaciones marinas 22, 85–101. https://doi.org/10.4067/S0717-71781994002200007

Porter, S.C., 1981. Glaciation in the Southern of Chile. Quaternary Research 16, 263–292.

Porter, S.E., Mosley-Thompson, E., Thompson, L.G., Wilson, A.B., 2021. Reconstructing an interdecadal pacific oscillation index from a pacific basin–wide collection of ice core records. Journal of Climate 34, 3839–3852. https://doi.org/10.1175/JCLI-D-20-0455.1

Portilho-Ramos, R.C., Chiessi, C.M., Zhang, Y., Mulitza, S., Kucera, M., Siccha, M., Prange, M., Paul, A., 2017. Coupling of equatorial Atlantic surface stratification to glacial shifts in the tropical rainbelt. Scientific Reports 7, 1561. https://doi.org/10.1038/s41598-017-01629-z

Price, B.N., Stansell, N.D., Fernández, A., Licciardi, J.M., Lesnek, A.J., Muñoz, A., Sorensen, M.K., Jaque Castillo, E., Shutkin, T., Ciocca, I., Galilea, I., 2022. Chlorine-36 Surface Exposure Dating of Late Holocene Moraines and Glacial Mass Balance Modeling, Monte Sierra Nevada, South-Central Chilean Andes (38°S). Frontiers in Earth Science 10, 1–21. https://doi.org/10.3389/feart.2022.848652

Putnam, A.E., Denton, G.H., Schaefer, J.M., Barrell, D.J.A., Andersen, B.G., Finkel, R.C., Schwartz, R., Doughty, A.M., Kaplan, M.R., Schlüchter, C., 2010. Glacier advance in southern middle-latitudes during the Antarctic Cold Reversal. Nature Geoscience 3, 700–704. https://doi.org/10.1038/ngeo962

Putnam, A.E., Schaefer, J.M., Denton, G.H., Barrell, D.J.A., Birkel, S.D., Andersen, B.G., Kaplan, M.R., Finkel, R.C., Schwartz, R., Doughty, A.M., 2013. The Last Glacial Maximum at 44°S documented by a 10Be moraine chronology at Lake Ohau, Southern Alps of New Zealand. Quaternary Science Reviews 62, 114–141. https://doi.org/10.1016/j.quascirev.2012.10.034

Quintana, J., Aceituno, P., 2012. Changes in the rainfall regime along the extratropical West coast. Atmósfera 25, 1–22.

Rabatel, A., Castebrunet, H., Favier, V., Nicholson, L., Kinnard, C., 2011a. Glacier changes in the Pascua-Lama region, Chilean Andes (29° S): recent mass balance and 50 yr surface area variations. The Cryosphere 5, 1029–1041. https://doi.org/10.5194/tc-5-1029-2011

Rabatel, A., Castebrunet, H., Favier, V., Nicholson, L., Kinnard, C., 2011b. Glacier changes in

the Pascua-Lama region, Chilean Andes (29° S): recent mass balance and 50 yr surface area variations. The Cryosphere 5, 1029–1041. https://doi.org/10.5194/tc-5-1029-2011

Rabatel, A., Jomelli, V., Naveau, P., Francou, B., Grancher, D., 2005. Dating of Little Ice Age glacier fluctuations in the tropical Andes: Charquini glaciers, Bolivia, 16°S. Comptes Rendus Geoscience 337, 1311–1322. https://doi.org/10.1016/j.crte.2005.07.009

Raymo, M.E., 1997. The timing of major climate terminations. Paleoceanography 12, 577–585. https://doi.org/10.1029/97PA01169

Reid, T.D., Brock, B.W., 2014. Assessing ice-cliff backwasting and its contribution to total ablation of debris-covered Miage glacier, Mont Blanc massif, Italy. Journal of Glaciology 60, 3–13. https://doi.org/10.3189/2014JoG13J045

Reynhout, S.A., Sagredo, E.A., Kaplan, M.R., Aravena, J.C., Martini, M.A., Moreno, P.I., Rojas, M., Schwartz, R., Schaefer, J.M., 2019. Holocene glacier fluctuations in Patagonia are modulated by summer insolation intensity and paced by Southern Annular Mode-like variability. Quaternary Science Reviews 220, 178–187. https://doi.org/10.1016/j.quascirev.2019.05.029

Riquelme, R., Rojas, C., Aguilar, G., Flores, P., 2011. Late Pleistocene-early Holocene paraglacial and fluvial sediment history in the Turbio valley, semiarid Chilean Andes. Quaternary Research 75, 166–175. https://doi.org/10.1016/j.yqres.2010.10.001

Rivera, A., Acuña, C., Cassasa, G., Bown, F., 2002. Use of remotely sensed and field data to estimate the contribution of Chilean glaciers to eustatic sea-level rise. International Glaciological Society 34, 367–372.

Rojas, M., Moreno, P., Kageyama, M., Crucifix, M., Hewitt, C., Abe-Ouchi, A., Ohgaito, R., Brady, E.C., Hope, P., 2009. The Southern Westerlies during the last glacial maximum in PMIP2 simulations. Climate Dynamics 32, 525–548. https://doi.org/10.1007/s00382-008-0421-7

Röthlisberger, F., 1986. 10000 Jahre Gletschergeschichte der Erde. Aarau.

Ruddiman, W.F., 2006. Ice-driven CO2 feedback on ice volume. Climate of the Past 2, 43–55. https://doi.org/10.5194/cpd-2-43-2006

Rutllant, J., Fuenzalida, H., 1991. Synoptic aspects of the central chile rainfall variability associated with the southern oscillation. International Journal of Climatology 11, 63–76. https://doi.org/10.1002/joc.3370110105

Sagredo, E.A., Kaplan, M.R., Araya, P.S., Lowell, T. V., Aravena, J.C., Moreno, P.I., Kelly, M.A., Schaefer, J.M., 2018. Trans-pacific glacial response to the Antarctic Cold Reversal in the southern mid-latitudes. Quaternary Science Reviews 188, 160–166. https://doi.org/10.1016/j.quascirev.2018.01.011

Sagredo, E.A., Lowell, T. V., Kelly, M.A., Rupper, S., Aravena, J.C., Ward, D.J., Malone, A.G.O., 2017. Equilibrium line altitudes along the Andes during the Last millennium: Paleoclimatic implications. The Holocene 27, 1019–1033. https://doi.org/10.1177/0959683616678458

Sagredo, E.A., Moreno, P.I., Villa-Martínez, R., Kaplan, M.R., Kubik, P.W., Stern, C.R., 2011.

Fluctuations of the Última Esperanza ice lobe (52°S), Chilean Patagonia, during the last glacial maximum and termination 1. Geomorphology 125, 92–108. https://doi.org/10.1016/j.geomorph.2010.09.007

Sagredo, E. A., Moreno, P.I., Villa-Martínez, R., Kaplan, M.R., Kubik, P.W., Stern, C.R., 2011. Fluctuations of the Última Esperanza ice lobe (52°S), Chilean Patagonia, during the last glacial maximum and termination 1. Geomorphology 125, 92–108. https://doi.org/10.1016/j.geomorph.2010.09.007

Sagredo, E.A., Rupper, S., Lowell, T. V., 2014. Sensitivities of the equilibrium line altitude to temperature and precipitation changes along the Andes. Quaternary Research 81, 355–366. https://doi.org/10.1016/j.yqres.2014.01.008

Sakai, A., Takeuchi, N., Fujita, K., Nakawo, M., 2000. Role of supraglacial ponds in the ablation process of a debris-covered glacier in the Nepal Himalayas, in: Debris-Covered Glaciers. IAHS, Seattle, Washington, pp. 119–130.

Santana, R., 1967. Rasgos de la glaciación cuaternaria en "El Manzanar". Valle del Cachapoal. Andes de Rancagua. Revista Geográfica de Valparaíso 1, 85–98.

Scapozza, C., Castelletti, C., Soma, L., Dall'Agnolo, S., Ambrosi, C., 2014. Timing of LGM and deglaciation in the Southern Swiss Alps. Géomorphologie : relief, processus, environnement 20, 307–322. https://doi.org/10.4000/geomorphologie.10753

Schaefer, J.M., Denton, G.H., Barrell, D.J.A., Ivy-Ochs, S., Kubik, P.W., Andersen, B.G., Phillips, F.M., Lowell, T. V., Schlüchter, C., 2006. Near-Synchronous Interhemispheric Termination of the Last Glacial Maximum in Mid-Latitudes. Science 312, 1510–1513. https://doi.org/10.1126/science.1122872

Schaefer, J.M., Denton, G.H., Kaplan, M., Putnam, A., Finkel, R.C., Barrell, D.J.A., Andersen, B.G., Schwartz, R., Mackintosh, A., Chinn, T., Schlüchter, C., 2009. High-frequency holocene glacier fluctuations in new zealand differ from the northern signature. Science 324, 622–625. https://doi.org/10.1126/science.1169312

Schomacker, A., 2008. What controls dead-ice melting under different climate conditions? A discussion. Earth-Science Reviews 90, 103–113. https://doi.org/10.1016/j.earscirev.2008.08.003

Schomacker, A., 2007. Dead-ice under different climate conditions: Processes, landforms, sediments and melt rate in Iceland and Svalbard. Lund University.

Schomacker, A., Benediktsson, Í.Ö., Ingólfsson, Ó., 2014. The Eyjabakkajökull glacial landsystem, Iceland: Geomorphic impact of multiple surges. Geomorphology 218, 98–107. https://doi.org/10.1016/j.geomorph.2013.07.005

Schomacker, A., Kjaer, K.H., 2007. Origin and de-icing of multiple generations of ice-cored moraines at Brúarjökull, Iceland. Boreas 36, 411–425. https://doi.org/10.1080/03009480701213554

Schomacker, A., Kjær, K.H., 2008. Quantification of dead-ice melting in ice-cored moraines at the high-Arctic glacier Holmströmbreen, Svalbard. Boreas 37, 211–225. https://doi.org/10.1111/j.1502-3885.2007.00014.x

SERNAGEOMIN, 2004. Mapa geológico de Chile: versión digital 1:1.000.000.

Shaw, T.E., Ulloa, G., Farías-Barahona, D., Fernandez, R., Lattus, J.M., McPhee, J., 2021. Glacier albedo reduction and drought effects in the extratropical Andes, 1986–2020. Journal of Glaciology 67, 158–169. https://doi.org/10.1017/jog.2020.102

Shroder, J.F., Bishop, M.P., Copland, L., Sloan, V.F., 2000. Debris-covered glaciers and rock glaciers in the Nanga Parbat Himalaya, Pakistan. Geografiska Annaler, Series A: Physical Geography 82, 17–31. https://doi.org/10.1111/j.0435-3676.2000.00108.x

Solomina, O.N., Bradley, R.S., Jomelli, V., Geirsdottir, A., Kaufman, D.S., Koch, J., McKay, N.P., Masiokas, M., Miller, G., Nesje, A., Nicolussi, K., Owen, L.A., Putnam, A.E., Wanner, H., Wiles, G., Yang, B., 2016. Glacier fluctuations during the past 2000 years. Quaternary Science Reviews 149, 61–90. https://doi.org/10.1016/j.quascirev.2016.04.008

Soteres, R.L., Sagredo, E.A., Kaplan, M.R., Martini, M.A., Moreno, P.I., Reynhout, S.A., Schwartz, R., Schaefer, J.M., 2022. Glacier fluctuations in the northern Patagonian Andes (44°S) imply wind-modulated interhemispheric in-phase climate shifts during Termination 1. Scientific Reports 12, 10842. https://doi.org/10.1038/s41598-022-14921-4

Stephens, B.B., Keeling, R.F., 2000. The influence of antarctic sea ice on glacial-interglacial CO2 variations. Nature 404, 171–174. https://doi.org/10.1038/35004556

Stone, J.O., 2000. Air pressure and cosmogenic isotope production. Journal of Geophysical Research: Solid Earth 105, 23753–23759. https://doi.org/10.1029/2000JB900181

Strand, P.D., Schaefer, J.M., Putnam, A.E., Denton, G.H., Barrell, D.J.A., Koffman, T.N.B., Schwartz, R., 2019. Millennial-scale pulsebeat of glaciation in the Southern Alps of New Zealand. Quaternary Science Reviews 220, 165–177. https://doi.org/10.1016/j.quascirev.2019.07.022

Strelin, J.A., Denton, G.H., Vandergoes, M.J., Ninnemann, U.S., Putnam, A.E., 2011. Radiocarbon chronology of the late-glacial Puerto Bandera moraines, Southern Patagonian Icefield, Argentina. Quaternary Science Reviews 30, 2551–2569. https://doi.org/10.1016/j.quascirev.2011.05.004

Stroeven, A.P., Fabel, D., Harbor, J.M., Fink, D., Caffee, M.W., Dahlgren, T., 2011. Importance of sampling across an assemblage of glacial landforms for interpreting cosmogenic ages of deglaciation. Quaternary Research 76, 148–156. https://doi.org/10.1016/j.yqres.2011.04.004

Stroup, J.S., Kelly, M.A., Lowell, T. V., Applegate, P.J., Howley, J.A., 2014. Late holocene fluctuations of Qori Kalis outlet glacier, Quelccaya Ice Cap, Peruvian Andes. Geology 42, 347–350. https://doi.org/10.1130/G35245.1

Stuiver, M., Reimer, P.J., 1993. Extended 14 C Data Base and Revised CALIB 3.0 14 C Age Calibration Program. Radiocarbon 35, 215–230. https://doi.org/10.1017/S0033822200013904

Sutherland, J.L., Carrivick, J.L., Evans, D.J.A., Shulmeister, J., Quincey, D.J., 2019. The Tekapo Glacier, New Zealand, during the Last Glacial Maximum: An active temperate glacier influenced by intermittent surge activity. Geomorphology 343, 183–210.

https://doi.org/10.1016/j.geomorph.2019.07.008

Swift, D.A., Cook, S.J., Graham, D.J., Midgley, N.G., Fallick, A.E., Storrar, R., Toubes Rodrigo, M., Evans, D.J.A., 2018. Terminal zone glacial sediment transfer at a temperate overdeepened glacier system. Quaternary Science Reviews 180, 111–131. https://doi.org/10.1016/j.quascirev.2017.11.027

Thompson, D.W.J., Wallace, J.M., 2000. Annular Modes in the Extratropical Circulation. Part I: Month-to-Month Variability*. Journal of Climate 13, 1000–1016. https://doi.org/10.1175/1520-0442(2000)013<1000:AMITEC>2.0.CO;2

Toggweiler, J.R., Russell, J.L., Carson, S.R., 2006. Midlatitude westerlies, atmospheric CO 2 , and climate change during the ice ages. Paleoceanography 21, n/a-n/a. https://doi.org/10.1029/2005PA001154

Valero-Garcés, B.L., Jenny, B., Rondanelli, M., Delgado-Huertas, A., Burns, S.J., Veit, H., Moreno, A., 2005. Palaeohydrology of Laguna de Tagua Tagua (34° 30′ S) and moisture fluctuations in Central Chile for the last 46 000 yr. Journal of Quaternary Science 20, 625–641. https://doi.org/10.1002/jqs.988

van Woerkom, T., Steiner, J.F., Kraaijenbrink, P.D.A., Miles, E.S., Immerzeel, W.W., 2019. Sediment supply from lateral moraines to a debris-covered glacier in the Himalaya. Earth Surface Dynamics 7, 411–427. https://doi.org/10.5194/esurf-7-411-2019

Vandergoes, M.J., Dieffenbacher-Krall, A.C., Newnham, R.M., Denton, G.H., Blaauw, M., 2008. Cooling and changing seasonality in the Southern Alps, New Zealand during the Antarctic Cold Reversal. Quaternary Science Reviews 27, 589–601. https://doi.org/10.1016/j.quascirev.2007.11.015

Veit, H., 1996. Southern Westerlies during the Holocene deduced from geomorphological and pedological studies in the Norte Chico, Northern Chile (27- 33°s). Palaeogeography, Palaeoclimatology, Palaeoecology 123, 107–119. https://doi.org/10.1016/0031-0182(95)00118-2

Villa-Martínez, R., Villagrán, C., Jenny, B., 2004. Pollen evidence for late-Holocene climatic variability at Laguna de Aculeo, Central Chile (lat. 34°S). The Holocene 14, 361–367. https://doi.org/10.1191/0959683604hl712rp

Villagrán, C., Varela, J., 1990. Palynological Evidence for Increased Aridity on the Central Chilean Coast during the Holocene. Quaternary Research 34, 198–207. https://doi.org/10.1016/0033-5894(90)90031-f

Villalba, R., 1994. Fluctuaciones climáticas en latitudes medias de América del Sur durante los últimos 1000 años : sus relaciones con la Oscilación del Sur. Revista Chilena de Historia Natural 67, 453–461.

Villalba, R., Lara, A., Masiokas, M.H., Urrutia, R., Luckman, B.H., Marshall, G.J., Mundo, I.A., Christie, D.A., Cook, E.R., Neukom, R., Allen, K., Fenwick, P., Boninsegna, J.A., Srur, A.M., Morales, M.S., Araneo, D., Palmer, J.G., Cuq, E., Aravena, J.C., Holz, A., Lequesne, C., 2012. Unusual Southern Hemisphere tree growth patterns induced by changes in the Southern Annular Mode. Nature Geoscience 5, 793–798. https://doi.org/10.1038/ngeo1613

Wachter, P., Beck, C., Philipp, A., Höppner, K., Jacobeit, J., 2020. Spatiotemporal Variability of the Southern Annular Mode and its Influence on Antarctic Surface Temperatures. Journal of Geophysical Research: Atmospheres 125. https://doi.org/10.1029/2020JD033818

Watson, C.S., Quincey, D.J., Smith, M.W., Carrivick, J.L., Rowan, A. V., James, M.R., 2017. Quantifying ice cliff evolution with multi-temporal point clouds on the debris-covered Khumbu Glacier, Nepal. Journal of Glaciology 63, 823–837. https://doi.org/10.1017/jog.2017.47

Wayne, W., Corte, A., 1983. Multiple glaciations of the Cordon del Plata, Mendoza Argentina. Palaeogeography, Palaeoclimatology, Palaeoecology 42, 185–209.

Wilson, R., Mernild, S.H., Malmros, J.K., Bravo, C., Carrión, D., 2016. Surface velocity fluctuations for Glaciar Universidad, central Chile, between 1967 and 2015. Journal of Glaciology 62, 847–860. https://doi.org/10.1017/jog.2016.73

Wolff, E.W., Fischer, H., Fundel, F., Ruth, U., Twarloh, B., Littot, G.C., Mulvaney, R., Röthlisberger, R., de Angelis, M., Boutron, C.F., Hansson, M., Jonsell, U., Hutterli, M.A., Lambert, F., Kaufmann, P., Stauffer, B., Stocker, T.F., Steffensen, J.P., Bigler, M., Siggaard-Andersen, M.L., Udisti, R., Becagli, S., Castellano, E., Severi, M., Wagenbach, D., Barbante, C., Gabrielli, P., Gaspari, V., 2006. Southern Ocean sea-ice extent, productivity and iron flux over the past eight glacial cycles. Nature 440, 491–496. https://doi.org/10.1038/nature04614

Yokoyama, Y., Lambeck, K., De Deckker, P., Johnston, P., Fifield, L.K., 2000. Timing of the Last Glacial Maximum from observed sea-level minima. Nature 406, 713–716. https://doi.org/10.1038/35021035

Zech, R. (2012). A late pleistocene glacial chronology from the Kitschi-Kurumdu Valley, Tien Shan (Kyrgyzstan), based on $^{10}$Be surface exposure dating. *Quaternary Research*, *77*(2), 281–288. https://doi.org/10.1016/j.yqres.2011.11.008

Zech, J., Terrizzano, C., García-Morabito, E., Veit, H., Zech, R., 2017. Timing and extent of late pleistocene glaciation in the arid central andes of Argentina and Chile (22°-41°s). Cuadernos de Investigacion Geografica 43, 697–718. https://doi.org/10.18172/cig.3235

Zech, R., Kull, C., Kubik, P.W., Veit, H., 2007. Exposure dating of Late Glacial and pre-LGM moraines in the Cordon de Doña Rosa, Northern/Central Chile (~31° S). Climate of the Past 3, 1–14. https://doi.org/10.5194/cp-3-1-2007

Zech, R., Kull, C., Veit, H., 2006. Late Quaternary glacial history in the Encierro Valley, northern Chile (29°S), deduced from 10Be surface exposure dating. Palaeogeography, Palaeoclimatology, Palaeoecology 234, 277–286. https://doi.org/10.1016/j.palaeo.2005.10.011

Zech, R., May, J., Kull, C., Ilgner, J., Kubik, P.W., Veit, H., 2008. Timing of the late Quaternary glaciation in the Andes from ∼15 to 40° S. Journal of Quaternary Science 23, 635–647. https://doi.org/10.1002/jqs.1200

**ANEXOS**

**CHARACTERISTICS OF THE SAMPLED BOULDERS IN THE MORAINE UNI IV**

**UNI 1801**

**Characteristics**

- Well-striated boulder
- Faceted in the north and south sides
- Next to UNI 1803
- Embedded in lateral margin of moraine B
- Length: 270 cm
- Width: 227 cm
- Height: 124 cm

**UNI 1802**

**Characteristics**

- Striated boulder, especially in the south and east faces
- Faceted in the north and south sides
- Next to UNI 1803
- Embedded in lateral margin of moraine B
- Length: 192 cm
- Width: 145 cm
- Height: 118 cm

**UNI 1803**

**Characteristics**

- Striated boulder
- Faceted in the north, east and south sides
- Next to UNI 1802 (upper left side in the image)
- On lateral moraine ridge of moraine B
- Length: 173 cm
- Width: 107 cm
- Height: 90 cm

**UNI 1903**

**Characteristics**

- Striated top
- Faceted in the east and west sides
- On frontal moraine ridge of moraine B
- Length: > 500 cm
- Width: > 300 cm
- Height: 240 cm

**UNI 1904**

**Characteristics**

- Striated top
- Irregular sides with shallow fractures
- Faceted in the south and west sides
- Embedded in the flute field between moraines $D_2$ and E
- Next to UNI 1905
- Length: 260 cm
- Width: 240 cm
- Height: 103 cm

**UNI 1905**

**Characteristics**

- Striated and superimposed boulder
- Faceted in the east and south sides
- Sides with shallow fractures
- Located in the flute field between moraines $D_2$ and E
- Next to UNI 1904
- Length: 110 cm
- Width: 70 cm
- Height: 103 cm

| UNI 2013 | Characteristics |
|---|---|
| | – Superimposed boulder<br>– Striated surface<br>– Fractures on the south-east side<br>– Next to UNI 2014<br>– Length: 260 cm<br>– Width: 170 cm<br>– Height: 120 cm |

| UNI 2012 | Characteristics |
|---|---|
| | – Embedded boulder<br>– Well-striated surface<br>– Faceted sides<br>– Length: 289 cm<br>– Width: 172 cm<br>– Height: 110 cm |

| UNI 2014 | Characteristics |
|---|---|
| | – Superimposed boulder<br>– Striated surface<br>– Faceted on the west side<br>– Next to UNI 2013<br>– Length: 135 cm<br>– Width: 93 cm<br>– Height: 99 cm |

| UNI 2015 | Characteristics |
|---|---|
| | – Embedded boulder<br>– Striated surface<br>– Faceted<br>– Length: 273 cm<br>– Width: 243 cm<br>– Height: 134 cm |

| UNI 2011 | Characteristics |
|---|---|
| | – Superimposed boulder<br>– Striated surface<br>– Faceted and with fractures on the south and east sides<br>– Length: 184 cm<br>– Width: 132 cm<br>– Height: 158 cm |

| UNI 1901 | Characteristics |
|---|---|
| | – Embedded boulder<br>– Well-striated surface<br>– Sides with shallow fractures<br>– Faceted on the east and west sides<br>– Located on till surface distal to moraine A<br>– Faceted on east and west sides<br>– Length: 340 cm<br>– Width: 200 cm<br>– Height: 135 cm |

| UNI 1902 | Characteristics |
|---|---|
| | – Embedded boulder<br>– Well-striated top<br>– Faceted and fractured in their sides<br>– Length: ~10000 cm<br>– Width: ~600 cm<br>– Height: 390 cm |

| UNI 2002 | Characteristics |
|---|---|
| | – Striated surface<br>– Sides with shallow fractures<br>– Faceted on the north, east, and south sides<br>– Length: 330 cm<br>– Width: 315 cm<br>– Height: 148 cm |

| UNI 2003 | Characteristics |
|---|---|
| | – Embedded boulder<br>– Well-striated surface<br>– Bullet nose shape<br>– Length: 177 cm<br>– Width: 110 cm<br>– Height: 81 cm |

| UNI 2009 | Characteristics |
|---|---|
| | – Embedded boulder<br>– Striated surface<br>– Length: 77 cm<br>– Width: 74 cm<br>– Height: 51 cm |

| **UNI 1907a,b** | **Characteristics** |
|---|---|
| | – Striated surface<br>– Faceted<br>– Length: 205 cm<br>– Width: 160 cm<br>– Height: 120 cm |

| **UNI 1906** | **Characteristics** |
|---|---|
| | – Well-striated surface<br>– Bullet nose shape<br>– Faceted on the east side<br>– Length: 450 cm<br>– Width: 320 cm<br>– Height: 283 cm |

| UNI 1805 | Characteristics |
|---|---|
| | – Striated surface<br>– Sides with shallow fractures<br>– Length: 398 cm<br>– Width: 250 cm<br>– Height: 236 cm |

| UNI 1909 | Characteristics |
|---|---|
| | – Embedded boulder<br>– Striated surface<br>– Sides with shallow fractures<br>– Faceted on the north, east, west, and south sides<br>– Length: 170 cm<br>– Width: 135 cm<br>– Height: 113 cm |

| UNI 1908 | Characteristics |
|---|---|
| | – Striated surface<br>– Sides with shallow fractures<br>– Length: 398 cm<br>– Width: 250 cm<br>– Height: 236 cm |

## CHARACTERISTICS OF THE SAMPLED BOULDERS IN THE MORAINE UNI III

| UNI 1809 | Characteristics |
|---|---|
| | – Embedded boulder<br>– Polished surface<br>– Faceted on the north side<br>– Fractured on the south side<br>– Length: 260 cm<br>– Width: 200 cm<br>– Height: 110 cm |

| UNI 1810 | Characteristics |
|---|---|
| | – Embedded boulder<br>– Polished surface<br>– Length: 160 cm<br>– Width: 125 cm<br>– Height: 50 cm |

| UNI 1811 | Characteristics |
|---|---|
| | – Embedded boulder<br>– Polished surface with shallow fractures<br>– Length: 150 cm<br>– Width: 95 cm<br>– Height: 70 cm |

| UNI 1812 | Characteristics |
|---|---|
| | – Embedded boulder<br>– Polished surface<br>– Shallow fractures on the sides<br>– Length: 145 cm<br>– Width: 130 cm<br>– Height: 70 cm |

| UNI 2016 | Characteristics |
|---|---|
| | – Embedded boulder<br>– Polished surface<br>– Length: 186 cm<br>– Width: 130 cm<br>– Height: 90 cm |

| UNI 2017 | Characteristics |
|---|---|
| | – Embedded boulder<br>– Fractures on the sides<br>– Length: 520 cm<br>– Width: 260 cm<br>– Height: 290 cm |

| UNI 1813 | Characteristics |
|---|---|
| | – Faceted boulder<br>– Weathered surface<br>– Length: 180 cm<br>– Width: 135 cm<br>– Height: 95 cm |

## CHARACTERISTICS OF THE SAMPLED BOULDERS IN THE MORAINE UNI II

| **UNI 1806** | **Characteristics** |
|---|---|
| | – Faceted boulder<br>– Irregular and weathered surface<br>– Length: 280 cm<br>– Width: 230 cm<br>– Height: 170 cm |

| **UNI 1808** | **Characteristics** |
|---|---|
| | – Faceted boulder<br>– Weathered surface<br>– Polished on the north side<br>– Length: 400 cm<br>– Width: 270 cm<br>– Height: 100 cm |

| UNI 1814 | Characteristics |
|---|---|
| | – Polished surface<br>– Faceted<br>– Length: 150 cm<br>– Width: 95 cm<br>– Height: 95 cm |

| UNI 1815 | Characteristics |
|---|---|
| | – Embedded boulder<br>– Polished and faceted<br>– Length: 100 cm<br>– Width: 85 cm<br>– Height: 55 cm |

| UNI 1816 | Characteristics |
|---|---|
| | – Embedded boulder<br>– Polished and weathered surface<br>– Faceted boulder<br>– Length: 120 cm<br>– Width: 91 cm<br>– Height: 80 cm |

| UNI 1817 | Characteristics |
|---|---|
| | – Polished surface<br>– Faceted<br>– Length: 110 cm<br>– Width: 80 cm<br>– Height: 60 cm |

| UNI 1910 | Characteristics |
|---|---|
| | – Embedded boulder<br>– Polished and weathered surface<br>– Faceted<br>– Length: 520 cm<br>– Width: 280 cm<br>– Height: 150 cm |

| UNI 1911 | Characteristics |
|---|---|
| | – Embedded boulder<br>– Polished and weathered surface<br>– Faceted<br>– Fracture splits the boulder in two pieces<br>– Length: 250 cm<br>– Width: 240 cm<br>– Height: 120 cm |

| UNI 1912 | Characteristics |
|---|---|
| | – Embedded boulder<br>– Polished and weathered surface<br>– Faceted<br>– Length: 290 cm<br>– Width: 195 cm<br>– Height: 115 cm |

| UNI 1913 | Characteristics |
|---|---|
| | – Polished and weathered surface<br>– Faceted<br>– Length: 150 cm<br>– Width: 120 cm<br>– Height: 85 cm |

| **UNI 1914** | **Characteristics** |
|---|---|
| | – Embedded boulder<br>– Polished and weathered surface<br>– Faceted<br>– Length: 290 cm<br>– Width: 195 cm<br>– Height: 115 cm |
| **UNI 1915** | Characteristics |
| | – Perched boulder<br>– Polished and weathered surface<br>– Faceted<br>– Length: 180 cm<br>– Width: 100 cm<br>– Height: 70 cm |

| UNI 1916 | Characteristics |
|---|---|
| | – Perched boulder<br>– Polished and weathered surface<br>– Faceted<br>– Length: 200 cm<br>– Width: 160 cm<br>– Height: 150 cm |

| UNI 2005 | Characteristics |
|---|---|
| | – Embedded boulder<br>– Polished and weathered surface<br>– Faceted<br>– Fractures on the sides<br>– Length: 435 cm<br>– Width: 130 cm<br>– Height: 175 cm |

| **UNI 2006** | **Characteristics** |
|---|---|
| | – Embedded boulder<br>– Polished and weathered surface<br>– Faceted<br>– Length: 100 cm<br>– Width: 75 cm<br>– Height: 50 cm |

| **UNI 2007** | **Characteristics** |
|---|---|
| | – Embedded boulder<br>– Polished and weathered surface<br>– Faceted<br>– Length: 170 cm<br>– Width: 155 cm<br>– Height: 130 cm |

| UNI 2008 | Characteristics |
|---|---|
| | – Embedded boulder<br>– Polished and weathered surface<br>– Faceted<br>– Length: 130 cm<br>– Width: 130 cm<br>– Height: 95 cm |

## CHARACTERISTICS OF THE SAMPLED BOULDERS IN THE MORAINE UNI I

| **UNI 1818** | **Characteristics** |
|---|---|
| | – Embedded boulder<br>– Polished and weathered surface<br>– Faceted<br>– Length: 235 cm<br>– Width: 165 cm<br>– Height: 120 cm |

| **UNI 1820** | **Characteristics** |
|---|---|
| | – Embedded boulder<br>– Polished and highly weathered surface<br>– Length: 136 cm<br>– Width: 130 cm<br>– Height: 110 cm |

| UNI 1821 | Characteristics |
|---|---|
| | – Embedded boulder<br>– Polished and highly weathered surface<br>– Length: 145 cm<br>– Width: 120 cm<br>– Height: 70 cm |